J. Fluid Mech. (1979), *vol.* 91, *part* 2, *pp.* 253–317
Printed in Great Britain

Two-dimensional analyses related to wave-energy extraction by submerged resonant ducts

By JAMES LIGHTHILL
Department of Applied Mathematics and Theoretical Physics, University of Cambridge

(Received 9 June 1978)

Submerged resonant ducts offer an approach to the design of wave-energy extraction devices consistent with the need for maximum seaworthiness. This paper gives a full account of one type of analysis of these systems, based upon two-dimensional wave hydrodynamics and linearized duct dynamics. The mathematical analyses are given in detail in § 2 while § 1 describes as concisely as possible (i) the assumptions underlying each analysis, (ii) its results and their implications for design, and (iii) any available experimental comparisons.

One theoretical prediction, unexpected when it was first made but since confirmed by experiment (Knott & Flower 1979), is that the effective pressure fluctuations to which a resonant duct responds can be substantially greater than those that would be present at the level of the duct mouth if the duct were absent. Other important predictions are concerned with added mass, radiation damping and the conditions for optimum energy extraction, calculated below for a wide variety of mouth design configurations and internal duct geometries. Broad tentative conclusions from the analyses are given at the end of § 1.

CONTENTS

1. Descriptive

1.1. *Introduction*

In middle latitudes, sources of energy not subject to depletion (the so-called 'renewable resources') include some which, with maximum availability in winter months, are suitable to regions with a winter energy-demand peak. Wind energy is in this category, but the wind at any one locality is immensely variable. Fortunately, ocean swell (that part of an ocean's response to winds which propagates over long distances) has far less variability (especially in winter) because the local swell energy flux responds to a spatially integrated effect of storms over a large oceanic area.

The significant energy source is not in those surface waves of moderate lengths (10–50 m) which may be most obvious to the eye. The swell energy that propagates

0022-1120/79/4157-6020 $02.00

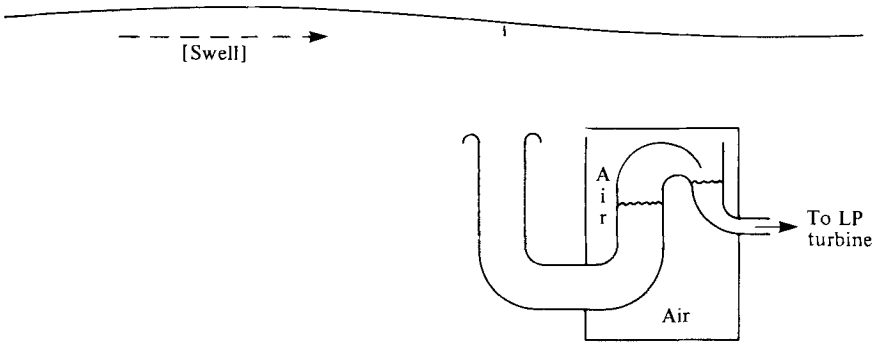

FIGURE 1. Schematic diagram of the Carey resonant duct.

over long distances is primarily in waves of length λ exceeding 50 m. Indeed, between different wave components of a given height and, therefore, given energy per unit sea-surface area, the eye is most sensitive to those of moderate lengths because they have greatest steepness; yet this energy flux (product of energy per unit area with the group velocity $(g\lambda/8\pi)^{\frac{1}{2}}$ at which the energy propagates) is substantially greater for the 'swell' with $\lambda > 50$ m.

Many promising projects for extracting energy from ocean swell depend upon devices operating where the energy is most readily available: at the sea surface. Nevertheless, it remains uncertain whether such surface devices, designed to derive energy mainly from storms in other parts of the ocean, can be made 'seaworthy' in the sense that they are proof against a *local* storm of particular severity. For this reason, a parallel research-and-development programme on the extraction of swell energy by devices which, to reduce their vulnerability to local storms, are submerged as much as 20 m below the surface, appears desirable. Such a programme, based on an invention (Carey & Meratla 1976) by Mr Dennis Carey, is being pursued by Vickers Ltd. The project is ultimately based on a quite simple idea, as follows.

In the Eastern Atlantic, about half of the swell energy flux is contained in waves with periods between 7 and 11 s (corresponding to wavelengths between about 80 and 200 m). From such swell a suitable device, although quite deeply submerged, might extract a significant amount of power if it could resonate with a period of about 9 s and with enough damping for its frequency response curve to have a breadth of $\pm 20\,\%$. With such an aim in view, certain types of mechanical resonator could be well worth pursuing. There is, however, yet another 'seaworthiness' attraction in a fixed resonator without any moving parts, such as the Vickers resonant duct.

Schematically, this can be represented as in figure 1. The resonating device is essentially a U-tube. Normally, however, a water column oscillating in a U-tube has air–water interfaces at both ends, and the vertical displacements of both interfaces contribute gravitational restoring forces that help to fix the resonant frequency. In Dennis Carey's invention, the gravitational restoring force is halved because there is no air–water interface at the end open to the ocean. That end, the 'mouth', which responds to the pressure fluctuations generated by the swell, need not therefore point vertically upwards as it does in figure 1. The resonant frequency, indeed, depends only on (i) the water-column length and on (ii) the restoring force at the *internal* air–water interface.

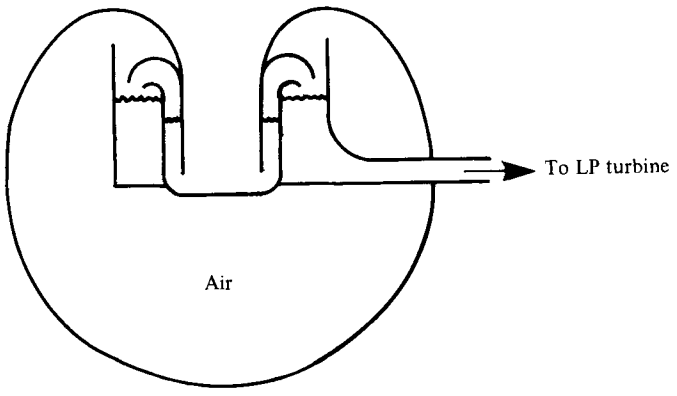

FIGURE 2. One of many alternative approaches to an engineering design based on the idea of figure 1 being pursued by Vickers Ltd.

We shall, in fact, see that model experiments have exhibited excellent resonance also in mouth-downwards and mouth-sideways configurations. Nevertheless, for a seaworthy device extracting energy from ocean swell, a mouth-upwards configuration has one great advantage: given the need for the *whole* device to be submerged at a depth great enough to avoid excessive loads in extreme sea states, we may wish to place as high as possible the *mouth*; that is, the part whose function is to respond, in normal sea states, to an ocean-swell pressure distribution that, of course, falls exponentially with depth. These issues are discussed more quantitatively below in the light of the mathematical models developed in this paper.

The rigid structure containing the air cavity needs to be attached firmly and rigidly to the sea bottom. The air cavity's main function is to supply a gravitational restoring force at the air–water interface; but the air's compressibility generates an additional restoring force which we may call 'pneumatic'. This is due to variations in the internal air pressure as the air–water interface rises and falls. That element in the restoring force makes the system reminiscent of a Helmholtz resonator. Its ratio to the gravitational element is at present expected to be much less than 1, but this ratio remains one of the free parameters available to be optimized in an ultimate engineering design.

The advantages for seaworthiness, inherent in a resonant device without moving parts, suggested also the preferred system for energy extraction. This is an 'overtopping' system, in which the oscillations of the air–water interface cause 'overspill' into a collecting duct that feeds a suitable low-pressure turbine. An overtopping system may have the advantage that it limits the amplitude of oscillations in the U-tube. The hope is that, under all normal conditions when the level of forcing-pressure fluctuations exceeds that able to supply the energy for overtopping oscillations, a high proportion of any excess energy may be utilized. In exceptionally heavy sea states, however, large nonlinear effects should de-tune the system so that it does not then show an excessive response.

Figure 1, as emphasized already, is purely schematic; indeed, a wide choice of geometrical configurations is available for the ultimate engineering design. At the mouth, however, figure 1 does call for a suitably rounded lip, because energy dissipation in jet eddies shed from any sharp lip is expected to be undesirably large; an expectation confirmed by experiments referred to in § 1.2. There is, furthermore, the

possibility of designing a much fuller bell-mouth geometry in an arrangement like that in figure 2. Here, an axisymmetric duct from a well rounded, centrally placed mouth divides into an annular duct of the same cross-sectional area and an annular air–water interface. There, overtopping would take place into an annular collecting duct. This arrangement, with an essentially spherical air cavity, is just one of the many alternative approaches to an engineering design now being considered.

The crudest possible mechanical analysis of a submerged resonant duct is as a forced mass–spring system with simple linear damping. The system's mass M may be taken as the average mass of fluid in the U-tube; possibly, with an 'added-mass' correction to allow for the open-end effect. The system's stiffness k is so defined that the fluid's displacement into the duct by a distance X is opposed by a restoring force kX, incorporating both gravitational and 'pneumatic' components. The period of resonant oscillations is then

$$2\pi(M/k)^{\frac{1}{2}}, \tag{1}$$

which needs as indicated above to be in the region of 9 s.

The forcing term is taken as

$$Fe^{i\omega t}; \tag{2}$$

that is, as a harmonic component with radian frequency ω in the force driving the U-tube oscillation. To a first approximation F can be taken as the area of the mouth multiplied by the amplitude of pressure fluctuations at the level of the mouth generated by the swell. However, the determination of a more accurate estimate of the forcing effect of incident swell on the motions in a submerged resonant duct is one of the primary objectives of this paper.

Among all the features of the very crude mechanical analysis here under discussion, the least realistic in detail is the assumption of linear damping. Nevertheless, many studies of resonant systems with nonlinear damping have shown that they are well represented by a model with a linear damping force $D\dot{X}$, provided that the coefficient D is so chosen that in each period of the oscillation it gives the same energy loss as in the real system. With this in mind we take the damping force as

$$(D_1+D_2)\dot{X}, \tag{3}$$

where D_1 and D_2 are so chosen that in each period of the oscillation $D_1\dot{X}$ and $D_2\dot{X}$ give energy losses corresponding, respectively, to the extraction of useful energy and the net wastage of energy.

According to the crude analysis given above, the oscillations are governed by the equation

$$M\ddot{X}+(D_1+D_2)\dot{X}+kX = Fe^{i\omega t}, \tag{4}$$

with its classical solution

$$X = \frac{Fe^{i\omega t}}{(k-M\omega^2)+(D_1+D_2)i\omega}. \tag{5}$$

The energy extraction rate (the mean value of $D_1\dot{X}^2$) is then

$$\frac{\frac{1}{2}D_1|F|^2\omega^2}{(k-M\omega^2)^2+(D_1+D_2)^2\omega^2}. \tag{6}$$

The maximum rate of energy extraction is obtained under the condition of resonance,

$$\omega = (k/M)^{\frac{1}{2}}, \tag{7}$$

which makes the period $2\pi/\omega$ equal to (1), and under the additional condition

$$D_1 = D_2, \tag{8}$$

which equalizes the wanted and unwanted rates of energy extraction.

This classical model gives the maximum rate of energy extraction as

$$|F|^2/(8D_2), \tag{9}$$

inversely proportional to the energy-wastage coefficient D_2 and directly proportional to the square of the forcing-effect amplitude $|F|$. Earlier, we suggested that $|F|$ should be proportional to the area of the duct mouth. Therefore, this crude analysis tends to focus attention on one major question: how much can be gained by increasing the width of the mouth in relation to other lengths in the problem (including the wavelength of the swell)? The present paper concentrates its main attention on this question, put to the author originally by Dennis Carey in October 1977.

We can now delimit precisely that portion of the whole analysis of the exceedingly complex Vickers project to which the present paper is devoted. In the first place, with all general engineering analysis of the project excluded, this paper is limited to fluid-mechanics aspects. Furthermore, out of the three main areas of fluid-mechanics research on the project, in which the author is involved either alone or with colleagues, the paper is confined to one only; in fact, to the one where researches have reached the point where publication has become appropriate.

Thus, we exclude here one major area of research, where the author's colleague Dr M. A. Swinbanks is especially involved; namely, the fully nonlinear fluid-mechanics analysis of resonant oscillations in a U-tube with energy extraction by overtopping. The present paper, in fact, will be limited to a treatment in which all energy-loss terms are represented as above by equivalent linear damping coefficients. The paper concentrates, instead, on the interactions between submerged resonant ducts and incident swell, and analyses the ensuing oscillations only as far as a linearized treatment of the energy-loss effects will allow. Studies which make use of the present calculations on duct–swell interactions as inputs to a fully nonlinear analysis of U-tube oscillations with overtopping are postponed to later papers.

Methods of analysis of the fluid mechanics of duct–swell interactions, furthermore, can be separated into two main types of method. For various reasons to be discussed below, two-dimensional models of the wave hydrodynamics of duct–swell interactions are highly informative. Furthermore, the classical method for solving two-dimensional hydrodynamic problems, based on conformal mapping, proves extremely powerful in this area, allowing very full and detailed analyses to be made. When all those analyses, together with satisfactory experimental checks, had been completed, it seemed appropriate to publish the material as a whole in the present paper. By contrast, because parallel work on three-dimensional models of the wave hydrodynamics, using quite different methods, is in an only partially developed state, publication of any of that work is, for the time being, postponed.

In this paper, then, several two-dimensional models relevant to experiments on the interaction between surface waves and resonant ducts are described, analysed and applied. For the convenience of readers uninterested in the details of analysis by conformal-mapping methods, the following section (§ 1.2) gives a straightforward description of the assumptions underlying each model and of all the quantitative

results derived from its use. Also, §1.2 makes improvements on the above mechanical description of the oscillations generated in the duct in several different ways (except that, as explained above, it continues to represent energy-loss terms by equivalent linear damping coefficients); for example, it calculates the effect of taper in the duct. Actually, the linearized dynamics of the duct motions is given in a form equally applicable to a two-dimensional or to a three-dimensional system. However, three quantities in that analysis (a forcing-pressure factor, an added-mass term and a radiation damping) need to be calculated from surface-wave theory, results of which are given here only for two-dimensional systems.

For power generation in the neighbourhood of a coastline on which a statistically uniform swell energy flux (in kW/m) is incident, we could imagine a truly two-dimensional realization of the scheme shown in figure 1, greatly extended in the direction perpendicular to the paper; that is, parallel to the coastline. Admittedly, it seems likely that consideration of the necessary civil engineering costs would give preference to a linear array of three-dimensional ducts, uniformly spaced parallel to the coastline.† Nevertheless, the behaviour of such an array may have much more in common with a purely two-dimensional system than with the completely three-dimensional behaviour of (say) an isolated duct. Again, tests of an isolated duct in waves propagated along a narrow wave tank may involve behaviour similar to that of a linear array of ducts, uniformly spaced perpendicular to the sides of the tank, with a strong two-dimensional component in the resulting response. These are reasons for paying serious attention in this paper to the results of two-dimensional analyses; some more such reasons are given in §1.2.

We have emphasized that a practical duct mouth must have rounded lips (figures 1 and 2) to reduce unwanted energy dissipation in jet eddies generated by flow separation at sharp lips. Nevertheless, the results of any analysis of a sharp-lipped duct by use of irrotational-flow theory, which permits no separation or energy dissipation, may be highly relevant to the real use of a duct using rounded lips to avoid dissipation; just as we know that the theoretical irrotational flow past an aerofoil with sharp leading edge gives a good representation of the general flow field about a real aerofoil with its leading edge sufficiently rounded to avoid separation. With these considerations in view, most of the analysis in this paper is for mathematical models of irrotational flow in and around sharp-lipped ducts; although we include one study (see figure 24) of the special effects of such a highly rounded bell-mouth as that illustrated in figure 2.

In addition to mouth-upwards models relevant to systems sketched in figures 1 and 2, we consider also mouth-sideways and mouth-downwards models, partly because various mouth arrangements are conceivable and it is still too early to finalize a choice between them. Also, certain experiments on mouth-downwards systems are particularly easy and afford a convenient test of resonant-duct principles and of associated theory.

Readers with a strictly practical interest in the fluid mechanics of submerged resonant ducts will find everything that they can obtain from this paper set out as concisely as possible in §1.2, to which they are now recommended to turn. Only those interested in details of the wave hydrodynamics for its own sake will wish to study its analysis by conformal mapping given in §§2.1 and 2.2.

† Possibly, with connected air cavities.

Here, we acknowledge briefly that the method used was pioneered especially by Levine & Rodemich (1958). Also, one of the quantities which we calculate (the reflexion coefficient for a mouth-upwards two-dimensional sharp-lipped duct without oscillating flow in the duct) had previously been derived by that method in a different form by Jarvis (1971), who gave extensive graphs of its computed values. In the present paper, all calculated quantities are expressed in terms of confluent hypergeometric functions; all of these have been found easy to compute using the rapidly convergent series for those functions; all, too, are readily expressible in terms of functions tabulated by Macdonald (1949), which was continually helpful as a check on the work. It is noteworthy also that a key aspect of the duct energetics is found to depend [see equation (192)] on a property of the Wronskian of two solutions of the confluent hypergeometric equation.

Between the full analysis of the highly accurate although inevitably complex two-dimensional swell–duct interaction theory given in §2.2, and the brief statements of the results and their applications (including some satisfactory comparisons with experiment) given in §1.2, we have an intermediate section (§2.1). This is concerned with a simpler type of model which we call a 'local' model. Although it is less accurate, it has the advantage that the calculations can be made 'in a few lines' (although they still use conformal mapping) and can be carried out successfully even for complicated geometries, such as bell-mouths. Local models are described for these reasons and because comparisons with the accurate 'fully interactive' theories of §2.2 lead us to appreciate the conditions under which the conclusions from them can be relied upon. We emphasize again, however, that, for every model, readers of §1.2 alone will derive a sufficiently clear picture of its assumptions, results and uses.

1.2. *Description of models: assumptions, results, uses*

For resonant ducts responding to incident swell, one important question has been indicated already in §1.1: as the duct width increases (for given wavelength), how will the effective forcing-pressure amplitude change? This question presupposes an expected fact (actually proved in §2.2) regarding motions in a very *narrow* duct: that they are driven by forcing pressures with the same amplitude as the pressure fluctuations found at the level of the mouth when the duct is absent. For wider ducts, that amplitude is presumably modified, by a modification factor which we call K. One might expect that $K < 1$ (in other words, that this modification is a reduction) on the grounds that a wide duct ought to be sensitive to a sort of averaged pressure distribution; that is, to an average of those sinusoidally distributed pressures that would be felt across the area actually occupied by its mouth if the duct were absent.

To test the correctness or otherwise of that expectation, a two-dimensional model appears particularly appropriate. Clearly, a two-dimensional model of the response of a vertical duct to waves will analyse how a *channel*, with parallel plane vertical walls, responds to waves with crests parallel to those walls. Any reduction in forcing-pressure amplitude due to averaging should be even more marked for such a 'two-dimensional duct' than for an axisymmetrical duct of the same width (in waves of the same wavelength). Therefore, the following calculations from two-dimensional models which indicate for many interesting cases that $K > 1$ (so that the modification represents an amplification, rather than a reduction, of forcing effect) strongly suggest that in axisymmetrical ducts a similar conclusion should be valid.

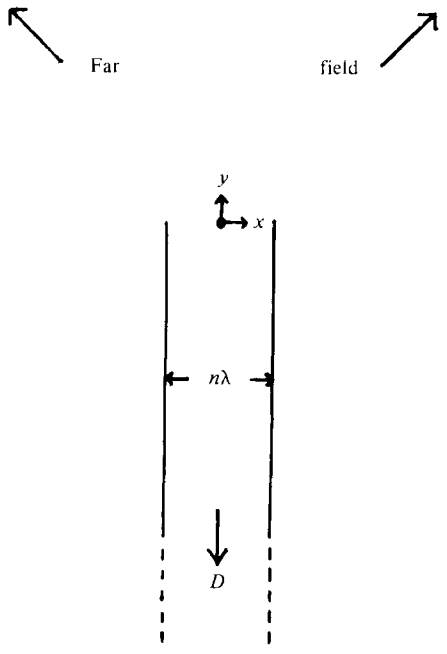

FIGURE 3. The mouth-upwards 'local' model seeks to determine how the pressure in the 'depths' D of the duct shown responds to the far field (10).

The calculation is performed first for a preliminary, highly simplified model of the type that we call a 'local' model. Local models can be analysed very simply indeed, and all the local models we use are worked out in detail in the relatively short section 2.1.

The model is concerned (figure 3) with how a two-dimensional channel of width $n\lambda$ (where $0 < n < 1$) responds to far-field pressures†

$$p_e = (p_0 e^{2\pi y/\lambda})\, e^{-2\pi i x/\lambda}, \tag{10}$$

varying exponentially with y and sinusoidally with x as in waves on deep water with wavelength λ. Here, p_e stands for excess pressure (excess over the hydrostatic pressure distribution); the origin is at the centre of the duct mouth and the y axis is vertically upwards. Evidently, p_0 would be the excess pressure at the centre of the mouth ($x = y = 0$) if the duct were absent; for waves of length λ on deep water it must fluctuate with a radian frequency

$$\omega = (2\pi g/\lambda)^{\frac{1}{2}}, \tag{11}$$

and, indeed, must be proportional to $e^{+i\omega t}$ for waves travelling in the $+x$ direction. We calculate the forcing-pressure modification factor

$$K = p_D/p_0, \tag{12}$$

where p_D is the excess pressure sensed in the depths D of the duct.

This model suffers from the defect that it regards the far field (10) as extending indefinitely far from the duct mouth, whereas the true pressure distribution (10)

† In this section, wherever we equate a physical quantity like p_e to a complex expression as in (10), we mean that p_e is equal to that expression's real part.

n	0	0·1	0·2	0·3	0·4	0·5	0·6	0·7	0·8	0·9	1·0
K	1	1·302	1·448	1·492	1·445	1·315	1·116	0·864	0·584	0·284	0

TABLE 1

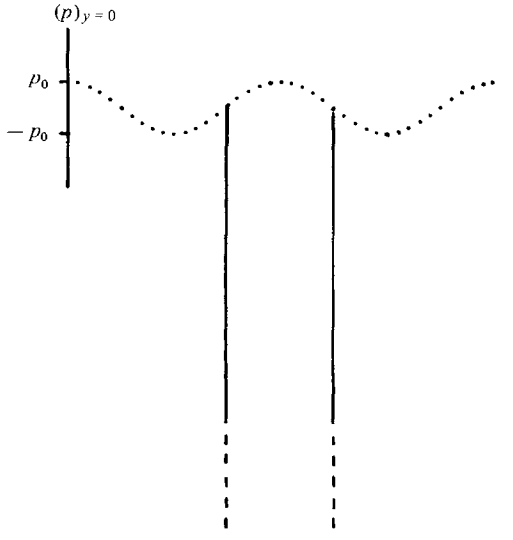

FIGURE 4. The local model in the case $n = 0{\cdot}5$ is concerned with a far field which at the level of the duct mouth would follow the dotted curve, varying between $-p_0$ and $+p_0$; yet, it predicts that the duct responds with an internal pressure $1{\cdot}315\ p_0$.

extends only up to the free surface, at which special boundary conditions need to be applied. In short, this is a 'local' model: it calculates the duct's response to the local distribution of pressure (10), and ignores any back-reaction of the presence of the duct on conditions at the free surface. This model also assumes zero flow in the duct. Although we soon replace it by a model free of both these restrictions, there are advantages in obtaining some preliminary information about the modification factor (12) from a model so simple that its physical significance can be easily probed.

Evaluation of this factor K is extremely straightforward for the local model (§2.1) and yields already some rather surprising numerical results, shown in table 1. Although considerations of averaging (see above) would be expected to make $K < 1$, we find that, for a useful range of values of the ratio n of duct width to wavelength, the modification factor K *exceeds* unity.

Figure 4 re-emphasizes the surprising nature of this conclusion, by an illustration for the case $n = 0{\cdot}5$. The dotted line represents the sinusoidal distribution of the excess pressure (10) that (with p_0 positive) would be present at the level of the duct mouth if the duct were absent. This has maximum p_0 at the centre of the mouth and, furthermore, it actually falls to zero at both lips; yet the duct responds with an excess pressure $1{\cdot}315\ p_0$.

We can interpret this physically by studying the mathematical processes used in the model. The reason why the presence of the duct modifies the far-field pressure distribution (10) is that gradients of that pressure distribution generate accelerations which are blocked by the duct walls. In figure 4, for example, we see that the far field

involves pressure gradients at the duct walls which tend to produce accelerations *outwards* (from the inside of the duct towards the outside). Evidently, the duct would prevent any such normal accelerations from occurring; indeed, in the mathematical model, we calculate the modifying pressure field (tending to zero far from the duct) which must be added to that far field to cancel those outward accelerations on the duct walls. Physically, then, the calculation is equivalent to saying that the vertical duct walls, by blocking any outward acceleration that the gradients of the far-field pressure distribution would otherwise produce, re-direct a substantial additional pressure *downwards into the depths of the duct*, where accordingly a pressure response in excess of p_0 can be found.

For some rather more refined physical discussion of the numerical values of K in table 1, see §2.1. It turns out that K is the product of two factors. One of these does exactly allow for an averaging across the duct of the sinusoidal distribution of far-field pressures. The other can be interpreted in terms of the idea that a duct responds, not directly to the pressures at the level of its mouth, but rather to pressure distributions at a level 'beyond' (in this case, above) its mouth; no doubt, because only at that level do pressure distributions avoid such a blocking action of the duct walls. To state briefly the results of a lengthy discussion of local models, a two-dimensional duct of width around $\frac{1}{16}\lambda$, $\frac{1}{8}\lambda$, $\frac{1}{4}\lambda$ or $\frac{1}{2}\lambda$ is found to respond, essentially, to pressure at distances of about 0·5, 0·4, 0·3 or 0·2 duct widths, respectively, beyond its mouth.

Either physical interpretation tends to confirm the view that a vertical duct with its mouth upwards can be effective even when the duct width is a significant fraction of the wavelength. Indeed, forcing-pressure amplitudes may be still greater in a wide duct than in a narrow one, as well as acting over a greater area. This suggestion that wide ducts may respond effectively encourages us to explore whether similar conclusions are valid for more realistic models.

Fortunately, calculations proved possible also with a far more refined (although still two-dimensional) model. This takes full account of the duct's interaction with the free sea-surface, where the usual (linearized) boundary condition is applied exactly. It also takes into account the dynamics of the internal fluctuating flows with which the duct responds to the forcing pressures. For such 'fully interactive' models in general, see §2.2; here, we describe only the model's assumptions, results, and uses.

We consider incident swell with the sinusoidal free-surface waveform

$$a\,e^{i(\omega t-\kappa x)}. \tag{13}$$

Here, $2a$ is the crest-to-trough height of the waves. For the free-surface condition to be satisfied with waves on deep water, the wavenumber $\kappa = 2\pi/\lambda$ must be equal to ω^2/g as in (11). We calculate the irrotational flow field representing the duct's response to an incident wave of the general sinusoidal form (13). Such a calculation, of course, will allow us to infer its behaviour in a wave system of arbitrary spectrum.

The duct's mouth is taken to be at a depth h below the surface, and the duct is again taken as a vertical channel of width $n\lambda$ (figure 5) with its walls at $x = \pm\frac{1}{2}n\lambda$. The excess pressure p_0 which would be found at the centre of the duct mouth if the duct were absent is then

$$p_0 = (\rho g a\, e^{-2\pi h/\lambda})\, e^{i\omega t}, \tag{14}$$

showing the classical exponential dependence on depth.

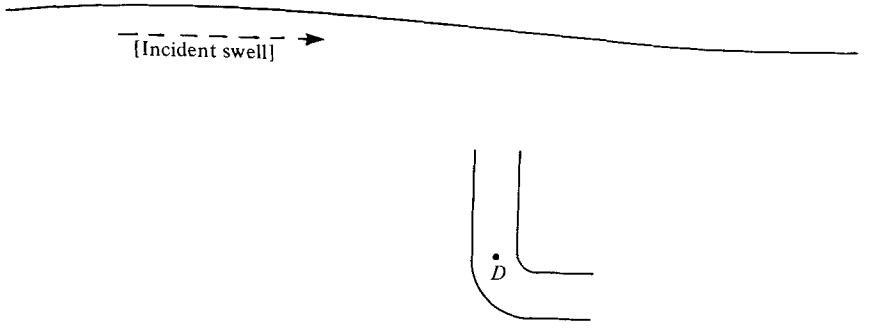

FIGURE 5. The fully interactive model for the mouth-upwards case seeks to determine how the pressure in the 'depths' D of the duct responds to the incident swell (13).

Although the duct by no means consists only of vertical elements, but rather is more of the nature of a U-tube (figure 1), we assume that the bend in the tube occurs at a level far enough below the mouth for the exponential decay of wave pressures and motions with depth to make its influence negligible (figure 5). The wave-hydrodynamics problem is solved, then, with an essentially vertical duct disturbing the incident waves (13). We determine the pressure at a point D which we may still think of as being in the 'depths' of the duct; however, that pressure already has a very simple, well defined form, for a given flow rate in the duct, provided that D is at least two duct widths below the level of the mouth. (This is where the velocity distribution across the duct width has become uniform.) Afterwards, we do a separate calculation of the duct dynamics, in which the motions in the U-tube are determined given its detailed geometry and this relationship between the pressure at D and the flow rate in the duct.

We proceed immediately to give the results obtained by solving the wave-hydrodynamics problem in the above fully interactive model. For clarity, we present these results in two stages. In the second stage, we give results when there is flow in the duct. In the first stage, however, we give results corresponding to the case (treated previously with the local model) of zero flow in the duct. In other words, we first present results for the case 'when the duct is not working'.

In that case, the model gives the excess pressure p_D in the depths D of the duct in a form

$$(Ke^{-i\alpha})\,p_0. \tag{15}$$

Here, K is as before the modification factor, defined as the ratio of the forcing-pressure amplitude $|p_D|$ to the amplitude $|p_0|$ of pressures at the level of the mouth if the duct were absent. The quantity α (positive and rather small, for all cases here calculated) is the phase lag with which the pressure fluctuations at D respond to those that would occur at the centre of the mouth if the duct were absent. The form

$$p_D = (Ke^{-2\pi h/\lambda})\,\rho g a\, e^{i(\omega t-\alpha)}, \tag{16}$$

obtained by combining (15) and (14), should make the above interpretations still clearer.

The variation of K with the ratios n and h/λ (of duct width and mouth depth, respectively, to the wavelength λ) is the most important of the model's outputs. That is why we display it graphically in three different ways.

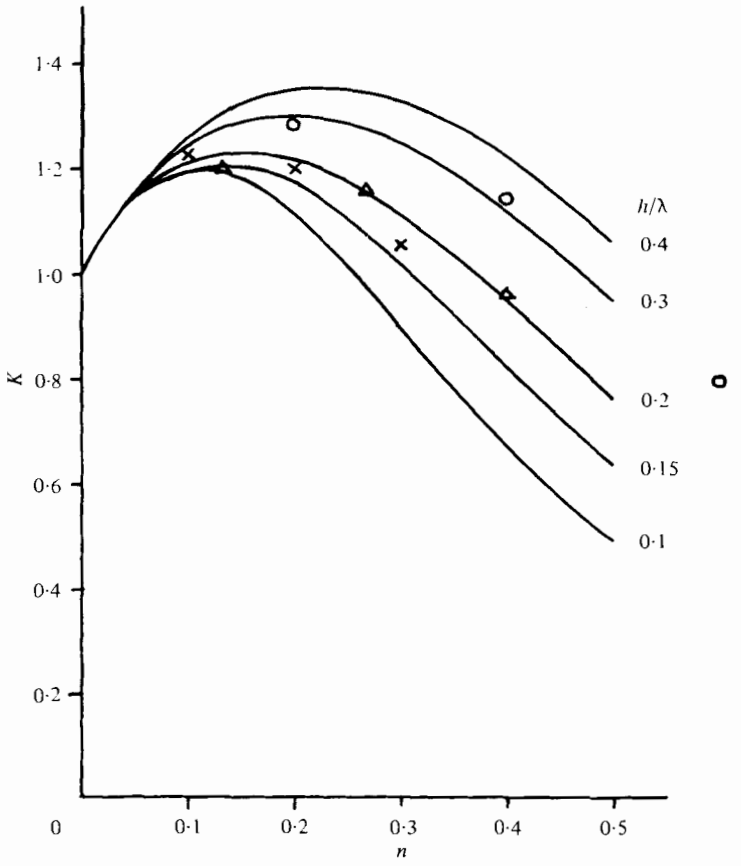

FIGURE 6. The pressure modification factor K in the mouth-upwards case, plotted as a function of the ratio n of duct width to wavelength for different values of the ratio h/λ of the mouth depth to wavelength. Curves: fully interactive theory. Experimental points (Knott & Flower 1979): ○, $h/\lambda = 0{\cdot}3$; △, $h/\lambda = 0{\cdot}2$; ×, $h/\lambda = 0{\cdot}15$.

Figure 6 shows how K varies with n for five different values of h/λ. Because the prime motive for using submerged resonant ducts is to avoid the risks which devices close to the free-surface wave motions may incur, we exclude values of h/λ less than 0·1. Conversely, values greater than 0·4 are excluded; essentially, because pressure fluctuations are hardly strong enough to be effective at a depth of $0{\cdot}5\lambda$ (where the exponential factor in (14) is 0·043) even after amplification by resonance effects.

For all five values of h/λ there is quite a substantial range of values of n for which $K > 1$. It extends to $n = 0{\cdot}25$, 0·31, 0·37, 0·46, 0·53 for $h = 0{\cdot}1$, 0·15, 0·2, 0·3, 0·4, respectively. The margin by which K exceeds 1 is significant, although not so large as was indicated in the values for the local model given in table 1. However, values quite close to those are found for the larger values of h/λ.

The fully interactive model confirms, then, the at first sight surprising conclusion that the modification factor K can exceed unity for interesting values of n; although, for this purpose, it directs attention to rather smaller values of n (around 0·2) than does the local model. The curves in figure 6 were shown at a Society for Underwater Technology seminar on 6 January 1978, and within three weeks one of the participants, Dr G. Knott, had used the wave tank at the University of Sussex to derive

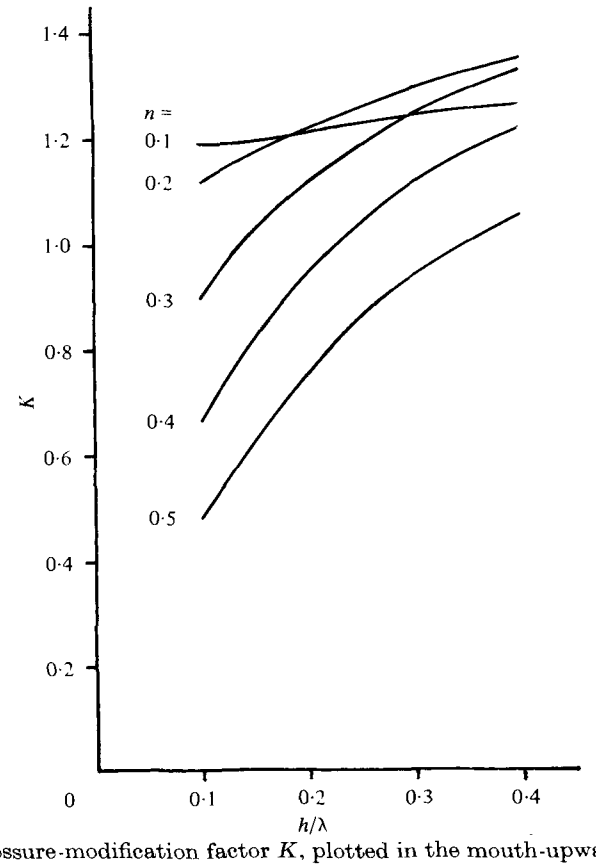

FIGURE 7. The pressure-modification factor K, plotted in the mouth-upwards case as a function of the depth–wavelength ratio h/λ for different values of the width–wavelength ratio n.

experimental values of K for the two-dimensional case of deep-water waves incident upon a parallel-sided vertical channel. Pressure fluctuations at a point corresponding to D in figure 5 were measured by a pressure transducer while an electromechanical gauge measured the undisturbed wave height. Values of K as defined by (16) were calculated from the data. The excellent agreement with the theoretical curves (figure 6) gives general support to the mathematical method used in this paper, and confirms the qualitative conclusion that forcing-pressure amplification can occur. For full details of the experiments, see Knott & Flower (1979).

Figure 7 gives an alternative plot of K, as a function of h/λ for five different values of n. This re-emphasizes that for many interesting values of h/λ the maximum forcing-pressure amplitude is found for values of n around 0·2.

Often, of course, we may be interested in how the behaviour of a particular duct configuration, as specified by its 'aspect-ratio' $h/n\lambda$ (mouth depth over duct width), changes in waves of varying lengths. Figure 8 gives graphs of K for three constant aspect-ratios $h/n\lambda$, equal to 0·5, 1 and 2. The last two values (with mouth depth either equal to the duct width, or twice as great) give values of K significantly greater than 1 for all $n < 0{\cdot}5$.

The curve marked ∞ represents the values of K given by the local theory (table 1 above, or §2.1 below) which, indeed, is proved in §2.2 to constitute a valid limit of

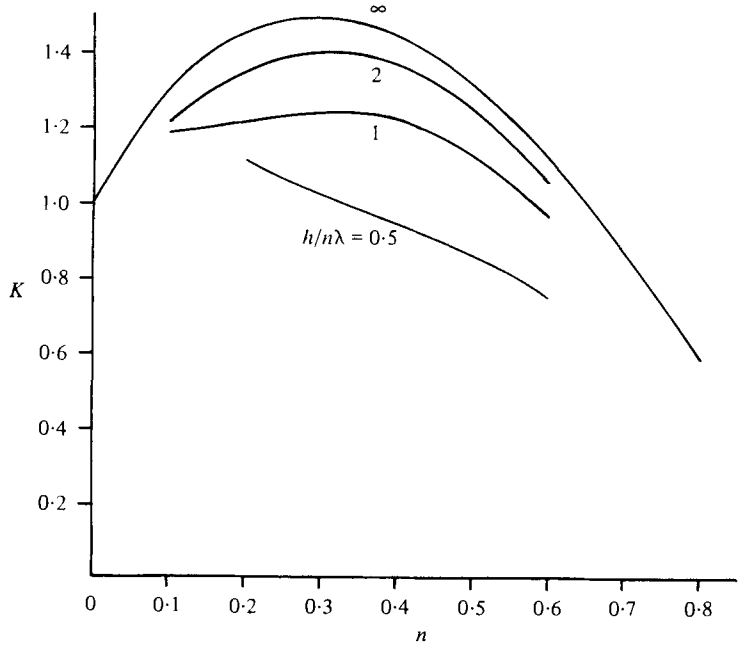

FIGURE 8. The pressure-modification factor K, plotted in the mouth-upwards case as a function of the ratio n of duct width to wavelength for different values of the aspect ratio $h/n\lambda$ (ratio of mouth depth to duct width). The curve $h/n\lambda = \infty$ represents the results (table 1) given by the 'local' model.

the fully interactive theory as the aspect-ratio $h/n\lambda$ becomes large. This was expected because a local model regards the free surface as essentially 'at infinity' and therefore is valid in the limit as the distance h to the free surface becomes large compared with the duct width. Actually, figure 8 shows that the results given by the local theory are already sufficiently accurate for most purposes when $h/n\lambda \geqslant 2$.

Although, in the present zero-flow case (when 'the duct is not working'), by far the most interesting quantity which we can calculate from the model is K, nevertheless the values of certain other quantities are worth recording. One of these is the ratio between the strengths of symmetric and antisymmetric components of the flow field near the mouth of the duct.

We find, in fact, that the disturbance-flow field generated by the interaction of the incident swell and the duct is a linear combination of two modes: one symmetric and one antisymmetric. However, the antisymmetric mode generates no excess pressure in the depths D of the duct; thus, for all n, the pressure (15) depends solely on the strength of the *symmetric* disturbance to the flow field. Indeed, that pressure (15) can be regarded as a suitable *measure* of the strength of this symmetric component. The corresponding strength of the antisymmetric component can be written

$$\{K_1 \exp[i(\tfrac{1}{2}\pi - \alpha_1)]\} p_0. \tag{17}$$

The extra phase term $\frac{1}{2}\pi$ reflects the fact that the antisymmetric component responds to horizontal (forward) motions in the incident-wave field, which have a phase lead of $\frac{1}{2}\pi$ over those vertical (downward) motions to which the symmetric component (15)' corresponds. The correction α_1 (positive, like α, and rather small for all the cases here calculated) represents a small phase lag in response to those horizontal motions.

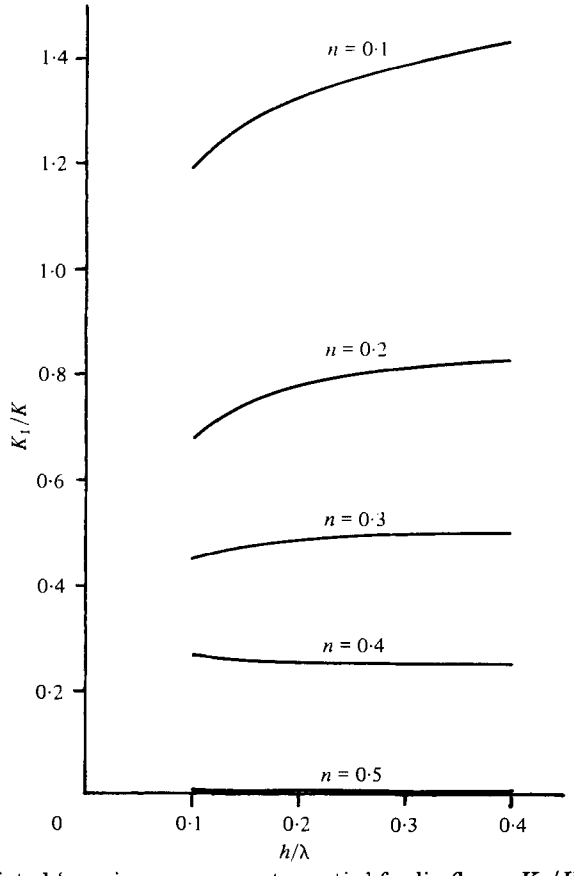

FIGURE 9. The predicted 'maximum asymmetry ratio' for lip flows, K_1/K, plotted as a function of the depth–wavelength ratio h/λ for different values of the ratio n of duct width to wavelength.

The relative importance of the antisymmetric and symmetric components is indicated by the ratio

$$K_1/K \tag{18}$$

of their amplitudes. Actually, we can show that this 'asymmetry ratio' (18) compares the antisymmetric and symmetric components in terms of the strengths of the *lip flows* (figure 9). Here we use the idea, well established in aerofoil theory, that a calculated irrotational-flow pressure distribution near a sharp edge gives a good measure of the true flow strength around a practical rounded edge; together with the fact that the ratio (18) is the calculated value of the limiting ratio of amplitudes of antisymmetric and symmetric motions as the lip is approached.†

Figure 9 shows that this asymmetry ratio is slightly greater than 1 for $n = 0{\cdot}1$ but quickly becomes much smaller as n increases; finally, for $n = 0{\cdot}5$, the motions become perfectly symmetrical. Actually, the corresponding studies when the duct is working show that the antisymmetric lip-flow strength is then unchanged, but the symmetric lip-flow strength is increased, so that the quantity plotted in figure 9 can be described as a *maximum* asymmetry ratio.

† Note, however, that the phase difference between the antisymmetric and symmetric motions is $\frac{1}{2}\pi + \alpha - \alpha_1$, implying by figure 10 that the moments in the cycle when the symmetric and antisymmetric motions attain their maxima are about 90° out of phase.

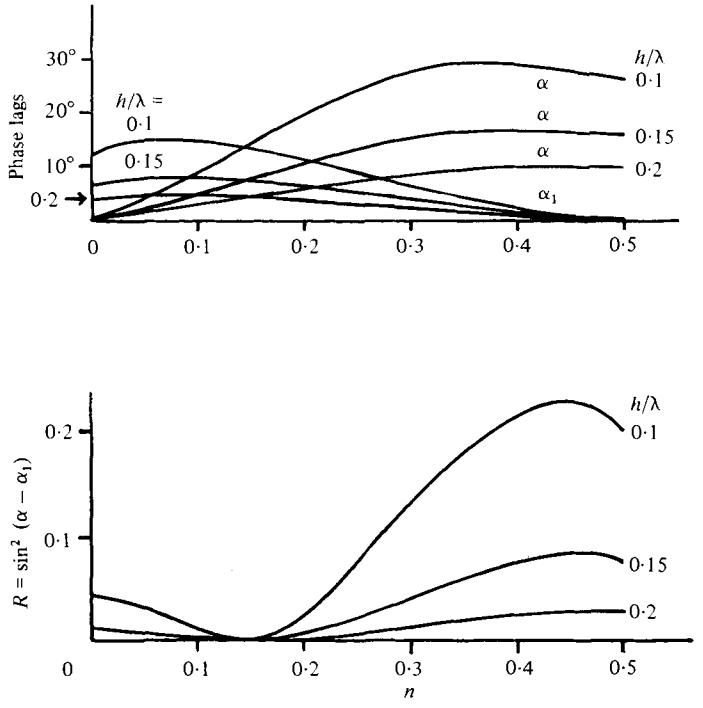

FIGURE 10. The phase lags α and α_1 in the symmetrical and antisymmetrical components of duct response in the mouth-upwards case, plotted as functions of the width–wavelength ratio n for different values of the depth–wavelength ratio h/λ. Lower graph: deduced values of the ratio R of reflected energy to incident energy in circumstances when there is no flow in the duct.

Figure 10 plots both the phase lags which have been referred to: the lag α for the duct pressures p_D associated with the symmetric motion, and the lag α_1 for the antisymmetric motions. Both remain quite small, and for $h/\lambda \geqslant 0{\cdot}3$ become insignificant.

One more quantity of interest can be obtained from the model for the case of zero flow in the duct, though values of this quantity have previously been computed by Jarvis (1971). Our results agree with his; and, also, with the following general form for the proportion R of incident wave energy which is reflected; a form known to apply to wave reflexion by any two-dimensional system with one symmetric and one antisymmetric degree of freedom (Newman 1975). This is the formula

$$R = \sin^2(\alpha - \alpha_1), \tag{19}$$

which when applied to the values of α and α_1 calculated in terms of confluent hypergeometric functions in §2.2 gives results (figure 10) that are in numerical agreement with those computed differently by Jarvis.

Figure 10 shows that, for the values of n and h/λ of interest here, the two-dimensional submerged duct without flow reflects rather little energy: less than 23%, 9% or 3% for $h/\lambda = 0{\cdot}1$, $0{\cdot}15$ or $0{\cdot}2$ respectively. Furthermore, where the curves for the phase lags α and α_1 cross over (that is, where n is about $0{\cdot}14$), the proportion R of reflected energy actually falls to zero.

This result, found also previously by Jarvis (1971), has, in addition, been checked experimentally (Knott & Flower 1979) for $h/\lambda = 0{\cdot}15$ and $0{\cdot}2$. Figure 11 compares the

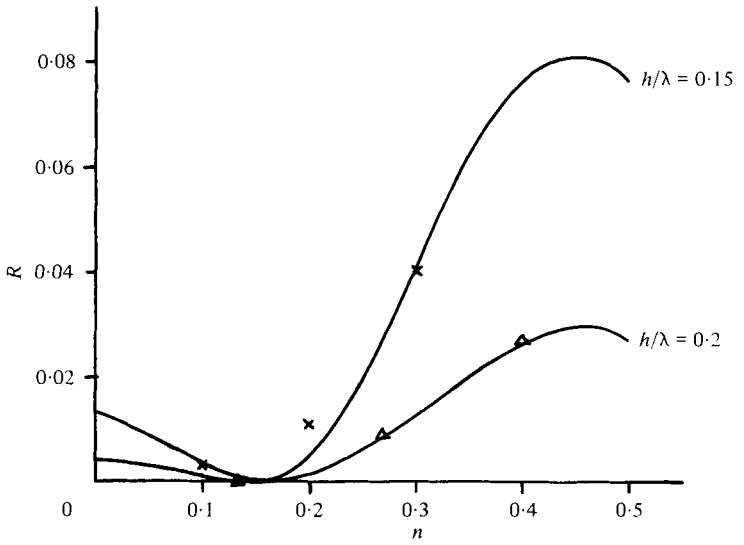

FIGURE 11. Comparison of the theoretically predicted reflexion coefficient R, in circumstances when there is no flow in the duct, with experimental data (Knott & Flower 1979) as follows: $\triangle$, $h/\lambda = 0{\cdot}2$; $\times$, $h/\lambda = 0{\cdot}15$.

experimental points with expanded versions of those two theoretical curves from figure 10. Once more, excellent agreement is found. The generally encouraging results from applying the theory when 'the duct is not working' spur us on to study the theory also in the case when the duct responds to the forcing pressures with a non-zero fluctuating flow.

We prepare for that with a brief reminder of how the excess pressure p_e (excess over the hydrostatic value) is distributed in a duct incorporating a fluctuating volume flow. We take this volume flow, directed into the duct from the mouth, as given by the complex exponential

$$Q_a e^{i\omega t} \tag{20}$$

with amplitude Q_a. We give the results in a form which is valid also in a three-dimensional duct, for which (20) has dimensions $\mathrm{m^3\ s^{-1}}$. When used with two-dimensional models, however, (20) will be the volume flow per unit breadth (called the volume *flux* in the detailed theory of §2.2), with dimensions $\mathrm{m^2\ s^{-1}}$.

We develop the analysis for a duct whose cross-sectional area $A(s)$ (or, for two-dimensional models, area per unit breadth) may exhibit a gradual variation with distance s measured along the centre-line from the mouth (figure 12). One reason for allowing such variation will be found to be its value in resonant-duct design for ensuring that a duct resonates at a frequency corresponding to the peak swell-energy-flux frequency at its destined location.

First, we give results according to a linear theory with every source of internal damping (whether due to energy extraction or to friction) neglected. The volume flow (20) implies a mean velocity

$$Q_a[A(s)]^{-1} e^{i\omega t} \tag{21}$$

at the cross-section $A(s)$, and therefore, on linear theory, an *acceleration*

$$i\omega Q_a[A(s)]^{-1} e^{i\omega t}. \tag{22}$$

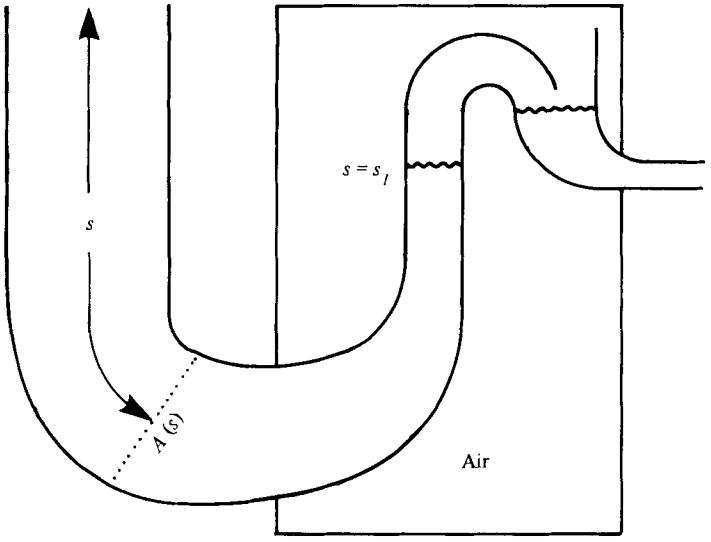

FIGURE 12. Schematic diagram of a resonant duct with tapered cross-section.

Then the gradient $(-\partial p_e/\partial s)$ of excess pressure along the duct equals the density ρ times this fluid acceleration, giving

$$p_e = \left\{\text{constant} - \rho i\omega Q_a \int_0^s [A(s)]^{-1}\, ds\right\} e^{i\omega t}. \tag{23}$$

We find that the results of hydrodynamic analysis of the interaction of incident swell with duct motions can be set out most clearly by expressing the constant in (23) as a sum of three separate terms, as follows:

$$p_e = Ke^{-i\alpha}p_0 - \rho\omega Q_a \left(D_r + i\left\{[A(0)]^{-1} l + \int_0^s [A(s)]^{-1}\, ds\right\}\right) e^{i\omega t}. \tag{24}$$

Here, the first term is the response already calculated in the case $Q_a = 0$, and the other two terms are 'open-end' corrections. Thus l is the *effective added length* of duct, due to 'added mass' of water outside its mouth $s = 0$. Also, we assign to D_r (which is found to be necessarily positive) the name *radiation damping coefficient.*

Note that, although internal damping has been neglected, a well-defined external damping is provided by such a positive coefficient D_r in (24) generating suctions $(-p_e)$ at the mouth in phase with the volume flow. These extract energy from the duct motions at a rate

$$\tfrac{1}{2}\rho\omega D_r |Q_a|^2. \tag{25}$$

In an irrotational-flow theory, the only possible mechanism for external loss of energy, of course, is by the fluctuating flow in the duct generating new surface waves; and we verify in §2.2 that the fluctuating flow by itself does indeed radiate surface waves with energy flux (25).

Inspection of (24) shows that we have defined the radiation damping coefficient D_r so that, although for three-dimensional systems it has the dimensions m^{-1}, nevertheless for two-dimensional systems (with Q_a and $A(s)$ as volume flow and cross-sectional area per unit breadth) D_r is dimensionless. Calculation of its value for

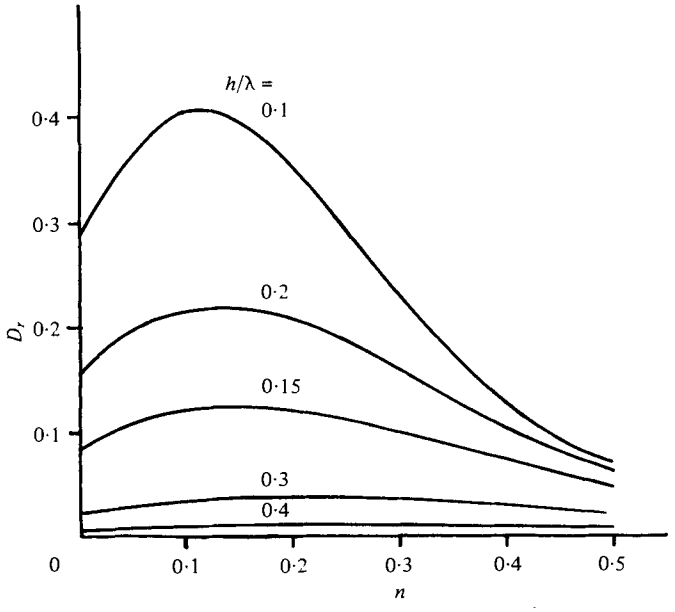

FIGURE 13. Radiation damping coefficient D_r for mouth-upwards duct, calculated on two-dimensional theory as a function of the width–wavelength ratio n for different values of the depth–wavelength ratio h/λ. This coefficient D_r is defined so that the energy radiated in new surface waves takes the form (25) per unit breadth, when the duct volume flow per unit breadth oscillates with amplitude Q_a.

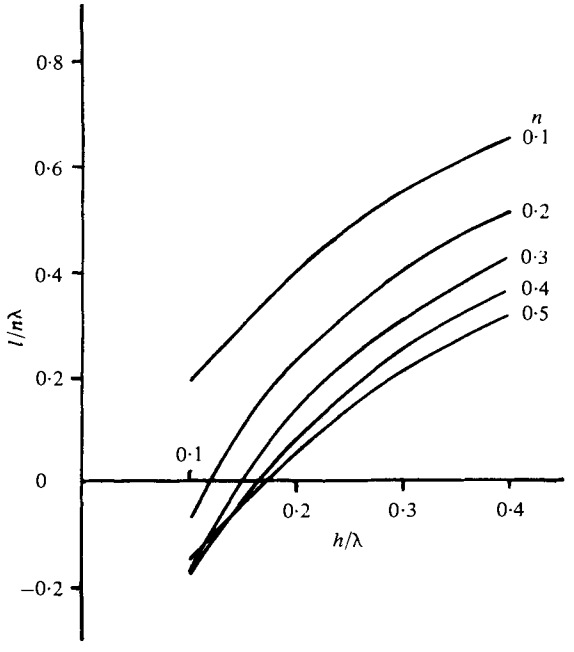

FIGURE 14. Added-mass curves in the mouth-upwards case, giving the ratio $l/n\lambda$ of the effective added length of duct to the width $n\lambda$ of the duct mouth, as a function of the ratio h/λ of mouth depth to wavelength.

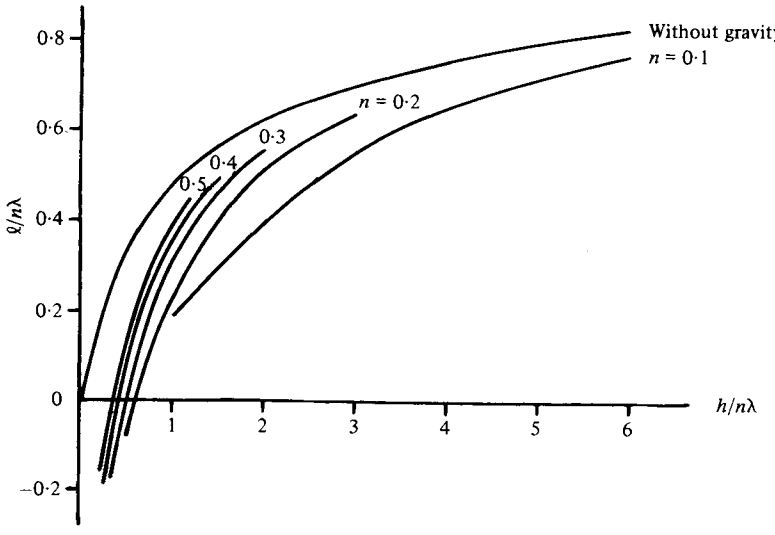

FIGURE 15. The data of figure 14 re-plotted as a function of the aspect-ratio $h/n\lambda$, and compared with the added-mass curve for a simplified problem with gravity neglected.

two-dimensional systems (§2.2) shows, in fact, that D_r is related to the forcing-pressure modification factor K plotted in figures 6, 7 and 8 by the simple equation

$$D_r = (Ke^{-2\pi h/\lambda})^2. \tag{26}$$

Equation (26) is a special case of the general reciprocal theorem which fixes the relation between the response of a symmetrical two-dimensional system to incident waves and the generation of waves by symmetrical oscillations of that system (Newman 1975; Evans 1976). Values of D_r calculated from (26) are plotted in figure 13; see later for a detailed study of their implications.

In certain well-known (for example, acoustical) cases, open-end corrections are found to involve, not only such radiation damping, but also a substantial added-mass component. By contrast, in the present problem, the effective added length of duct l turns out to be negligibly small for the most interesting values of the parameters. Thus, figure 14 shows that with h/λ between 0·1 and 0·2, and n between 0·2 and 0·5, the ratio $l/n\lambda$ of added length to duct width lies between $-0{\cdot}2$ and $+0{\cdot}2$.

By studying the mathematical theory leading to this conclusion we can discern one important reason underlying it: above all, the *proximity of the free surface* (at which the duct mouth is pointing) restricts the added length. Already from the solution of a rather elementary added-mass problem (figure 15) we can partially understand this. It is the problem with gravity neglected, when the free surface, as a surface of zero excess pressure, acts already to limit the possible build-up of negative excess pressure in the duct in phase with downward acceleration. In this problem the added mass is half of that associated, in unbounded fluid, with a certain anti-symmetrical problem: one in which the duct operates together with its mirror-image in the free surface (whose inflow acts in antiphase). The ratio $l/n\lambda$ is then a simple function (figure 15) of the aspect-ratio $h/n\lambda$ alone, which falls to zero as that aspect-ratio becomes small (allowing the flow to shoot back and forth between the duct and its image).

The fully interactive theory shows that when gravity is taken into account the added mass is necessarily *reduced* below the above-mentioned simple value with gravity neglected; presumably, because gravity restricts the motions of the free surface. Figure 15 shows how this reduction brings down the value of $l/n\lambda$ in cases of particular interest to the numerically low levels mentioned earlier.

Now, we can turn to the dynamics of motion in the duct; again, with all internal damping neglected. This requires (figure 12) that we relate the excess pressure (24) at the internal air–water interface $s = s_I$ to the motions of that interface. These have velocity (21) and therefore displacement

$$Q_a[i\omega A(s_I)]^{-1}\, e^{i\omega t}. \tag{27}$$

If the air at the interface were at constant absolute pressure p, then the excess pressure $p_e = p + \rho g y$ (excess over hydrostatic) would exhibit fluctuations equal to ρg times the fluctuating displacement (27) of the interface. We take, however,

$$p_e = \rho g_+ Q_a[i\omega A(s_I)]^{-1}\, e^{i\omega t} \quad \text{at} \quad s = s_I, \tag{28}$$

where g_+ is equal to the gravitational acceleration g plus a 'pneumatic-stiffness' correction due to any fluctuations in the pressure p of the air itself.

Actually, we can express the correction $g_+ - g$ in terms of the *capacitance* C of the air cavity. Here, C is the product of the air's volume (or, in two-dimensional models, volume per unit breadth) and its compressibility; thus, C specifies the air's volume *reduction* per unit increase of pressure. The displacement (27) produces an increase

$$C^{-1}Q_a(i\omega)^{-1}\, e^{i\omega t} \tag{29}$$

in air pressure (C^{-1} times the associated volume reduction). Therefore, the excess pressure $p_e = p + \rho g y$ exhibits the fluctuation (28) with

$$g_+ = g + (\rho C)^{-1} A(s_I). \tag{30}$$

In practical designs the pneumatic-stiffness correction $g_+ - g$ is expected to represent only a small proportional addition to the gravitational acceleration g.

Equating (28) to the value of (24) for $s = s_I$ gives

$$Ke^{-i\alpha}p_0 = \rho\omega Q_a\left(D_r + i\left\{[A(0)]^{-1}l + \int_0^{s_I}[A(s)]^{-1}\,ds - g_+\omega^{-2}[A(s_I)]^{-1}\right\}\right). \tag{31}$$

Here, in the large parentheses, we have a fixed real part D_r (the radiation damping) and an imaginary part which varies with the duct's internal geometry. Therefore, the amplitude $|Q_a|$ of volume-flow fluctuations is a maximum when the length s_I of the water column and the variation in duct cross-section $A(s)$ for $0 < s < s_I$ satisfy the resonance condition, specified by equating to zero that imaginary part (the contents of the braces). At resonance, then,

$$g_+\omega^{-2} = [A(s_I)]\left\{\int_0^{s_I}[A(s)]^{-1}\,ds + [A(0)]^{-1}l\right\}. \tag{32}$$

Equation (32) is potentially useful for design purposes because it suggests how a duct of given overall length s_I can be tuned to respond maximally to a desired

frequency as suggested by the swell-energy-flux spectrum at its destined location. Actually, we have seen that the added-mass correction l and the pneumatic-stiffness correction $g_+ - g$ are small, and we can explain the design approach most clearly if we temporarily neglect them. Then, (32) shows that a duct of *uniform* cross-section $A(s)$ would be limited to a water-column length $s_I = g\omega^{-2}$, giving for example $s_I = 20$ m for a 9 s wave period $2\pi\omega^{-1}$. In practice, any strict limitation to a particular value of the water-column length to achieve resonance at a particular wave period (such as 9 s) might conflict inconveniently with other design requirements. Use of a non-uniform cross-section, however, could avoid such conflict.

Thus, (32) also shows that increasing the duct length would not necessarily violate resonance provided that the duct were given sufficient *taper*. Then, $A(s)$ would be made a gradually decreasing function of s so that (if we again neglected l and $g_+ - g$) the quantity

$$A(s_I)\int_0^{s_I}[A(s)]^{-1}\,ds \tag{33}$$

would take the desired value $g\omega^{-2}$. Physically, we would be compensating for excess 'hydraulic inertia' in an over-long duct by using taper to provide extra 'hydraulic stiffness'; that is, extra gravitational restoring pressures associated with given volume displacements at the internal air–water interface.

Under the condition of resonance, (31) becomes

$$Ke^{-i\alpha}p_0 = \rho\omega Q_a D_r, \tag{34}$$

so that the volume flow (20) is in phase with the forcing pressures (15). Then the rate (25) of energy radiation by the duct motions is exactly equal to the rate of energy input by the forcing pressures. Thus, as with resonant systems in general, the resonant response Q_a adjusts its phase so that it can gain maximum energy from the forcing effect, and its amplitude so that energy gain and energy loss are in balance.

When internal damping (whether by frictional effects or by energy extraction, or both) is taken into account, we can again assume that the resonant response satisfies the same energy balance condition. Here, we express that condition formally as if both frictional damping and energy extraction were governed by linear damping coefficients, with the energy loss rate for volume flow $Q_a e^{i\omega t}$ given by

$$\tfrac{1}{2}\rho\omega D_f|Q_a|^2, \quad \tfrac{1}{2}\rho\omega D_1|Q_a|^2 \tag{35}$$

respectively, in addition to the loss (25) by radiation damping. Then the energy input (rate of working by forcing pressures (15) in phase with volume flow) balances the sum of the energy loss rates (25) and (35):

$$\tfrac{1}{2}K|p_0|\,|Q_a| = \tfrac{1}{2}\rho\omega(D_r + D_f + D_1)\,|Q_a|^2, \tag{36}$$

giving

$$|Q_a| = \frac{K|p_0|}{\rho\omega(D_r + D_f + D_1)}; \tag{37}$$

while the energy extraction rate $\frac{1}{2}\rho\omega D_1|Q_a|^2$ becomes

$$\tfrac{1}{2}D_1\frac{K^2|p_0|^2}{\rho\omega(D_r + D_f + D_1)^2}. \tag{38}$$

As in §1.1, we find under these assumptions of linear damping that the energy

extraction is greatest when the wanted and unwanted energy loss rates are equal; that is, when

$$D_1 = D_r + D_f. \tag{39}$$

The maximum energy extraction rate, achieved under this condition, is

$$\frac{K^2|p_0|^2}{8\rho\omega(D_r+D_f)}. \tag{40}$$

We can compare this with the rate of energy flux in the incident waves (13), equal to their wave energy density $\frac{1}{2}\rho g a^2$ per unit horizontal area times their energy propagation velocity $\frac{1}{2}g\omega^{-1}$ (that is, their group velocity, which is half their phase speed). Dividing the power extracted (40), with expression (14) for p_0, by this incident power $\frac{1}{4}\rho g^2 a^2 \omega^{-1}$, we obtain

$$\frac{\text{power extracted}}{\text{incident power}} = \frac{(Ke^{-2\pi h/\lambda})^2}{2(D_r+D_f)} = \frac{D_r}{2(D_r+D_f)}. \tag{41}$$

Here, we have used expression (26) for D_r.

When the frictional damping D_f is neglected, (41) agrees with a general law for two-dimensional wave-energy extraction devices with fore-and-aft symmetry, analysed on frictionless linear theory (Evans 1976): the maximum energy extraction rate is half the incident wave-energy flux (see also § 2.2 for yet another derivation of this result). Evans's law follows from the general reciprocal theorem which (in its application to the present problem) gives (26), making the radiation damping coefficient D_r equal to the square of the duct response coefficient $Ke^{-2\pi h/\lambda}$. In the frictionless case, this means that the apparent advantage of increasing the forcing-pressure modification factor K is exactly counterbalanced by the resulting increase in D_r.

A different picture emerges, however, when we take into account additional effects, beginning with the frictional damping. Then (41) implies a further requirement for optimal energy extraction: the condition

$$D_r \gg D_f, \tag{42}$$

which requires the radiation damping to be so much larger than the frictional damping that the frictionless upper limit 0·5 of the ratio (41) is almost reached. The requirement (42) has two sides to it. One is the need to reduce D_f by every possible means, including especially the use of rounded lips, or a bell-mouth, to minimize frictional dissipation in jet eddies shed from sharp orifice lips (see below). After that has been done, however, satisfaction of condition (42) may still require that (26) is sufficiently large. This condition in turn, after h/λ has been made large enough to meet the requirements for seaworthiness, emphasizes the importance of K^2 being as big as possible.

It is at first sight paradoxical that, according to a two-dimensional model, energy extraction may be made more effective by having the radiation damping as big as possible. The reason, of course, lies in the necessary truth of the reciprocal relationship (26) between radiation damping and the square of the forcing-pressure amplitudes. Given only condition (42), that the radiation damping is made *large* compared with the frictional damping, then the reciprocal relationship allows the full frictionless optimum (one-half of the incident swell energy flux) to be extracted. (Under those circumstances, as shown in § 2.2, the other half is re-radiated equally in both directions.)

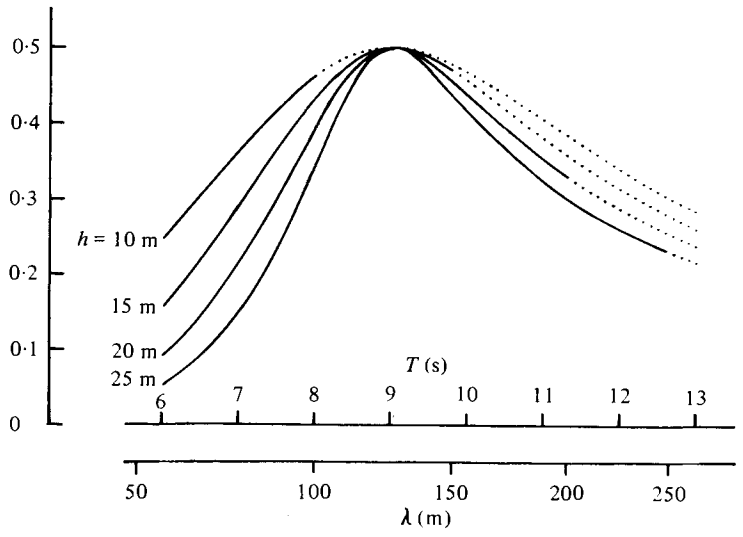

FIGURE 16. Specimen graphs, based on linear damping coefficients, giving the fraction of incident swell energy flux captured by a two-dimensional system with mouth width $n\lambda$ equal to the mouth depth h and with duct width tapering to 9 m at the internal interface. The period T takes the value 9 s at resonance. Parts of curves corresponding to wavelengths $\lambda > 10h$ are shown dotted.

The theory indicates also a second advantage in D_r being relatively large. Whatever be the frequency of the peak in the swell-energy-flux spectrum, there is a substantial band of frequencies around it within which the average swell energy flux takes values within (say) 50 % of the peak. An effective device for wave-energy absorption must have a sufficiently broad-band response to be able to absorb a significant fraction of the energy at those frequencies also. This, in turn, calls for a large enough value for the total damping, which under conditions (39) and (42) is essentially $2D_r$.

A specimen calculation, leading to a very rough numerical idea of this requirement as indicated by two-dimensional linear theory, may be given by taking the resonant period once more as 9 s and taking $A(s_I)$ in (31) as 9 m, with g_+ as 11 ms^{-2}. Then, as the wave period in seconds, $T = 2\pi\omega^{-1}$, varies, the expression in braces in (31), with $-0{\cdot}031T^2$ as its last term, must be equal to

$$0{\cdot}031(T_R^2 - T^2), \tag{43}$$

since it vanishes when T takes its resonant value $T_R = 9$. Adding this imaginary part to a total real damping coefficient now increased to $2D_r$ is found to reduce the proportion of swell energy flux extracted from $\frac{1}{2}$ to

$$D_r/\{(2D_r)^2 + [0{\cdot}031(T_R^2 - T^2)]^2\}^{\frac{1}{2}}. \tag{44}$$

Here, the term in square brackets varies by ± 1 as T, the wave period in seconds, varies between 7 and 10·6. At the ends of that frequency band, then, the proportion of swell energy flux extracted will fall only from $\frac{1}{2}$ to $\frac{1}{4}$ provided that D_r is around 0·3. This suggests that a submerged resonant duct may need to operate at values of the radiation damping coefficient around 0·3 if it is to be sensitive to a broad enough spectrum of swell energy flux. Figure 13 shows how this tends to fix h/λ between 0·1 and 0·15 and n between 0 and 0·25.

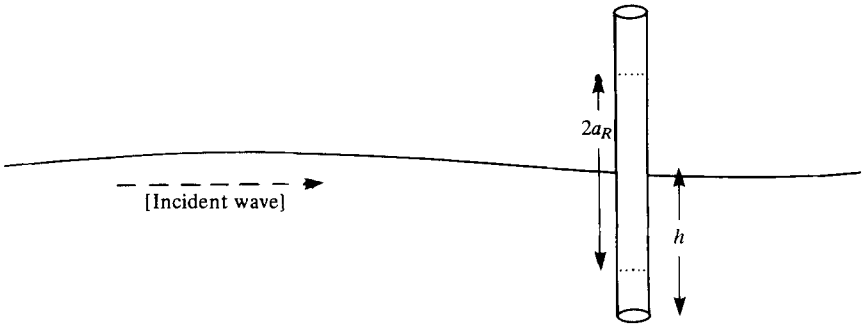

FIGURE 17. A simple 'mouth-downwards' experiment to test resonant-duct principles.

For a particular duct, however, we cannot regard D_r as fixed since λ varies as a function of wave period. Figure 16 takes this into account by showing how the proportion (44) of swell energy flux extracted varies with T for a duct with aspect-ratio $h/n\lambda = 1$ at various values of the depth h (equal in this case to the mouth width $n\lambda$). Parts of the curves for which $h < 0{\cdot}1\lambda$, with the duct mouth perhaps undesirably near the surface for waves of the wavelength concerned, are shown dotted.

Although the assumptions underlying figure 16 are somewhat arbitrary, so that the absolute values have no significance, the figure does give a broad feel for the problems involved in the choice of the mouth depth h. Placing the mouth too deep could make the resonance curves too narrow, while placing it too near the surface could make it dangerously sensitive to the longer waves. These considerations may suggest some kind of compromise in the general neighbourhood of $h = 20$ m.

One extensive series of experiments to test resonant-duct principles has been conducted with an extremely simple, but inverted, system. This makes use of a *mouth-downwards* configuration. An open vertical tube (figure 17) with its lower end, the 'mouth', inserted to a certain depth h in a travelling sinusoidal wave, resonates for a particular value of h, producing very large peak amplitudes of oscillation a_R of the water level in the tube (greatly exceeding the corresponding amplitude a in the wave). It is easy to measure how the amplitude at resonance varies with wavelength, wave amplitude, duct width, etc. At a more sophisticated level of experimentation, the upper end of the tube in figure 17 can be placed in a chamber at reduced air pressure (which raises the undisturbed level in the tube), in order to test the behaviour of an overtopping system. To obtain theoretical insight into both types of experiment, a mouth-downwards analysis directly comparable to the mouth-upwards analysis described above has been made.

The whole mouth-downwards analysis turns out to be surprisingly similar to that in the mouth-upwards case. Indeed, in the simple version described earlier as a 'local' model and found to be a good approximation for large aspect-ratio $h/n\lambda$, the only change needed is a substitution of $(-n)$ for n (§2.1). The forcing-pressure modification factor K then takes the values shown in table 2; essentially, the values of the function in table 1 with n replaced by $-n$.

This time, K is seen to be a true 'reduction factor'. We can understand this in terms of the quite different geometries characterizing the two cases. The mouth-downwards duct itself excludes the entire region of substantial pressure fluctuations that would otherwise be present above its mouth; therefore, it must respond primarily

n	0	0·1	0·2	0·3	0·4	0·5	0·6	0·7	0·8	0·9	1·0
K	1	0·755	0·646	0·575	0·524	0·484	0·452	0·426	0·404	0·384	0·368

TABLE 2

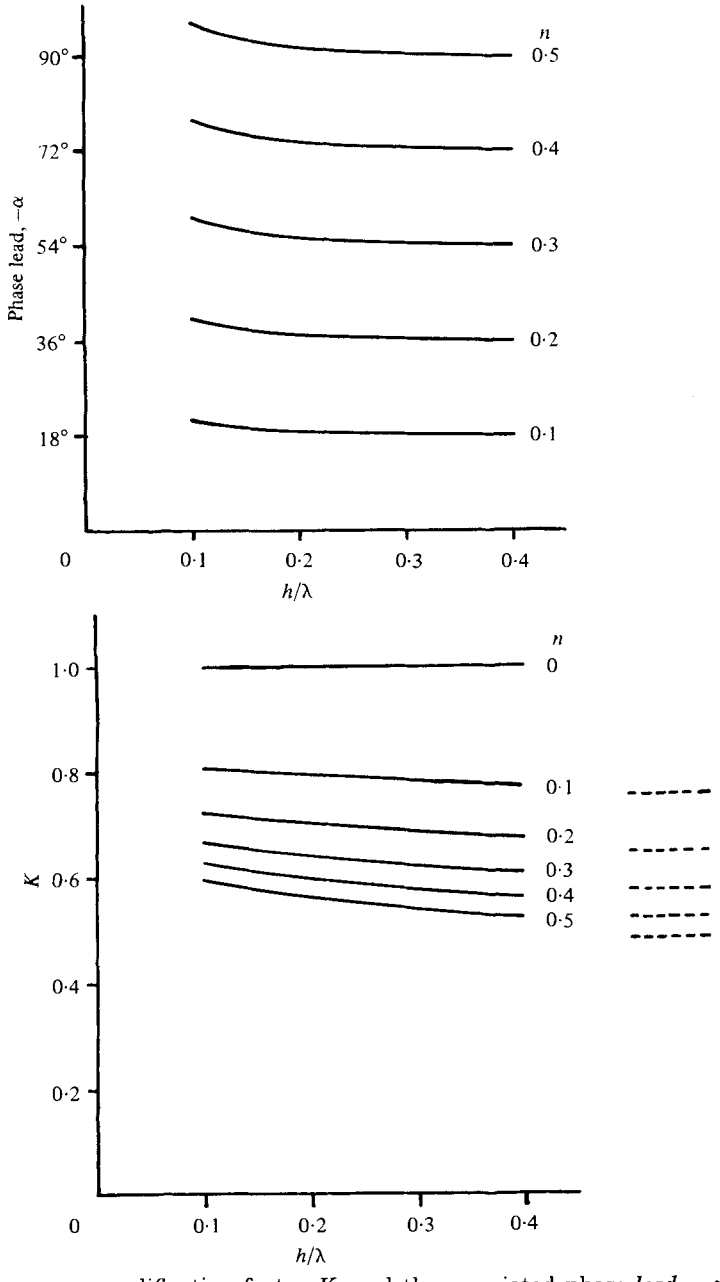

FIGURE 18. The pressure modification factor K, and the associated phase *lead* $-\alpha$, plotted in the mouth-downwards case against the ratio h/λ of the mouth depth to wavelength for different values of the width–wavelength ratio. Broken lines: asymptotic values given (table 2) by the 'local' model.

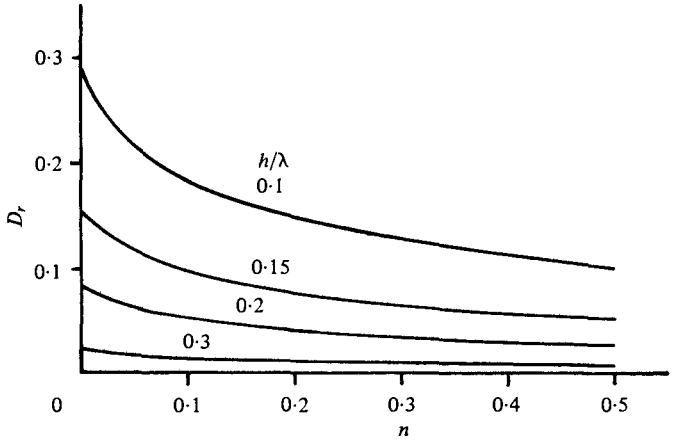

FIGURE 19. Radiation damping coefficient D_r for a mouth-downwards duct, calculated on two-dimensional theory as a function of the width–wavelength ratio n for different values of the ratio h/λ of mouth depth to wavelength (compare figure 13 in the mouth-upwards case).

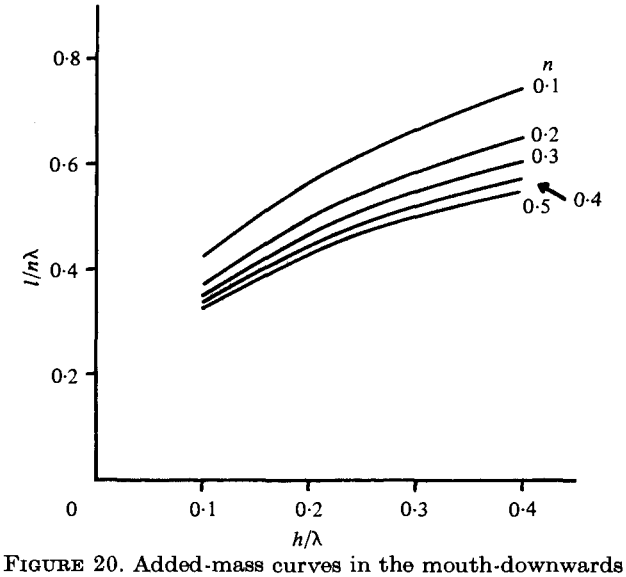

FIGURE 20. Added-mass curves in the mouth-downwards case (compare figure 14 in the mouth-upwards case).

to pressures immediately *outside* the duct. The local model supports this view by predicting that the forcing pressures in the duct are in phase with those which would be found at the position of the *lip nearest the incident waves* if the duct were absent. Thus the quantity α, defined in (15) as the phase lag of the forcing pressure behind the pressure which would be found at the position of the duct *centre* if the duct were absent, takes the negative value $(-n\pi)$ corresponding to a phase lead (the waves would reach the nearest lip before reaching the centre). In addition, the tendency noted earlier for a duct to respond to pressures 'beyond' (here, below) its mouth contributes to making $K < 1$.

In the mouth-downwards case, the fully interactive model (§2.2) gives results even closer to those of the local model than in the mouth-upwards case. Figure 18

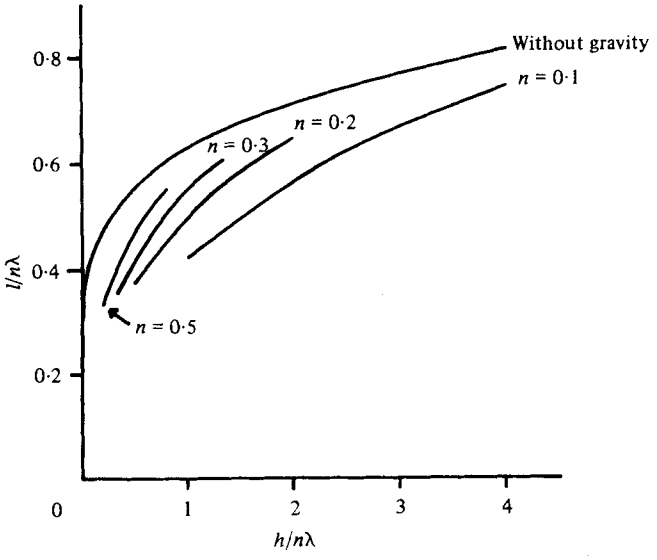

FIGURE 21. The ratio $l/n\lambda$, of effective added length of duct to mouth width, plotted in the mouth-downwards case as a function of the aspect-ratio $h/n\lambda$ (ratio of mouth depth to duct width), and compared with the added-mass curve for a simplified problem with gravity neglected.

shows the values of K as a function of h/λ for $n = 0{\cdot}1$, $0{\cdot}2$, $0{\cdot}3$, $0{\cdot}4$ and $0{\cdot}5$, together with the asymptotic values given by table 2. It shows also the phase lead $(-\alpha)$ tending still more rapidly to the asymptotic values $n\pi$ (marked, this time, on the vertical scale). Broadly speaking, the local theory gives sufficient accuracy now when the aspect-ratio $h/n\lambda$ exceeds 1 (instead of 2 for the mouth-upwards theory).

The low values of the forcing-pressure modification factor K in figure 18 produce a still greater reduction in the radiation damping coefficient D_r, given as before by (26). Figure 19 plots D_r as a function of n for $h/\lambda = 0{\cdot}1$, $0{\cdot}15$, $0{\cdot}2$ and $0{\cdot}3$, and these values can be compared with the much larger values in figure 13 for the mouth-upwards case. We earlier noted reasons why relatively large values of D_r may be needed in practical applications of resonant ducts: optimal energy capture may require D_r to be large compared with the corresponding frictional damping coefficient D_f; while substantial values of D_r (around $0{\cdot}3$) may be required for a broad enough resonance curve. Figure 19 hardly encourages, therefore, any attempt to devise practical systems based on a mouth-downwards configuration.

Yet another difference between the two configurations lies in the magnitudes of the *added mass*. Figure 20 shows the effective additional length of tube l (see (24) above) as a fraction $l/n\lambda$ of the duct width. The values predicted are significantly higher than in the mouth-upwards case (figure 14), especially for the most interesting values of $h/\lambda \leqslant 0{\cdot}2$.

We can understand this new feature by studying the corresponding elementary added-mass problem with gravity neglected. Then the value of $l/n\lambda$ is just a function of the aspect-ratio $h/n\lambda$ as in figure 15 but its values are already much higher (figure 21) than in the corresponding mouth-upwards problem. Physically, this is because the duct is now pointing *away* from the free surface. This change essentially explains the difference between the two configurations, since figures 15 and 21 show the reductions due to gravity to be comparable. Although our mouth-downwards model,

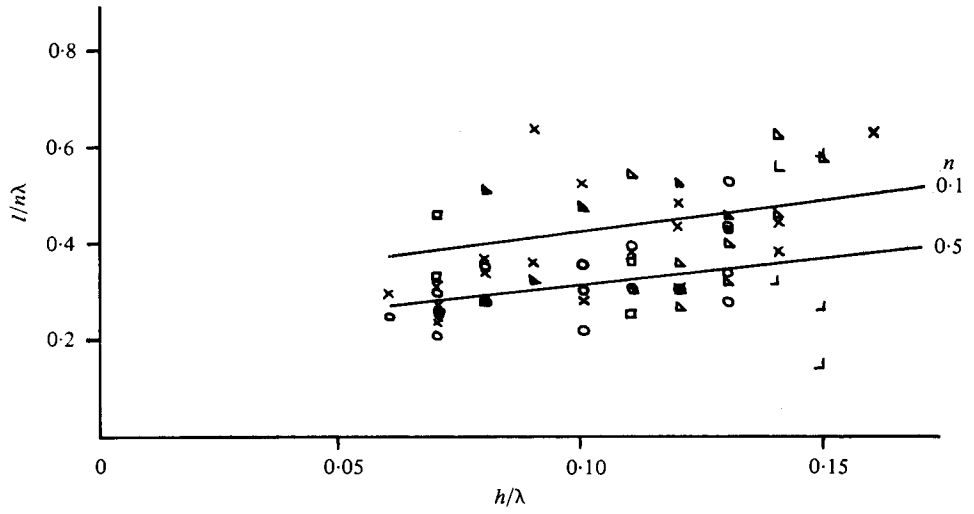

FIGURE 22. Experimentally determined ratios $l/n\lambda$ of effective added length of duct to mouth width, determined (Carey, unpublished) for the simple mouth-downwards experiment of figure 17. Curves: theory of figure 10. Points: □, $a/\lambda = 0{\cdot}0250$; ◣, $a/\lambda = 0{\cdot}0139$; ×, $a/\lambda = 0{\cdot}0111$; ∟, $a/\lambda = 0{\cdot}0104$; ○, $a/\lambda = 0{\cdot}0045$; ◺, $a/\lambda = 0{\cdot}0042$; ⌟, $a/\lambda = 0{\cdot}0023$.

like all models in this paper, is two-dimensional, such broad quantitative comparisons which it suggests are probably applicable also to three-dimensional ducts, where we can similarly expect pressure modification factors K considerably less than 1, together with substantial added-mass effects.

Confirmation of this last conclusion comes from the simple experiment illustrated in figure 17. The condition (32) for resonance, with $g_+ = g$ and with the tube area $A(s)$ constant, becomes

$$g\omega^{-2} = s_I + l = h + l, \tag{45}$$

since in the experiment of figure 17 the distance s_I from the duct mouth to the internal air–water interface is equal to the mouth depth h. Therefore, by observing the depth h at which resonance to waves of frequency ω occurs, we can determine the added length from (45) as

$$l = g\omega^{-2} - h = (\lambda/2\pi) - h. \tag{46}$$

Values of the ratio $l/n\lambda$ so determined for different values of h/λ less than $\frac{1}{2}\pi = 0{\cdot}159$ were found (figure 22) to be mainly clustered in the region 0·3–0·5, as predicted by two-dimensional theory (figure 20) in that range of h/λ.

From such experiments it is possible also to infer information about damping, by measuring the amplitude a_R by which the level in the tube varies about its undisturbed position under resonant conditions. The two-dimensional model predicts the value of a_R from (37), in which the volume-flow amplitude

$$|Q_a| = Un\lambda, \quad \text{where} \quad U = \omega a_R \tag{47}$$

is the velocity amplitude. With zero energy-extraction coefficient D_1 and with p_0 as in (14), (37) then gives

$$\rho\omega(D_r + D_f)(\omega a_R)(n\lambda) = K\rho g a e^{-2\pi h/\lambda}, \tag{48}$$

which with $\omega^2\lambda = 2\pi g$ as in (11) implies that

$$2\pi n(D_r + D_f)\, a_R = (Ke^{-2\pi h/\lambda})\, a \simeq 0{\cdot}4a. \tag{49}$$

Here, even for a circular tube (figure 17), the forcing-pressure modification factor K might be expected to diverge relatively little from its value on two-dimensional theory. In that case, the product $Ke^{-2\pi h/\lambda}$ turns out to be close to 0·4 in the present experiments, because increasing n makes the value of l/λ increase, so that, by (46), h/λ *decreases*; actually, in such a way that the effects on $Ke^{-2\pi h/\lambda}$ practically cancel. On that assumption, measured values of the amplitude ratio a/a_R might be used in (49) to infer $D_r + D_f$.

Here D_r, while more likely than K to depart significantly from its two-dimensional value,† should nevertheless be independent of amplitude, while D_f should increase with amplitude. This suggests that their values could be separately found if the experiment were repeated for several values of the wave amplitude.

Specifically, we defined D_f in (35) so that frictional dissipation of energy occurs at an average rate

$$\tfrac{1}{2}\rho\omega D_f |Q_a|^2. \tag{50}$$

It is interesting to test the hypothesis that with a sharp-lipped tube the frictional dissipation occurs mainly in jet-like eddies shed from the lip in outflow and, possibly, also in an inflow phase involving lip separation. In a two-dimensional model this would make the average dissipation rate (50) proportional to the average flow of kinetic energy across the mouth; that is, to the average of

$$\tfrac{1}{2}\rho(U\cos\omega t)^2\, |U\cos\omega t|\, n\lambda \tag{51}$$

with the velocity amplitude U given by (47). Putting (50) equal to (51) multiplied by a coefficient $\theta \leqslant 1$, we get

$$\tfrac{1}{2}\rho\omega D_f (Un\lambda)^2 = \tfrac{1}{2}\rho U^3 n\lambda (4/3\pi)\,\theta, \tag{52}$$

where $4/3\pi$ is the average of $|\cos\omega t|^3$. Thus,

$$D_f(n\lambda) = a_R(4/3\pi)\,\theta, \tag{53}$$

confirming the dependence of D_f on amplitude.

We can conveniently test our hypothesis by plotting all measurements of a_R in the form of graphs of $\lambda a/a_R$ against a_R for fixed tube width $n\lambda$. The theoretical relations (49) and (53) would suggest that

$$\lambda a/a_R = 5\pi[D_r(n\lambda) + (4\theta/3\pi)\, a_R], \tag{54}$$

making such graphs for different tube widths $n\lambda$ into straight lines, all of the same slope $\frac{20}{3}\theta$ but with different intercepts $(5\pi D_r n\lambda)$ on the axis $a_R = 0$. Results of experiments shown in figure 23 do in fact strongly suggest a common slope for the graph of $\lambda a/a_R$ against a_R for each of five different tube widths $n\lambda = 61$, 45·5, 30, 19·5 and 9·3 cm. Just the three *ringed* points were so much out of line with nearby data that they were ignored. A least-squares fit to the remaining points by five lines of identical slope, shown on the diagram, gave a satisfactory interpretation of all those data, and determined this slope, equal to $\frac{20}{3}\theta$ according to the theory, as 6·0, making

$$\theta = 0{\cdot}9. \tag{55}$$

† Because its value is no longer tied to that of K by the reciprocal relationship (26).

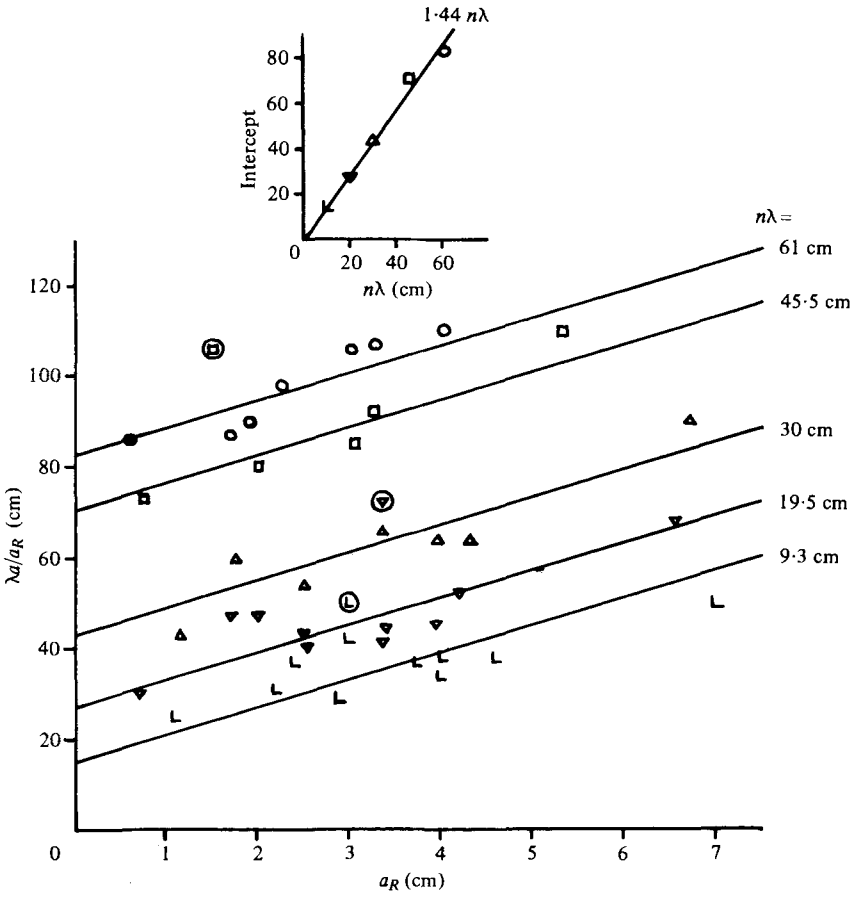

FIGURE 23. Experimentally determined values (Carey, unpublished) of $\lambda a/a_R$ for waves of amplitude a and length λ incident upon a mouth-downwards vertical cylinder as in figure 17, for different values $n\lambda$ of the cylinder's diameter: ○, $n\lambda$ = 61 cm; □, $n\lambda$ = 45·5 cm; △, $n\lambda$ = 30 cm; ▽, $n\lambda$ = 19·5 cm; ∟, $n\lambda$ = 9·3 cm. The three ringed points were so much out of line with nearby data that they were discarded. The straight lines represent a least-squares fit to the remaining points by lines of identical slope for each value of $n\lambda$. This slope is 6·0. The inset diagram plots the intercept of these lines on the vertical axis a_R = 0 as a function of the cylinder diameter $n\lambda$, showing that this intercept remains close to $1{\cdot}44n\lambda$. In summary, the data are well represented by an equation $\lambda a/a_R = 1{\cdot}44n\lambda + 6{\cdot}0a_R$.

This means that practically all of the kinetic-energy flow across the mouth (both outwards and inwards) is dissipated in jet eddies. The conclusions do also imply that boundary-layer dissipation was negligible compared with jet-eddy dissipation, since their *ratio* should be proportional to the aspect-ratio $h/n\lambda$, and the above slope was found insensitive to variation of $h/n\lambda$ by an order of magnitude.

The intercepts in figure 23 are close to a constant multiple $1{\cdot}44n\lambda$ (see inset) of the tube width $n\lambda$. From (54) this implies a radiation damping coefficient

$$D_r = 1{\cdot}44/5\pi = 0{\cdot}09. \tag{56}$$

This is just over half the value of radiation damping, $D_r = 0{\cdot}16$, which in a strictly two-dimensional system would follow by (26) from the value 0·4 which we have taken for $Ke^{-2\pi h/\lambda}$. There is, in fact, no need for the relationship (26) between the two coef-

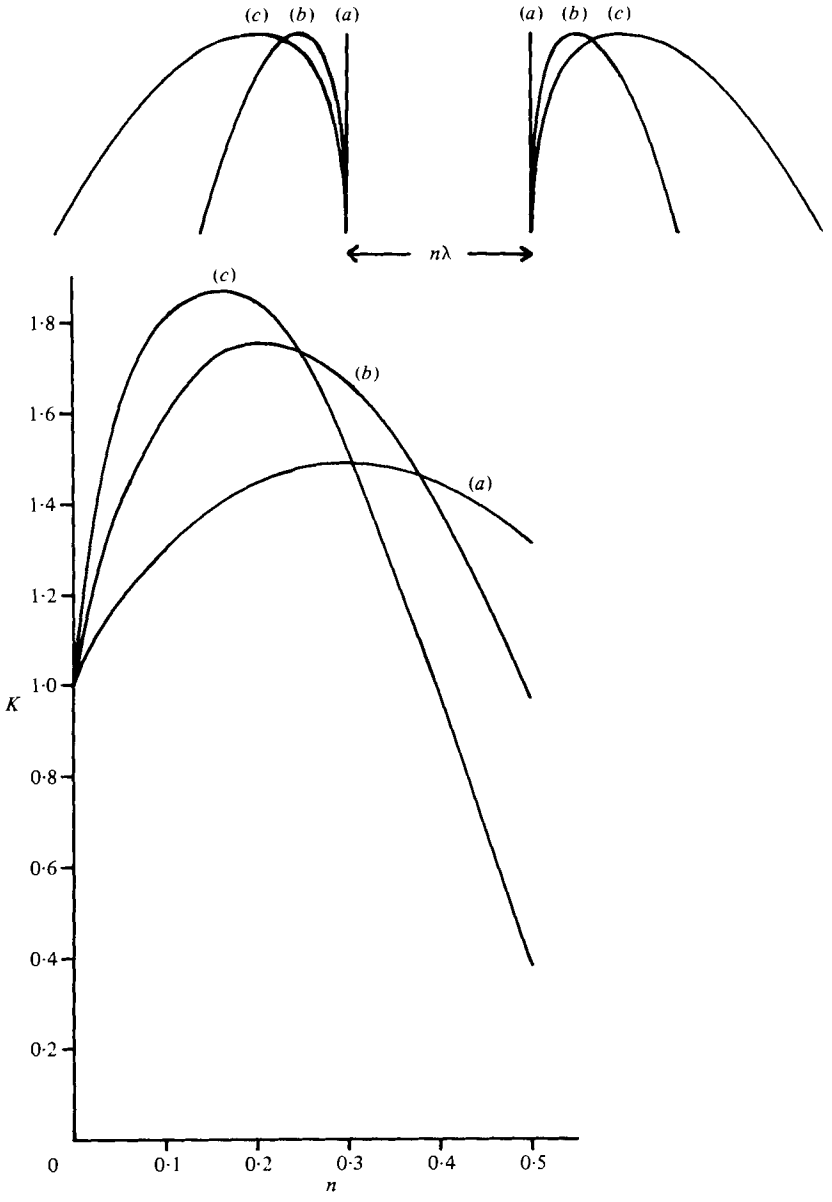

FIGURE 24. Two bell-mouth shapes (*b*) and (*c*), for which a two-dimensional 'local' theory gives a pressure-modification factor varying with K as shown (curves *b* and *c*). The corresponding sharp-lipped mouth, (*a*), has values of K given (on the same theory) in table 1, represented here by curve (*a*).

ficients to hold for an axisymmetric duct, even in a wave tank with vertical side walls. It is interesting, however, that an extensive body of data on that system for a wide range of values of n can be interpreted by use of a constant radiation damping coefficient, just over half that appropriate on two-dimensional theory.

One important, although not unexpected, conclusion from the set of experiments just described and their analysis, was that sharp lips are a potent source of energy dissipation associated with separation both of the outflow and of the inflow at the

lips. More recent experiments, to be reported in later papers, imply that D_f may be reduced by more than a factor of 10 through the use of suitably rounded lips. Then the dominance of frictional dissipation at the larger amplitudes disappears.

When a wide bell-mouth is used, these recent experiments have indicated that even the limiting value of the resonant amplitude a_R for zero frictional damping is augmented. This suggested an analysis of whether the forcing-pressure modification factor K might be increased by use of a bell-mouth. Fortunately, it proved possible to calculate this (§2.1), within the limitations of a 'local' model, with results shown in figure 24. For values of n around 0·2, a bell-mouth shape rather similar to that in the project sketch of figure 2 produces (on this admittedly crude theory) a considerable augmentation of K which may prove to be significant.

One more special configuration is studied by means of a local model in §2.1. This is a mouth-sideways duct with the mouth facing the swell. The conclusion from the analysis is simply that the forcing pressures to which such a duct is sensitive are those which (in the absence of the duct) would be found at a level between 20 and 25 % of the duct width *below* the duct's upper lip. Even so, it may still be too soon to rule out mouth-sideways configurations, because they could lead to economical simplifications of duct geometry.

Nevertheless, the broad tentative conclusions from analyses in this section tend to favour a configuration something like that in figure 2, with a bell-mouth, at a mouth depth of around 20 m. The duct width might also be around 20 m (to utilize the high values of K for values of n from 0·1 to 0·2); but taper (that is, duct cross-sectional area $A(s)$ reducing as the distance s from the mouth increases) should be used to help fix the resonance period at 9 s. Suggestions from experiments that frictional damping could be made negligible and radiation damping reduced to about half its two-dimensional value indicate that practically all the swell energy incident upon such a duct might be captured.

2. Analytical

2.1. *Local models of forcing-pressure modification*

This section is concerned with a simple preliminary model of forcing-pressure modification which ignores interaction between the duct and the free surface. Such a 'local' model is of value for the mouth-upwards duct because it shows 'in a few lines' why the modification need not be a reduction but can be an amplification. Quantitatively, the results turn out to be a valid asymptotic limit of the fully interactive theory (§2.2) when the ratio $h/n\lambda$ of mouth depth to duct width is large; and they are sufficiently accurate when $h/n\lambda \geqslant 2$.

The corresponding local model in the mouth-downwards case leads to an equally brief calculation suggesting why the modification must in that case be a reduction. This latter calculation is open, as we shall see, to apparently grave objections regarding convergence; yet, the full theory taking into account interaction with the free surface shows that the local model is again a valid limit for large $h/n\lambda$ and, indeed, is already sufficiently accurate when $h/n\lambda \geqslant 1$. Lastly, the success of a local model in both these cases encourages us to use a local model also to estimate the modification factor for a 'mouth-sideways' configuration, which would not lend itself to treatment by a fully interactive theory, and for a 'bell-mouth' arrangement.

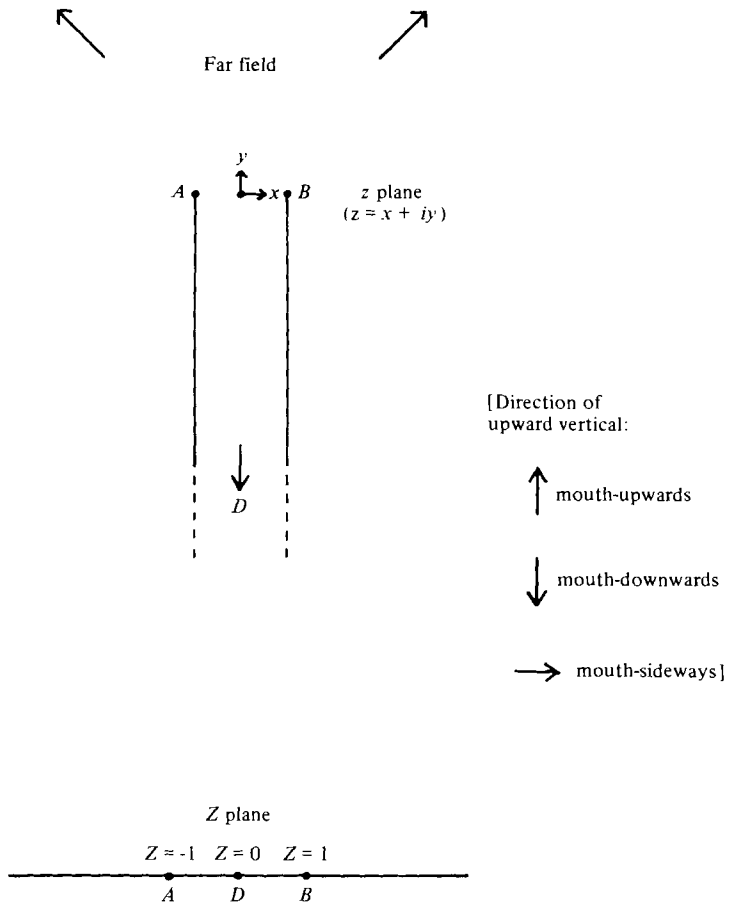

FIGURE 25. Diagram illustrating, for 'local' models, the z plane and its transformation (64) into the Z plane.

A local theory is concerned, essentially, with how the duct mouth responds to the fluctuating pressure distribution in its close neighbourhood. It regards all other influences, such as the free surface and the bend in the U-tube, as so remote from the duct mouth that, mathematically, they are 'at infinity'. Then the geometry of the problem is reduced to that of a semi-infinite duct in *otherwise unbounded* fluid (figure 25).

The present model, like all others in this paper, is two-dimensional in that the duct is taken as the channel between two plane parallel walls. The fluctuations of excess pressure inside it are calculated for the case of zero duct flow. Nothing would be gained by seeking to incorporate modifications due to duct flow in this model, since for example added mass must be logarithmically infinite for a two-dimensional duct in otherwise unbounded fluid.

The fluid dynamics is expressed most economically in terms of a velocity potential ϕ and stream function ψ, where for zero duct flow we can take the boundary condition as

$$\psi = 0 \text{ on both duct walls: } \quad x = \pm \tfrac{1}{2}n\lambda, \quad y < 0. \tag{57}$$

Here, the origin is taken at the centre of the duct mouth (figure 25).

Far from the duct mouth (which for a 'local' model means 'at infinity') the complex potential

$$\phi + i\psi = f(x+iy) = f(z) \tag{58}$$

is given the 'far-field' value

$$f_\infty(z) = f_0 e^{-2\pi i x/\lambda} e^{2\pi y/\lambda} = f_0 e^{-2\pi i z/\lambda}, \tag{59}$$

varying sinusoidally with x and exponentially with y as in waves on deep water. Here, f_0 is the value which $f(z)$ would have at the centre of the mouth if the duct were absent. We seek to determine $f_D = f(-i\infty)$, the purely real value of the complex potential in the 'depths' of the duct (where (57) implies that $\psi = 0$) as the real part,†

$$f_D = \mathrm{Re}\,(Ke^{-i\alpha} f_0), \tag{60}$$

of a multiple of this value f_0.

When the far field $f_\infty(z)$ is a sinusoidal wave travelling in the $+x$ direction, f_0 is necessarily proportional to $e^{i\omega t}$, where ω satisfies (11). The complex potential $f(z)$, representing the duct's response to that far field, is then also a multiple of $e^{i\omega t}$, so that the definition (60) of $Ke^{-i\alpha}$ agrees with the earlier definition (15) in terms of the excess pressure p_e. In fact,

$$p_e = -\rho\,\partial\phi/\partial t = \mathrm{Re}\,[-\rho i\omega f(z)]; \tag{61}$$

accordingly, $Ke^{-i\alpha}$ can be thought of as the ratio of the complex quantities

$$-\rho i\omega K e^{-i\alpha} f_0 \quad \text{and} \quad -\rho i\omega f_0$$

(each proportional to $e^{i\omega t}$) whose real parts are, respectively, the excess pressure in the depths of the duct and the excess pressure at the centre of the duct mouth if the duct were absent.

The 'local-model' problem is readily solved by a conformal mapping. The Schwarz–Christoffel rule for mapping the inside of any polygon in the z plane on to the upper half Z plane is to write

$$dz/dZ = C\Pi(Z-c)^{(\theta-\pi)/\pi}; \tag{62}$$

this product Π includes a term for each finite point $Z = c$ on the real axis corresponding to a vertex where the interior angle of the polygon is θ. The constant C is used to adjust the polygon's scale and orientation.

Applying this rule to the region of figure 25, regarded as a polygon with interior angles of 2π at both A and B, and with an interior angle of 0 at the point $Z = 0$ corresponding to the 'depths' D of the duct, we obtain

$$\frac{dz}{dZ} = \frac{n\lambda}{i\pi} \frac{(Z-1)(Z+1)}{Z}. \tag{63}$$

The value $(n\lambda/i\pi)$ for the constant C is chosen so that in the upper half Z plane the change in z from the left of D to the right (namely, $(-\pi i)$ times the residue of (63) at $Z = 0$) is the duct width $n\lambda$. The resulting value of z is

$$z = \frac{n\lambda}{i\pi} [\tfrac{1}{2}(Z^2-1) - \log(-iZ)] \tag{64}$$

† Throughout the 'mathematical' sections (§§2.1 and 2.2), the operation Re (taking the real part) is always written explicitly, rather than being suppressed as in the 'engineering' sections (§§1.1 and 1.2).

if the constant of integration is chosen so that the origin $z = 0$ is at the centre of the duct mouth. Thus, we take the imaginary part of $\log(-iZ)$ as

$$\arg(-iZ) = \mp \tfrac{1}{2}\pi \quad \text{for real} \quad Z \gtrless 0, \tag{65}$$

where therefore $x = \mathrm{Re}\, z = \pm \frac{1}{2}n\lambda$; while $y = \mathrm{Im}\, z$ attains at $Z = \pm 1$ its maximum $y = 0$. The point at infinity in the Z plane is mapped on to the point at infinity in the z plane.

In the Z plane the far field (59) becomes

$$f_\infty(Z) = f_0 \exp[n(1-Z^2)](-iZ)^{2n}. \tag{66}$$

Now we write $f(Z)$ as the sum of this far field and a correction which is 'local' (vanishing at $Z = \infty$) and has imaginary part $-\mathrm{Im} f_\infty(Z)$ on the boundary $Z = 0$; thus,

$$f(Z) = f_\infty(Z) + \frac{1}{\pi}\int_{-\infty}^{\infty} \mathrm{Im} f_\infty(Z_1)\, \frac{dZ_1}{Z - Z_1}, \tag{67}$$

where the imaginary part of the integral, as Z tends to a point on the boundary, tends to π times the residue $[-\mathrm{Im} f_\infty(Z)]$ of the integrand at $Z_1 = Z$. Evidently, the correction ensures that the sum $f(Z)$ satisfies $\psi = \mathrm{Im} f(Z) = 0$ on the boundary as required by condition (57).

The value f_D of $f(z)$ in the duct's 'depths' ($z \to -i\infty$) corresponding to $Z = 0$, where $f_\infty(Z) = 0$, is given by (67) as

$$f_D = \frac{1}{\pi}\int_{-\infty}^{\infty} \mathrm{Im} f_\infty(Z_1)\, \frac{dZ_1}{(-Z_1)} = \mathrm{Re}\, \frac{i}{\pi}\int_{-\infty}^{\infty} \frac{f_\infty(Z)}{Z}\, dZ. \tag{68}$$

Equation (60) therefore, with (66), gives

$$Ke^{-i\alpha} = \frac{i}{\pi}\int_{-\infty}^{\infty} \exp[n(1-Z^2)](-iZ)^{2n}\, \frac{dZ}{Z}. \tag{69}$$

With $\arg(-iZ)$ determined by (65), this implies that

$$Ke^{-i\alpha} = \frac{2\sin n\pi}{\pi}\int_0^{\infty} \exp[n(1-Z^2)]\, Z^{2n-1} dZ. \tag{70}$$

Now, with nZ^2 as a new variable X, we use the standard factorial-function integral

$$\int_0^{\infty} e^{-X} X^{n-1} dX = (n-1)! \tag{71}$$

(called $\Gamma(n)$ in the older books) to obtain finally

$$Ke^{-i\alpha} = \left(\frac{\sin n\pi}{n\pi}\right)\left[\frac{n!}{(n/e)^n}\right]. \tag{72}$$

The fact that the right-hand side of (72) is real implies zero phase lag ($\alpha = 0$) in the duct's response, as analysed by a local model. The forcing-pressure modification factor K is equal, however, not to the value

$$\frac{1}{n\lambda}\int_{-\frac{1}{2}n\lambda}^{\frac{1}{2}n\lambda} e^{-2\pi i x/\lambda}\, dx = \frac{\sin n\pi}{n\pi} \tag{73}$$

obtained by averaging the value of the far-field pressures (59) across the duct mouth, but to this value multiplied by the quantity in square brackets; a quantity always

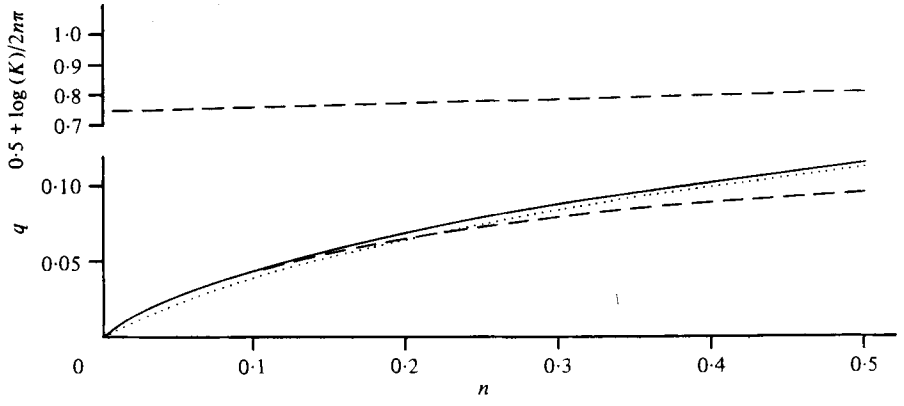

FIGURE 26. The lower diagram plots, for different local models, the quantity q, defined so that a two-dimensional duct of width $n\lambda$ (where λ = wavelength) responds to pressures which would be present at a distance $q\lambda$ beyond its mouth if the duct were absent. ——, value of q for mouth-upwards and mouth-downwards duct; ·····, approximation to this given by the simple equation (76); – – –, value of q for mouth-sideways duct. The upper diagram plots, for mouth-sideways ducts, the quantity (86). This specifies pressure fluctuations in the duct in terms of the level at which pressure fluctuations of that amplitude would appear if the duct were absent, by expressing the height of that level above the duct's *lower* lip as a fraction of the duct width.

greater than 1 for positive n. This is the quantity specified by Stirling's famous formula as asymptotically

$$(2\pi n)^{\frac{1}{2}}\left\{1+\frac{1}{12n}+O\left(\frac{1}{n^2}\right)\right\} \quad \text{for large} \quad n. \tag{74}$$

As a consequence, a rather good approximation for all positive n is

$$\left[\frac{n!}{(n/e)^n}\right] \doteqdot (2\pi n+1)^{\frac{1}{2}}, \tag{75}$$

a simple expression with practically the same asymptotic behaviour for large n and coinciding with the left-hand side at $n = 0$. (Elsewhere, it falls short of the left-hand side, but never by as much as 0·05.)

Essentially, this means that the duct responds to the far-field pressure averaged across the duct's width *at a different level* $y = q\lambda$, where

$$q \doteqdot \frac{1}{4\pi}\log(2\pi n+1); \tag{76}$$

this is the level where $e^{2\pi y/\lambda}$ takes the value (75). Evidently, the level $y = q\lambda$ is beyond the level of the mouth by an amount which for small n is close to the duct's *half-width* $\frac{1}{2}n\lambda$, but which increases more slowly for larger n. It seems physically reasonable that the duct of width $n\lambda$, if considered as a static-pressure tube, is sensitive to the pressures at such a distance $q\lambda$ beyond its mouth (where for this mouth-upwards duct 'beyond' means 'above'), averaged across the duct width.

Numerical values of K were given earlier (table 1) and compared (figure 8) with values derived from the fully interactive theory of §2.2. The local model was shown to be sufficiently accurate for a mouth at a depth exceeding two duct widths. Here, we show also a graph of q against n, derived from (76) (see the dotted line in figure 26);

with, for comparison (see the full line), the exact value of $q = y/\lambda$ for which $e^{2\pi q}$ is equal to the quantity in square brackets.

The corresponding local model for a mouth-downwards duct (see figure 17) will be found open to apparently grave convergence difficulties. Ignoring these, however, we derive from it results that agree still better with calculations (§2.2) by a fully interactive theory, and are sufficiently accurate for a mouth at a depth exceeding one duct width.

The derivation of these results is practically 'in one line': the same figure 25 can be used, provided it is understood that the vertically upward direction (pointing towards the free surface) is now 'down the page'. The far field (59) is then correct with λ replaced by $-\lambda$, but the unchanged duct width can be written

$$n\lambda = (-n)(-\lambda); \tag{77}$$

that is, as $-n$ times the new value of λ. We can expect, then, that the conclusion (72) for the mouth-upwards local model can be applied with n replaced by $-n$ to the mouth-downwards local model. This gives

$$Ke^{-i\alpha} = \left(\frac{\sin n\pi}{n\pi}\right) \frac{(-n)!}{(-n/e)^{-n}} = \frac{(n/e)^n}{n!}(-1)^n, \tag{78}$$

where the well-known identity

$$n!(-n)! = n\pi/\sin n\pi \tag{79}$$

has been used.

Unlike the corresponding mouth-upwards argument, this one appears mathematically unrigorous; especially, since the integral (70) is very far from being convergent with n replaced by $-n$. Also, the answer (78) is vague as regards phase, since $(-1)^n$ could mean either

$$e^{in\pi} \quad \text{or} \quad e^{-in\pi}, \quad \text{giving} \quad \alpha = -n\pi \quad \text{or} \quad +n\pi. \tag{80}$$

However, experience shows that many results derived from integral expressions for the factorial (or gamma) function continue to be valid after those integrals fail to converge. This makes it, perhaps, not too surprising that the fully interactive theory does confirm the above conclusions, with, actually, $\alpha = -n\pi$ as well as

$$K = \frac{(n/e)^n}{n!}, \tag{81}$$

as an asymptotic limit which for cases of practical interest is rather closely attained (figure 18).

The physical interpretation of the phase lead $-\alpha = n\pi$ is that the peak forcing pressure for a mouth-downwards duct occurs as soon as the wave crest reaches the nearest wall of the duct. Note that a mouth-downwards duct denies direct contact with the waves to the volume of fluid *above* its mouth, unlike a mouth-upwards duct, which responds most of all to the waves just above its centre. Thus, wave motions directly above the mouth are important (growing exponentially with the height y) in the mouth-upwards case, but the mouth-downwards duct excludes them. Accordingly, the strong signal to which the duct responds is that found when the crest reaches the duct's nearest wall, at a phase lead $-\alpha = n\pi$ relative to when the crest reaches the centre of the duct.

The value (81) for K is the *reciprocal* of that quantity in square brackets which satisfies the approximate equality (75). Physically, it means that once more the duct responds to the value of the far-field pressures at a distance $q\lambda$ 'beyond' the duct mouth, where q is given approximately by the broken line in figure 26, representing (76), or more accurately by the full line. The new features are twofold: for the mouth-downwards duct, 'beyond' means 'below'; while, also, the former 'averaging across the duct width' is replaced (see above) by taking the value under the duct's wall nearest to the incident waves. For the mouth-downwards case, numerical values of K derived from this local model were given earlier (table 2) and compared (figure 18) with values derived from the fully interactive theory of §2.2.

Another similar configuration of some interest lends itself especially to a local model. Experiments have been done on mouth-sideways ducts (Every, Priddin & Prosser 1977). A two-dimensional fully interactive model of such a duct would be difficult to work out and, also, physically unsatisfactory; thus, it would need to allow transmitted waves with a different (finite-depth) dispersion relationship from that of the incident wave; a feature probably absent from a real three-dimensional system. On the other hand, the power of a local model for estimating the forcing-pressure modification factor in the two cases treated above suggests that it might attain that limited aim in the mouth-sideways case.

We can still use figure 25 for a local model of the mouth-sideways configuration provided that the vertically upward direction is taken *to the right* on the figure. The far field is then

$$f_\infty(z) = f_0 e^{2\pi i y/\lambda} e^{2\pi x/\lambda} = f_0 e^{2\pi z/\lambda}, \tag{82}$$

representing an incident wave travelling in the $-y$ direction towards the duct mouth $-\frac{1}{2}n\lambda < x < \frac{1}{2}n\lambda$, $y = 0$. This time, the far field (82) is as if the wavelength in (59) were changed to $-i\lambda$; while the unchanged duct width can be written as the new value of λ multiplied by in, replacing the n of the mouth-upwards analysis.

This time, the integral (70) is convergent (if by a somewhat narrow margin!) and the result (72) is changed to

$$Ke^{-i\alpha} = \left(\frac{\sinh n\pi}{n\pi}\right)\left[\frac{(in)!}{(in/e)^{in}}\right]. \tag{83}$$

Here, the factor in large round brackets again represents a forcing-pressure modification derived by simply averaging over the duct mouth. On the other hand, it is well known that the result (79) with in replacing n gives

$$(in)! = \left(\frac{n\pi}{\sinh n\pi}\right)^{\frac{1}{2}} e^{-i\Omega(n)} \tag{84}$$

where the real function $\Omega(n)$ has been tabulated (Fock 1926). It follows that

$$\alpha = \Omega(n) + n\log(n/e), \quad K = [(\sinh n\pi)/n\pi]^{\frac{1}{2}} e^{\frac{1}{2}n\pi}, \tag{85}$$

where the $e^{\frac{1}{2}n\pi}$ factor in K comes from the i^{-in} factor in (83). Values of $\Omega(n)$, as well as of K, and of $-\alpha$ (in degrees), are given in table 3.

Note that the value of α given by (85) is negative because its negative second term is numerically greater than its positive first term. Thus, there is yet again a phase *lead*. Its magnitude accords with the idea that the duct is sensitive to pressures at a certain distance *beyond* its mouth, where in this instance 'beyond' means 'in the

n	0	0·05	0·1	0·15	0·2	0·25	0·3	0·35	0·4	0·45	0·5
$\Omega(n)$	0	0·0288	0·0573	0·0853	0·1123	0·1382	0·1682	0·1858	0·2072	0·2266	0·2441
K	1	1·084	1·180	1·289	1·414	1·557	1·721	1·909	2·125	2·371	2·655
$-\alpha$	0	9·8°	15·6°	20·0°	23·5°	26·3°	28·5°	30·5°	32·0°	33·4°	34·5°

TABLE 3

horizontal direction from which the incident waves are coming'. A phase lead $-\alpha$ means that the duct is sensitive to pressures at a distance $q\lambda$ beyond its mouth, where this time $q = -\alpha/2\pi$.

Figure 26 plots the quantity $q = -\alpha/2\pi$ as a function of n (broken line). The mouth-sideways tube is sensitive to pressures at a distance $q\lambda$ beyond the duct mouth, with q given by this broken line. Note that the corresponding q for mouth-upwards and for mouth-downwards ducts is given by the full line, or approximately by the dotted line with the very simple equation (76). The different lines remain rather close together; they all predict that ducts of width $\frac{1}{16}\lambda$, $\frac{1}{8}\lambda$, $\frac{1}{4}\lambda$ or $\frac{1}{2}\lambda$ respond to pressures at distances of about 0·5, 0·4, 0·3 or 0·2 duct widths, respectively, beyond the mouth.

We must ask also whether, in the mouth-sideways case, this sensitivity to the pressure at a particular distance beyond the mouth is a sensitivity to the pressure there *averaged over the duct width* (as in the mouth-upwards case) or to the pressure at the position of the *duct wall nearest to the incident waves* (as in the mouth-downward case). The truth for the mouth-sideways case, shown clearly in the expression (85), is given by the geometric mean of those two alternatives! Thus, it is given by the geometric mean of $(\sinh n\pi)/(n\pi)$, a modification factor describing an averaging over the duct width, and of $e^{n\pi}$, a modification factor which converts from the pressure at the centre of the mouth to the pressure at the duct wall which is *uppermost* (and, therefore, 'nearest to the waves').

The top graph in figure 26 gives the numerical significance of the result (85) for K in a different form. We can specify the amplitude Kp_0 of the forcing-pressure fluctuations in terms of the level at which the incident wave would exhibit pressure fluctuations of that amplitude if the duct were absent. The quantity plotted is the height of that level above the duct's lower wall, expressed as a fraction

$$\tfrac{1}{2} + (2n\pi)^{-1} \log K \tag{86}$$

of the duct width $n\lambda$. The graph implies that the amplitude of the forcing pressures is equal to the pressure amplitude in the undisturbed incident wave at a level which varies from 75 to 81% of the duct width above the duct's lower wall as n increases from 0 to 0·5.

In the light of this result we should not, perhaps, rule out the possibility that submerged resonant ducts with mouth-sideways intakes might respond usefully to incident swell. For a given depth of submergence of the duct's upper wall, fixed primarily by considerations of seaworthiness, the pressures to which the duct would respond might be those corresponding to a depth greater by a mere 25–19% of the duct width. One can imagine duct designs that might give a very substantial resonant response at such pressures. Nevertheless, we cannot feel the same degree of confidence in such conclusions from a purely local theory as we can in inferences from the fully interactive theories of §2.2.

We end this section by briefly developing one more local theory of a system too complicated for a fully interactive theory to be possible. This is the case of a mouth-upwards duct with lips so rounded that it can be called a bell-mouth. Considerations of reducing frictional damping suggest (§ 1.2) the importance of fitting bell-mouths to ducts, so it is interesting to inquire how the forcing-pressure modification factor K will be affected if such a bell-mouth is fitted.

The necessary modifications to the two-dimensional mouth-upwards local theory based on the conformal mapping (64) are very simple. We add a *real constant*, $(n\lambda/\pi)\,W$, to the derivative (63) of the mapping so that it becomes

$$\frac{dz}{dZ} = \frac{n\lambda}{i\pi}\left(\frac{Z^2-1}{Z} + iW\right). \tag{87}$$

The positive real part added to the previous pure-imaginary value allows the boundary in the z plane corresponding to the real Z axis to have, alongside its previous ups and downs, a movement to the right which is continuous, except for the discontinuous jump of $n\lambda$ corresponding to the pole at $Z = 0$. Note also that the other singularities of the mapping are moved below the real Z axis, to

$$Z = \pm(1-\tfrac{1}{4}W^2)^{\frac{1}{2}} - \tfrac{1}{2}iW, \tag{88}$$

so as to round off the previous sharp lips. The mapping becomes

$$z = (n\lambda/i\pi)\,[\tfrac{1}{2}(Z^2-1) - \log(-iZ) + iWZ], \tag{89}$$

and the boundary shape in the z plane is given parametrically by the equations

$$x = (n\lambda/\pi)\,(\tfrac{1}{2}\pi \operatorname{sgn} Z + WZ), \quad y = (n\lambda/\pi)\,[\log|Z| + \tfrac{1}{2}(1-Z^2)] \tag{90}$$

for real Z. These curves are shown for $W = \frac{1}{4}\pi$ and $\frac{1}{2}\pi$ as the bell-mouth shapes, (*b*) and (*c*) respectively, in figure 24 (compare the sharp-lipped duct *a*). The far field (59) is

$$f_\infty(Z) = f_0 \exp[n(1-Z^2-2iWZ)]\,(-iZ)^{2n}, \tag{91}$$

and we deduce as before that the phase lag α is zero and that the forcing-pressure modification factor K is given as the integral

$$K = \frac{1}{\pi}\left(\frac{e}{n}\right)^n \int_0^\infty e^{-X} X^{n-1} \sin[n\pi + 2W(nX)^{\frac{1}{2}}]\,dX, \tag{92}$$

which is easy to evaluate numerically after expanding it in powers of W. The results are shown in figure 24, for comparison with the results for the sharp-lipped duct obtained previously (table 1) and shown in graph (*a*).

The absolute values of K in figure 24 may not be very significant, since the local theory has been found to be only a crude approximation. Nevertheless, the shapes of the curves (*b*) and (*c*) for the narrower and wider bell-mouths *relative* to the previously obtained curve (*a*) (based on the same theory) for the sharp-lipped duct are probably significant. They indicate that, for values of n around 0·2, the use of a bell-mouth such as is in any case desirable for minimizing frictional damping should, additionally, increase the amplitude of the forcing pressure itself.

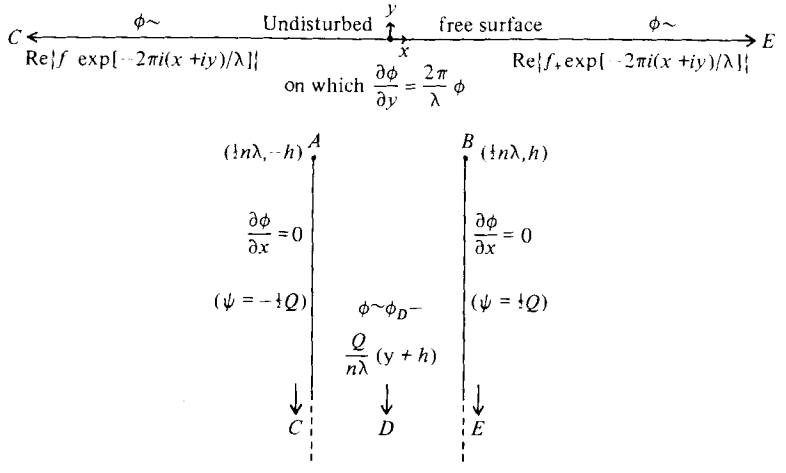

FIGURE 27. Boundary-value problem, in terms of the velocity potential ϕ and stream function ψ, to be solved in the fully interactive theory of the mouth-upwards case.

2.2. *Fully interactive models*

In this section we develop in detail a fully interactive model for the sharp-lipped, mouth-upwards case. The analysis, like all others in this paper, is two-dimensional. The motions, assumed irrotational, are calculated exactly except that, at the free surface, the usual linearized boundary condition is applied. From the calculation, we infer several aspects of the duct's response to an incident wave. These include forcing-pressure modification, added mass, and energy absorption, transmission and reflexion. Afterwards, we indicate the relatively minor changes in the analysis from which all the corresponding information in the mouth-downwards case is similarly derived.

Figure 27 specifies the mouth-upwards problem to be solved in terms of the velocity potential ϕ. The origin is now taken in the undisturbed free surface $y = 0$ over the centre $(0, -h)$ of the duct mouth. The two vertical lines $x = \pm \frac{1}{2}n\lambda$, $y < -h$ represent the duct's thin walls, on which $\partial\phi/\partial x = 0$. We expect that at the sharp lips A and B ($x = \pm \frac{1}{2}n\lambda$, $y = -h$) the velocity potential will have a square-root singularity, and we know from aerofoil theory how the strength of that singularity can be related to the real flow around a rounded orifice lip.

At any time t, we define Q as the *downward flux* (volume flow per unit breadth perpendicular to the paper) in the duct. The corresponding average vertical velocity across the duct width is

$$\partial\phi/\partial y = -Q/n\lambda. \tag{93}$$

We take

$$\phi + (Q/n\lambda)(y+h) \to \phi_D \tag{94}$$

in the 'depths' D of the duct; that is, far enough inside it for the vertical velocity (93) to have become uniform. Here, ϕ_D represents the duct's response in terms of all features of ϕ other than that which would be associated with an average flow velocity (93) distributed uniformly between (x, y) and $(x, -h)$. From (94) we can obtain the excess pressure in the depths of the duct as $-\rho\partial\phi/\partial t$.

At the free surface, the linearized boundary condition for motions with radian frequency ω is applied. We write this as

$$\partial\phi/\partial y = (2\pi/\lambda)\phi \quad \text{on} \quad y = 0, \tag{95}$$

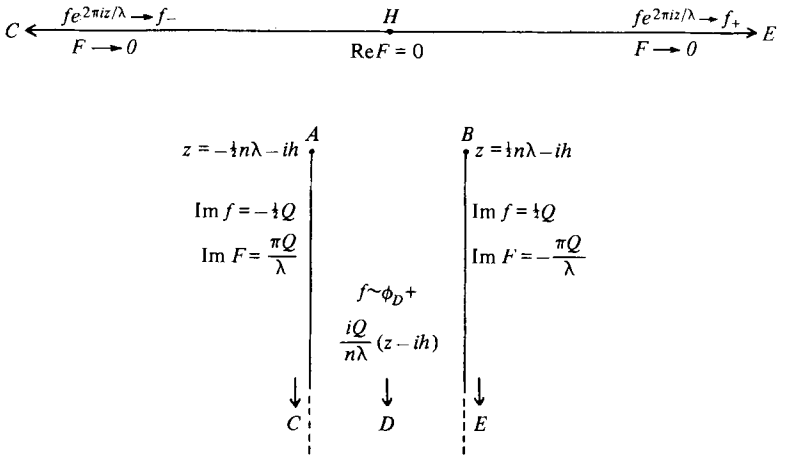

FIGURE 28. Boundary-value problem, in terms of the complex potential f and the auxiliary function F, to be solved in the complex z plane in the mouth-upwards case.

where we express the wavenumber

$$(2\pi/\lambda) = \omega^2/g \tag{96}$$

in terms of wavelength because the present analysis, like that of §2.1, involves the ratio n of duct width to wavelength as a frequently occurring exponent.

Far to the right ($x \to +\infty$) and to the left ($x \to -\infty$) of the duct we take

$$\phi - \mathrm{Re}\,(f_\pm e^{-2\pi i x/\lambda} e^{2\pi y/\lambda}) \to 0 \quad \text{as} \quad x \to \pm\infty, \tag{97}$$

so that ϕ tends to undisturbed sinusoidal-wave solutions. Later, we interpret f_- as the combination of incident and reflected waves

$$f_- = f_I e^{i\omega t} + f_R e^{-i\omega t} \tag{98}$$

(travelling to the right and to the left, respectively) and f_+ as the transmitted wave

$$f_+ = f_T e^{i\omega t} \tag{99}$$

(travelling to the right); here, f_I, f_R and f_T are complex amplitudes. The absence of any $e^{-i\omega t}$ term in f_+ expresses the radiation condition that the only energy 'coming in from infinity' is that in the incident wave.

We can expect that, at any time t, the above conditions determine uniquely a solution ϕ of Laplace's equation $\nabla^2\phi = 0$ in terms of three real quantities; that is, Q and the real and imaginary parts of the incident wave $f_I e^{i\omega t}$. Later, we use assumptions about the internal duct impedance associated with the dynamics of duct motions to relate Q to ϕ_D and, hence, to derive a solution in terms of f_I alone.

If ψ is the stream function, satisfying

$$\partial\psi/\partial y = \partial\phi/\partial x, \quad \partial\psi/\partial x = -\partial\phi/\partial y, \tag{100}$$

then we can take

$$\psi = \pm\tfrac{1}{2}Q \quad \text{on} \quad x = \pm\tfrac{1}{2}n\lambda, \quad y \leqslant -h \tag{101}$$

because the downward flux between these two streamlines is Q. Then the complex potential

$$\phi + i\psi = f(x + iy) = f(z) \tag{102}$$

is an analytic function of $z = x+iy$, for which (100) are the Cauchy–Riemann equations, and satisfies conditions set out in figure 28. In particular,

$$f-(iQ/n\lambda)(z+ih)-\phi_D \to 0 \tag{103}$$

in the depths of the duct. Also,

$$f-f_{\pm}e^{-2\pi iz/\lambda} \to 0 \quad \text{as} \quad z \to \pm\infty. \tag{104}$$

Furthermore, an auxiliary function

$$F(z) = \left(\frac{\partial}{\partial y}-\frac{2\pi}{\lambda}\right)(\phi+i\psi) = \left(i\frac{d}{dz}-\frac{2\pi}{\lambda}\right)f(z) \tag{105}$$

satisfies boundary conditions that are also specified on figure 28. The free-surface condition (95) becomes

$$\operatorname{Re} F = 0 \quad \text{on} \quad y = 0, \tag{106}$$

while (104) gives

$$F \to 0 \quad \text{as} \quad z \to \pm\infty. \tag{107}$$

In the depths of the channel, by (103),

$$F+(Q/n\lambda)+(2\pi/\lambda)[\phi_D+(iQ/n\lambda)(z+ih)] \to 0. \tag{108}$$

On the duct walls, where ψ satisfies (101), the imaginary part $\partial\psi/\partial y-(2\pi\psi/\lambda)$ of F satisfies

$$\operatorname{Im} F = \mp(\pi Q/\lambda) \quad \text{on} \quad x = \pm\tfrac{1}{2}n\lambda, \quad y \leqslant -h. \tag{109}$$

At the orifice lips $z = \pm\frac{1}{2}n\lambda - ih$, the square-root singularities of f imply *inverse-square-root* singularities of F.

The straightforward boundary conditions (106) and (109) for F enable it to be determined as a simple algebraic function (see (126) below). Then, to derive f (and hence ϕ) from it, we must solve (105) as a first-order linear differential equation with constant coefficients. Using the integrating factor $e^{2\pi iz/\lambda}$ and the forms (104) and (107) of f and F at $z = \pm\infty$, we obtain the two alternative results

$$f(z)\,e^{2\pi iz/\lambda} = f_{\pm} - i\int_{\pm\infty}^{z} F(z_1)\exp(2\pi iz_1/\lambda)\,dz_1, \tag{110}$$

where either the upper or lower signs may be used.

On the other hand, when we have found a form of F whose imaginary part

$$\partial\psi/\partial y-(2\pi\psi/\lambda)$$

satisfies (109), we cannot be sure that ψ itself will satisfy (101). It is, indeed, important to note that the boundary value of ψ could differ from (101) by any multiple of $e^{2\pi y/\lambda}$ without disturbing the correctness of (109). However, we can use (110) to express the condition that no such deviation is present, by considering the limiting form of the left-hand side as $z \to -i\infty$; that is, in the depths D of the duct. These are where (103) represents the true limiting form of f, and where any non-zero multiple of $e^{2\pi y/\lambda}$ in a boundary value of ψ would require f to deviate from that limiting form by

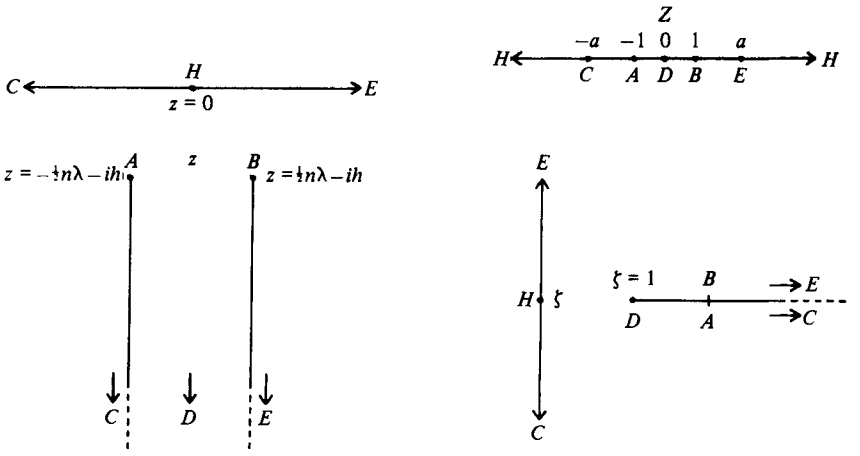

FIGURE 29. The three complex planes (z plane, Z plane and ζ plane) used in the mouth-upwards case.

a non-zero multiple of $e^{-2\pi iz/\lambda}$. In that case, the left-hand side of (110) would deviate by a non-zero constant from the value given by the limiting property (103). We express the fact that no such deviation occurs by requiring that

$$f_{\pm} = \lim_{z \to -i\infty} \left\{ [\phi_D + (iQ/n\lambda)(z+ih)] e^{2\pi iz/\lambda} + i \int_{\pm\infty}^{z} F(z_1) \exp(2\pi i z_1/\lambda)\, dz_1 \right\}. \quad (111)$$

The above arguments prove (111) rigorously provided that $n < \frac{1}{2}$. This is because, if an analytic function (103) has imaginary part zero on two parallel lines $x = \pm \frac{1}{2}n\lambda$, $y < -h$ and takes values between them which tend to zero as $y \to -\infty$, then those values are $O(e^{\pi y/n\lambda})$. This result is expected physically from the rate of decay of the lowest eigenfunction of the problem, proportional to $\cos(\pi x/n\lambda)$; while, mathematically, it is guaranteed by the Phragmén–Lindelöf theorem. Accordingly, even when the left-hand side of (103) is multiplied by $e^{2\pi iz/\lambda}$, its value must still tend to zero as assumed in (111) provided only that $n < \frac{1}{2}$. It is, in fact, relatively straightforward to extend the results derived below to values of $n \geqslant \frac{1}{2}$ but we save space by omitting such an analysis because ducts promising for practical applications all satisfy $n < \frac{1}{2}$.

As in §2.1, a Schwarz–Christoffel mapping (62) from the z plane to the upper half Z plane is the key to the problem's solution (figure 29). The z plane is, as before, a polygon with interior angles of 2π at both A and B (corresponding to $Z = -1$ and $+1$) and an interior angle of 0 at the point D (corresponding to $Z = 0$). This time, however, there are two additional vertices at infinity; namely, C and E (corresponding to $Z = -a$ and $+a$, where $a > 1$); each with a *negative* 'interior angle' $-\frac{1}{2}\pi$ since the edges diverge instead of converging towards the vertex. It follows that

$$\frac{dz}{dZ} = \frac{n\lambda}{i\pi} \frac{(Z-1)(Z+1)}{Z} \frac{a^3}{(a-Z)^{\frac{3}{2}}(a+Z)^{\frac{3}{2}}}. \quad (112)$$

Here, the right-hand factor, modifying the previous factor (63), tends to 1 as $Z \to 0$; accordingly, it does not disturb the correctness of the left-hand constant factor $n\lambda/i\pi$, chosen so as to make the duct width $n\lambda$.

The resulting value of z is

$$z = \frac{n\lambda}{i\pi}\left[\frac{a^3-a}{(a^2-Z^2)^{\frac{1}{2}}} + \tfrac{1}{2}\log\frac{(a^2-Z^2)^{\frac{1}{2}}+a}{(a^2-Z^2)^{\frac{1}{2}}-a}\right], \tag{113}$$

if the constant of integration is chosen this time so that the origin $z = 0$ corresponds to the point at infinity in the Z plane. Furthermore, the mapping is *symmetrical*, in that the positive imaginary axis, where $-iZ$ is positive, corresponds to the negative imaginary axis, where iz is positive, provided that both the many-valued functions of Z in square brackets are interpreted as the branches positive where $-iZ$ is positive. Note also that the value of a must be determined by the condition that $\mathrm{Im}\, z = -h$ at $Z = \pm 1$, giving

$$h = \frac{n\lambda}{\pi}\left[a(a^2-1)^{\frac{1}{2}} + \tfrac{1}{2}\log\frac{a+(a^2-1)^{\frac{1}{2}}}{a-(a^2-1)^{\frac{1}{2}}}\right]. \tag{114}$$

It will often prove convenient to use the auxiliary variable

$$\zeta = a/(a^2-Z^2)^{\frac{1}{2}} \tag{115}$$

which fills the right-hand half-plane cut from $+1$ to $+\infty$ (figure 29). In terms of ζ, (113) becomes

$$z = \frac{n\lambda}{i\pi}\left[(a^2-1)\zeta + \tfrac{1}{2}\log\frac{1+\zeta}{1-\zeta}\right], \tag{116}$$

which gives

$$dz = \frac{n\lambda}{i\pi}\left(a^2 - 1 + \frac{1}{1-\zeta^2}\right)d\zeta. \tag{117}$$

In (116), the function

$$\log\frac{1+\zeta}{1-\zeta} \tag{118}$$

is the branch specified above as positive when $-iZ$ is positive. In the ζ plane, then, it is positive on HD (where $0 < \zeta < 1$). By contrast, as $1-\zeta$ moves round the branch-point D at the tip of the cut, the function (118) acquires an imaginary part

$$+\pi \text{ on } DBE, \text{ but } -\pi \text{ on } DAC; \tag{119}$$

that is, on the upper and lower edges of the cut, respectively. (These results, when applied in (116), make the real part of z equal to $+\frac{1}{2}n\lambda$ on DBE and $-\frac{1}{2}n\lambda$ on DAC, of course.) By contrast, the function (118) has *real* part zero on EHC (where ζ is pure imaginary).

The boundary conditions on F itself are similar to these. By (109), its imaginary part is

$$-(\pi Q/\lambda) \text{ on } DBE, \text{ but } +(\pi Q/\lambda) \text{ on } DAC; \tag{120}$$

while by (106) its real part is zero on EHC. Combining (119) and (120), we deduce that the modified function F_m, defined as

$$F_m = \zeta\left(F + \frac{Q}{\lambda}\log\frac{1+\zeta}{1-\zeta}\right), \tag{121}$$

is purely real on the whole boundary; on DBE and DAC as the product of two real quantities, and on EHC as the product of two pure imaginary quantities.

A function F_m with this property is easily determined; especially, if we look for its value in the Z plane whose boundary (figure 29) is simply the real axis. We are given,

essentially, that F_m is analytic in the upper half Z plane and real on the real Z axis. Therefore, it can be continued by the Schwarz reflexion principle (which defines $F_m(Z)$ in the lower half-plane as $[F_m(Z^*)]^*$, where the star means complex conjugate), to give a function analytic in the whole Z plane.

As $|Z| \to \infty$ (that is, at the point H) we have $\zeta \to 0$, so that by (121), since F is bounded near an ordinary point H (where $z = 0$) of the free surface, $F_m \to 0$. This suggests the awkward possibility that F_m may be a function having no singularities anywhere in the whole Z plane and tending to zero as $|Z| \to \infty$. Such a function, of course, would be identically zero.

At this stage, however, it is necessary to remember that F, as defined by (105), has an inverse-square-root singularity at the points A and B in the z plane where f has square-root singularities (that is, at $z = \pm \frac{1}{2}n\lambda - ih$). Since these correspond to points $Z = \pm 1$ where the derivative (112) of the mapping vanishes, the said inverse-square-root singularities in the z plane become simple poles in the Z plane; in fact,

$$(z \mp \tfrac{1}{2}n\lambda + ih)^{-\frac{1}{2}} \quad \text{becomes proportional to} \quad (Z \mp 1)^{-1} \quad \text{as} \quad Z \to \pm 1. \tag{122}$$

It follows that F_m is an analytic function in the whole Z plane except for simple poles at $Z = \pm 1$. Also,

$$F_m = O(|Z|^{-1}) \quad \text{as} \quad |Z| \to \infty \tag{123}$$

by (115) and (121). Finally, then, the function $(Z^2-1)\,F_m(Z)$ has no singularities at all in the complex plane, and satisfies

$$(Z^2-1)\,F_m(Z) = O(|Z|) \quad \text{as} \quad |Z| \to \infty. \tag{124}$$

Such a function can only be a first-order polynomial, which we write

$$(Z^2-1)\,F_m(Z) = (2\pi/\lambda)\,(F_0 + F_1 Z) \tag{125}$$

where F_0 and F_1 are constants and the factor $2\pi/\lambda$ has been inserted purely for reasons of convenience. Evidently, the constants F_0 and F_1 must be real since (125) is given to be real on the real Z axis. By (121), the general solution for F is therefore

$$F = \frac{2\pi}{\lambda}\,\frac{F_0 + F_1 Z}{(Z^2-1)\,\zeta} - \frac{Q}{\lambda}\log\frac{1+\zeta}{1-\zeta}, \tag{126}$$

depending on three real quantities F_0, F_1 and Q as foreshadowed earlier on physical grounds.

One of these quantities, F_0, is closely related to the quantity ϕ_D which we particularly wish to calculate. This is because the left-hand side of (108) tends to zero in the depths of the duct, where $Z \to 0$ and $\zeta \to 1$ and z is given by (116). Equation (126) for F implies, therefore, that the limit as $\zeta \to 1$ of

$$-\frac{2\pi}{\lambda}F_0 - \frac{Q}{\lambda}\log\frac{1+\zeta}{1-\zeta} + \frac{Q}{n\lambda} + \frac{2\pi}{\lambda}\left[\phi_D + \frac{Q}{\pi}\left(a^2 - 1 + \tfrac{1}{2}\log\frac{1+\zeta}{1-\zeta}\right) - \frac{Qh}{n\lambda}\right] \tag{127}$$

(where the first part is the limiting form of the first two terms in (108), and the second part is the limiting form of the last term) is zero. Therefore, since (127) is actually independent of ζ, it must be identically zero, giving

$$\phi_D = F_0 + bQ, \quad \text{where} \quad b = \frac{h}{n\lambda} - \frac{a^2-1}{\pi} - \frac{1}{2n\pi}. \tag{128}$$

For given Q, then, the value of F_0 determines the required quantity ϕ_D specifying the velocity potential (94) (and hence also the excess pressure $-\rho\,\partial\phi/\partial t$) in the depths of the channel. Later, this relationship, together with a value of the duct's 'internal impedance' (specifying the dynamics of motions within it), is used to determine the value of Q and hence the rate of energy absorption.

In the meantime, we note that the second constant F_1 (the coefficient of an antisymmetric part of F) derives its significance mainly from its ratio to F_0 (the coefficient of a symmetric part). Indeed, (126) implies that the residues of F at the poles $Z = \pm 1$ are in the ratio

$$(F_0+F_1)/(F_0-F_1). \tag{129}$$

By (122), then, this is the ratio between the strengths of the inverse-square-root singularities of $F(z)$ at the corresponding points $z = \pm n\lambda - ih$. This in turn, by (105), is the ratio of the square-root singularities of $f(z)$ at those points; strengths which give a measure of the strengths of the real flows around any rounded orifice lips such as may be represented by the sharp lips of figure 27. Since the strengths of those flows are in the ratio (129), we can say that the strengths of the symmetric and antisymmetric elements in the lip motions (see figure 9) are in the ratio F_0/F_1.

We now obtain equations from which the quantities F_0, F_1 and Q can be related to the behaviour of the waves at large distances; that is, to f_-, representing by (98) the incident and reflected waves, and to f_+, representing the transmitted waves. We shall find that these relations determine all three constants, and also the transmitted and reflected waves, when both the incident wave and the internal duct impedance are given.

We start from (111); note that the limiting value of the term in square brackets appeared later, also in square brackets, as part of a quantity (127) *whose limit is zero.* Therefore, the term in square brackets in (111) can be replaced by

$$\left[F_0+\frac{Q}{2\pi}\left(\log\frac{1+\zeta}{1-\zeta}-\frac{1}{n}\right)\right]. \tag{130}$$

Also, by (116) we can write

$$e^{2\pi iz/\lambda} = \exp\left[2n(a^2-1)\,\zeta\right]\left(\frac{1+\zeta}{1-\zeta}\right)^n \tag{131}$$

in terms of ζ. Furthermore, by (115) we have

$$Z = +ia(1-\zeta^2)^{\frac{1}{2}}/\zeta \tag{132}$$

since ζ is positive when $-iZ$ is positive. In terms of ζ, then, (126) gives

$$F = -\frac{2\pi}{\lambda}\frac{F_0\zeta+F_1 ia(1-\zeta^2)^{\frac{1}{2}}}{a^2(1-\zeta^2)+\zeta^2}-\frac{Q}{\lambda}\log\frac{1+\zeta}{1-\zeta}, \tag{133}$$

and the integral in (111) runs from $\pm i\infty$ to ζ with dz given by (117). Equation (111) then becomes

$$f_\pm = \lim_{\zeta\to 1}\left\{\left[F_0+\frac{Q}{2\pi}\left(\log\frac{1+\zeta}{1-\zeta}-\frac{1}{n}\right)\right]e^{2\pi iz/\lambda} + i\int_{\pm i\infty}^{\zeta} F\,e^{2\pi iz/\lambda}\,\frac{n\lambda}{i\pi}\,\frac{a^2(1-\zeta^2)+\zeta^2}{1-\zeta^2}\,d\zeta\right\}, \tag{134}$$

where furthermore the substitutions (131) and (133) must be made.

As it stands, equation (134) is not one where the upper limit in the integral can

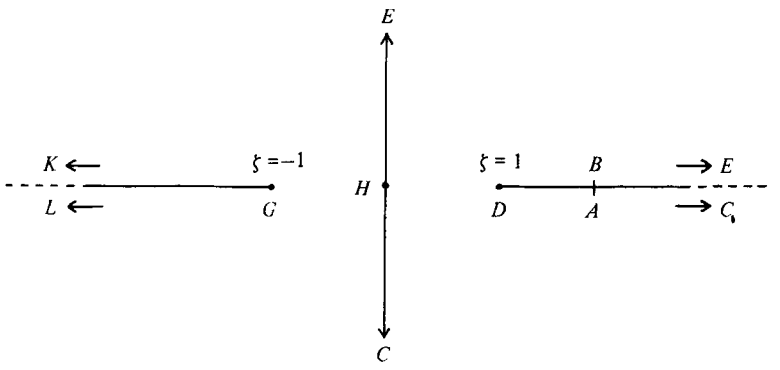

FIGURE 30. Illustrating the complete complex ζ plane in the mouth-upwards case, cut from $\zeta = 1$ to $\zeta = +\infty$ and from $\zeta = -1$ to $\zeta = -\infty$.

simply be replaced by 1, since the resulting integral would be divergent. However, a rearrangement analogous to integration by parts allows us to replace (134) by a single integral from $\pm i\infty$ to 1. We replace the term outside the integral (the first line of the expression in braces) by the integral of its derivative,

$$\int_{\pm i\infty}^{\zeta} d\left\{\left[F_0+\frac{Q}{2\pi}\left(\log\frac{1+\zeta}{1-\zeta}-\frac{1}{n}\right)\right]e^{2\pi iz/\lambda}\right\}=\int_{\pm i\infty}^{\zeta} e^{2\pi iz/\lambda}\frac{Q\,d\zeta}{\pi(1-\zeta^2)}$$
$$+\int_{\pm i\infty}^{\zeta}\left[F_0+\frac{Q}{2\pi}\left(\log\frac{1+\zeta}{1-\zeta}-\frac{1}{n}\right)\right]\frac{2\pi i}{\lambda}\,e^{2\pi iz/\lambda}\,\frac{n\lambda}{i\pi}\left(a^2-1+\frac{1}{1-\zeta^2}\right)d\zeta. \quad (135)$$

Then the limit (134), with its first line replaced by (135), becomes a convergent integral from $\pm i\infty$ to 1, for three reasons as follows. The logarithmic term appearing [see (133)] in F and so also in the second line of (134) is cancelled by the logarithmic term in (135); the first integral on the right-hand side of (135) is cancelled in the second such integral by the product of the $-Q/2\pi n$ term in square brackets and that part of the factor multiplying it which tends to infinity as $\zeta \to 1$; and the similar product of the F_0 term in square brackets with the factor multiplying it which tends to infinity as $\zeta \to 1$ cancels the contribution made by the F_0 term in expression (133) for F to the part of the second line in (134) which tends to infinity as $\zeta \to 1$.

We readily check, in fact, that the convergent integral from $\pm i\infty$ to 1 by which (134) can be thus replaced may be written as

$$f_{\pm} = F_0(A_0 \mp iB_0) - iF_1(A_1 \mp iB_1) - Q(A_2 \mp iB_2), \quad (136)$$

where the constants A_m and B_m are defined (in such a way that all are later found to be positive for $0 < n < \frac{1}{2}$) in terms of the integrals

$$A_0 \mp iB_0 = \int_{\pm i\infty}^{1}\left(\tfrac{1}{2}s+\frac{2n}{1+\zeta}\right)e^{\frac{1}{2}s\zeta}\left(\frac{1+\zeta}{1-\zeta}\right)^n d\zeta, \quad (137a)$$

$$A_1 \mp iB_1 = 2na\int_{\pm i\infty}^{1} e^{\frac{1}{2}s\zeta}\left(\frac{1+\zeta}{1-\zeta}\right)^n \frac{d\zeta}{(1-\zeta^2)^{\frac{1}{2}}}, \quad (137b)$$

$$A_2 \mp iB_2 = \frac{s}{4\pi n}\int_{\pm i\infty}^{1} e^{\frac{1}{2}s\zeta}\left(\frac{1+\zeta}{1-\zeta}\right)^n d\zeta. \quad (137c)$$

Here, the variable

$$s = 4n(a^2-1) \tag{138}$$

has been introduced because it turns out that each of these integrals can be expressed quite simply in terms of standard confluent hypergeometric functions of s.

In fact, the integrands in (137) are all regular in the whole ζ plane, provided that it is cut not only from $+1$ to $+\infty$ but also from $-\infty$ to -1 (figure 30). The integrals can therefore be evaluated by path deformations as follows:

$$\int_{i\infty}^{1} = \int_{EHD} = \int_{KHD} = \int_{KG} + \int_{GD}, \tag{139}$$

$$\int_{-i\infty}^{1} = \int_{CHD} = \int_{LHD} = \int_{LG} + \int_{GD}; \tag{140}$$

a pair of sums with the common element

$$\int_{GD} = \int_{-1}^{1}.$$

Now,

$$\int_{-1}^{1} e^{\frac{1}{2}s\zeta} \left(\frac{1+\zeta}{1-\zeta}\right)^n \frac{d\zeta}{1+\zeta} \tag{141}$$

can be evaluated, by expanding $e^{\frac{1}{2}s(\zeta+1)}$ in series, as

$$e^{-\frac{1}{2}s} \sum_{r=0}^{\infty} \frac{(\frac{1}{2}s)^n}{r!} \int_{-1}^{1} (1+\zeta)^{n+r-1} (1-\zeta)^{-n} d\zeta, \tag{142}$$

where the integral by itself has the well-known beta-function form

$$2^r(n+r-1)!\,(-n)!/r!. \tag{143}$$

Using this in (142) with $(-n)!$ replaced in terms of $n!$ by (79), the whole expression (142) becomes

$$\frac{\pi}{\sin n\pi} e^{-\frac{1}{2}s} \sum_{r=0}^{\infty} \frac{s^r}{(r!)^2} \frac{(n+r-1)!}{(n-1)!}. \tag{144}$$

Accordingly,

$$\int_{-1}^{1} e^{\frac{1}{2}s\zeta} \left(\frac{1+\zeta}{1-\zeta}\right)^n \frac{d\zeta}{1+\zeta} = \frac{\pi}{\sin n\pi} e^{-\frac{1}{2}s} M_n(s), \tag{145}$$

where we shall use $M_n(s)$ as a compact notation for the confluent hypergeometric series

$$M_n(s) = M(n, 1, s) = \sum_{r=0}^{\infty} \frac{s^r}{(r!)^2} n(n+1) \ldots (n+r-1), \tag{146}$$

also called ${}_1F_1(n; 1; s)$. Texts on special functions, such as Jeffreys & Jeffreys (1950), define this as one standard solution of the differential equation

$$\frac{d^2w}{ds^2} + \left(\frac{1}{s} - 1\right) \frac{dw}{ds} - nw = 0. \tag{147}$$

The somewhat surprising importance of the fact, that the quantity $M_n(s)$ appearing in expressions (137) for the constants A_m and B_m satisfies this differential equation with respect to a parameter s defined by (138), emerges later [see (192)].

Asymptotically, the solution (146) of (147) is known to satisfy

$$M_n(s) \sim e^s s^{n-1}/(n-1)! \quad \text{as} \quad s \to \infty. \tag{148}$$

We shall use also a second solution $U_n(s)$ of (147), called $U(n, 1, s)/(-n)!$ by Jeffreys & Jeffreys (1950). This solution tends to zero asymptotically, satisfying

$$U_n(s) \sim s^{-n}/(-n)! \quad \text{as} \quad s \to \infty. \tag{149}$$

Like $M_n(s)$, it can be written as a series convergent for all s; namely,

$$U_n(s) = \frac{\sin n\pi}{\pi} \sum_{r=0}^{\infty} \frac{s^r}{(r!)^2} n(n+1)\dots(n+r-1)\,[2F(r) - F(n+r-1) - \log s] \tag{150}$$

where $F(r)$ stands for $d(\log r!)/dr$; both series (146) and (150) are computed very readily indeed.

The importance of $U_n(s)$ is that it has the following integral expression closely parallel to (145):

$$\int_{-\infty}^{-1} e^{\frac{1}{2}s\zeta} \left(\frac{-1-\zeta}{1-\zeta}\right)^n \frac{d\zeta}{-1-\zeta} = \frac{\pi}{\sin n\pi} e^{-\frac{1}{2}s} U_n(s), \tag{151}$$

where the term in large round brackets is real and positive on the path of integration. By (140) and (151),

$$\int_{-i\infty}^{1} e^{\frac{1}{2}s\zeta} \left(\frac{1+\zeta}{1-\zeta}\right)^n \frac{d\zeta}{1+\zeta} = \int_{LG} + \int_{GD} = \frac{\pi}{\sin n\pi} e^{-\frac{1}{2}s}[-e^{-in\pi}U_n(s) + M_n(s)], \tag{152}$$

where the term in large round brackets in (152) is equal on the lower edge LG of the cut to $e^{-in\pi}$ times the corresponding term in (151). The similar integral (139) from $i\infty$ to 1 involves $\int_{KG}$ instead of $\int_{LG}$ and therefore is as in (152) but with $e^{+in\pi}$ replacing $e^{-in\pi}$; in short, it is the complex conjugate of (152).

Applying the operator $(d/ds) + \frac{1}{2}$ to (152) gives us the value of the one other type of integral occurring in (137):

$$\frac{1}{2}\int_{-i\infty}^{1} e^{\frac{1}{2}s\zeta} \left(\frac{1+\zeta}{1-\zeta}\right)^n d\zeta = \frac{\pi}{\sin n\pi} e^{-\frac{1}{2}s}[-e^{-in\pi}U_n'(s) + M_n'(s)], \tag{153}$$

with the integral from $i\infty$ to 1 again given by the complex conjugate. Using (152) and (153) twice each in (137), we obtain

$$C_0 = A_0 + iB_0 = \frac{\pi}{\sin n\pi} e^{-\frac{1}{2}s}\{sM_n'(s) + 2nM_n(s) - e^{-in\pi}[sU_n'(s) + 2nU_n(s)]\}, \tag{154a}$$

$$C_1 = A_1 + iB_1 = \frac{2n\pi a}{\cos n\pi} e^{-\frac{1}{2}s}[M_{n+\frac{1}{2}}(s) - e^{-i(n+\frac{1}{2})\pi}U_{n+\frac{1}{2}}(s)], \tag{154b}$$

$$C_2 = A_2 + iB_2 = \frac{s}{2n\sin n\pi} e^{-\frac{1}{2}s}[M_n'(s) - e^{-in\pi}U_n'(s)], \tag{154c}$$

for the constants $C_m = A_m + iB_m$ with the lower sign, the others being of course their complex conjugates $C_m^* = A_m - iB_m$.

To sum up, the constants C_m have the readily computable values (154) for use in (136), which with (98) and (99) can be written as

$$f_I e^{i\omega t} + f_R e^{-i\omega t} = f_- = F_0 C_0 - iF_1 C_1 - QC_2 \tag{155}$$

in terms of the incident and reflected waves, and as

$$f_T e^{i\omega t} = f_+ = F_0 C_0^* - iF_1 C_1^* - QC_2^* \tag{156}$$

in terms of the transmitted wave. Here, the quantities F_0, F_1 and Q are real. Solution of these equations can be facilitated by taking the complex conjugate of (156), to give

$$f_T^* e^{-i\omega t} = f_+^* = F_0 C_0 + iF_1 C_1 - QC_2. \tag{157}$$

By adding or subtracting (155) and (157) we can obtain the part of F_0 and F_1 proportional to $e^{i\omega t}$, in terms of the incident wave f_I alone together with the corresponding part of Q.

From this point onwards, we use subscript a for 'complex amplitude' so that, for example,

$$Q = \mathrm{Re}\,(Q_a e^{i\omega t}) = \tfrac{1}{2}(Q_a e^{i\omega t} + Q_a^* e^{-i\omega t}), \tag{158}$$

while F_{0a} and F_{1a} are defined similarly. Subtracting (157) from (155) gives

$$f_- - f_+^* = -2iF_1 C_1 = -iC_1(F_{1a} e^{i\omega t} + F_{1a}^* e^{-i\omega t}). \tag{159}$$

From the terms in $e^{i\omega t}$ (which on the left-hand side of (159) involve the incident wave alone) we deduce that

$$F_{1a} = iC_1^{-1} f_I: \tag{160}$$

the complex amplitude of the antisymmetric mode of orifice lip motion is iC_1^{-1} times the complex amplitude of the incident wave.

Results of greater practical interest are obtained by *adding* (155) and (157) to give

$$f_- + f_+^* = 2(F_0 C_0 - QC_2) = C_0(F_{0a} e^{i\omega t} + F_{0a}^* e^{-i\omega t}) - C_2(Q_a e^{i\omega t} + Q_a^* e^{-i\omega t}). \tag{161}$$

Now, from the terms in $e^{i\omega t}$, we obtain

$$F_{0a} = C_0^{-1} f_I + (C_2 C_0^{-1})\, Q_a. \tag{162}$$

With (128) which relates F_0 to ϕ_D, this gives an equation

$$\phi_{Da} = C_0^{-1} f_I + (C_2 C_0^{-1} + b)\, Q_a, \tag{163}$$

expressing the complex amplitude of the fluctuations of velocity potential in the depths of the duct as a linear combination of the complex amplitudes of the incident wave and of the downward flux Q.

From the first term in (163), we derive the pressure modification factor $Ke^{-i\alpha}$. This is defined in terms of the value ϕ_0 which the velocity potential in the incident wave would take at the centre $(0, -h)$ of the mouth if the duct were absent. By (97) and (98), ϕ_0 can be written in the form

$$\phi_0 = \mathrm{Re}\,(\phi_{0a} e^{i\omega t}) \quad \text{with} \quad \phi_{0a} = f_I e^{-2\pi h/\lambda}. \tag{164}$$

By (61), (163) and (164), the pressure modification factor can be calculated as the ratio of complex amplitudes of pressure fluctuations in the absence of duct flow to those in the absence of any duct at all:

$$Ke^{-i\alpha} = \frac{-\rho i\omega \phi_{Da}}{-\rho i\omega \phi_{0a}} = \frac{\phi_{Da}}{\phi_{0a}} = \frac{C_0^{-1} f_I}{f_I e^{-2\pi h/\lambda}} = e^{2\pi h/\lambda} C_0^{-1}. \tag{165}$$

Values of K and α calculated from this formula were given in figures 6, 7, 8 and 10.

The result (165) agrees with the simple conclusion (72) from a local model in the limit as $h/n\lambda$ becomes large, when (114) implies that a also is large, with

$$\pi h/n\lambda = a^2 - \tfrac{1}{2} + \log(2a) + o(1) \tag{166}$$

as $a \to \infty$. Then the asymptotic forms (148) and (149) show that, in the expression (154a) for C_0, the U_n terms are negligible and the dominant term for large $s = 4n(a^2-1)$ is

$$C_0 \sim \frac{n\pi}{\sin n\pi} e^{+\frac{1}{2}s} \frac{s^n}{n!}. \tag{167}$$

Accordingly, (165) gives

$$\frac{n\pi}{\sin n\pi} Ke^{-i\alpha} = \frac{n!}{s^n} \exp\left(\frac{2\pi h}{\lambda} - \tfrac{1}{2}s\right)$$
$$\sim \frac{n!}{(4na^2)^n} \exp\left[2n(a^2-\tfrac{1}{2}) + 2n\log(2a) - 2n(a^2-1)\right] = \frac{n!}{(n/e)^n} \tag{168}$$

exactly as in (72). Figure 8 has shown already that this limiting result is sufficiently accurate whenever $h/n\lambda > 2$.

Equation (163) when the flux is non-zero implies with (94) an expression for the potential ϕ in the depths of the duct. Its complex amplitude ϕ_a can be written as

$$\phi_a = \phi_{Da} - (Q_a/n\lambda)(y+h) = C_0^{-1} f_I - (Q_a/n\lambda)(y+h-l) - iD_r Q_a. \tag{169}$$

Here, the values of l and D_r are evident from (163):

$$l = n\lambda[\mathrm{Re}\,(C_2 C_0^{-1}) + b], \quad D_r = -\mathrm{Im}\,(C_2 C_0^{-1}). \tag{170}$$

Physically, l is an inertial term, representing an effective 'added length' of duct above the mouth; while D_r (which will be found to be necessarily positive) is a resistive term to be identified later as the radiation damping coefficient.

Using (128) for b, we can write the ratio of the added length l to the duct width $n\lambda$ as

$$\frac{l}{n\lambda} = \left\{\frac{h}{n\lambda} - \frac{a^2-1}{\pi}\right\} - \mathrm{Re}\left[\frac{1}{2n\pi} - \frac{C_2}{C_0}\right]. \tag{171}$$

The term in braces is of interest as representing the added-mass effect calculated for a much simpler problem: the case when gravity is neglected but the constant-pressure condition is applied on the surface $y = 0$. Then the properties of the function (118) imply that all the conditions for the complex potential f with flux Q in the duct are satisfied by

$$f = \frac{Q}{2\pi} \log \frac{1+\zeta}{1-\zeta}, \tag{172}$$

which by (116) is asymptotically

$$f = (Q/n\lambda)[iz - (h-l)] \tag{173}$$

in the depths ($\zeta \to 1$) of the duct, with

$$\frac{l}{n\lambda} = \left\{\frac{h}{n\lambda} - \frac{a^2-1}{\pi}\right\}. \tag{174}$$

This expression in braces in (171) and (174) is that plotted against $h/n\lambda$ in figure 15 as the curve 'without gravity effects'. Equations (154) show, furthermore, that the term in square brackets in (171) can be written in a form

$$\frac{1}{\pi} \frac{M_n(s) - e^{-in\pi} U_n(s)}{sM_n'(s) + 2nM_n(s) - e^{-in\pi}[sU_n'(s) + 2nU_n(s)]} \tag{175}$$

which may be expected (since U_n is typically much smaller than M_n) to have positive real part, and does so for all cases which the author has calculated (figure 15). Thus the effects of gravity in limiting the displacement of the free surface produce a reduction in added mass.

By analogy with (165) we write also

$$K_1 \exp(-i\alpha_1) = \exp(2\pi h/\lambda)\, C_1^{-1}. \tag{176}$$

This, by (160), means that

$$F_{1a} = K_1 \exp[i(\tfrac{1}{2}\pi - \alpha_1)]\, f_I \exp(-2\pi h/\lambda). \tag{177}$$

Here, F_{1a} is the complex amplitude of the antisymmetric lip motions. These tend to respond, not to the crest itself as do the symmetric motions, but to the horizontal acceleration peak which precedes the crest by a phase lead of $\frac{1}{2}\pi$. Then the phase difference α_1 represents a (rather small) lag in response to that peak horizontal acceleration.

Equation (177) implies that the ratio K_1/K, plotted in figure 9, is a ratio, in the zero-flux case (165), of the real amplitudes $|F_{1a}|$ and $|F_{0a}|$ of antisymmetric and symmetric lip motions [see the discussion following (129)]. These, however, are nearly 90° out of phase (the exact phase difference being $\frac{1}{2}\pi + \alpha - \alpha_1$). Note that flux in the duct would leave F_{1a} unaltered but, according to (162), would typically increase $|F_{0a}|$ so that K_1/K can be described as a sort of *maximum* asymmetry ratio.

We next determine the complex amplitudes f_T and f_R of the transmitted and reflected waves. Eliminating F from (156) and (157) we obtain

$$(C_1 f_+ + C_1^* f_+^*) = F_0(C_0 C_1^* + C_0^* C_1) - Q(C_1 C_2^* + C_1^* C_2), \tag{178}$$

where all three bracketed expressions are *real*. Equation (178) means that the real part of

$$2C_1 f_T e^{i\omega t} - F_{0a} e^{i\omega t}(C_0 C_1^* + C_0^* C_1) - Q_a e^{i\omega t}(C_1 C_2^* + C_1^* C_2) \tag{179}$$

vanishes for all t, which is possible for a multiple of $e^{i\omega t}$ only if it is identically zero. Therefore, f_T is given by

$$2C_1 f_T = F_{0a}(C_0 C_1^* + C_0^* C_1) - Q_a(C_1 C_2^* + C_1^* C_2). \tag{180}$$

Also, from the terms in $e^{-i\omega t}$ in (161), we have

$$f_R + f_T^* = C_0 F_{0a}^* - C_2 Q_a^*, \tag{181}$$

and multiplying this by $2C_1^*$ and using (180) for f_T we deduce

$$2C_1^* f_R = F_{0a}^*(C_0 C_1^* - C_0^* C_1) - Q_a^*(C_1^* C_2 - C_1 C_2^*). \tag{182}$$

An important check on the whole analysis can now be made. The *energy flux* (per unit crest length) in the incident wave can be written

$$\tfrac{1}{4}\rho\omega|f_I|^2; \tag{183}$$

this is the group velocity (half the phase velocity) multiplied by the wave energy per unit horizontal area. We expect the total rate E of energy absorption by the duct, per unit crest length, to be the part of the incident wave energy (183) that is neither transmitted nor reflected:

$$E = \tfrac{1}{4}\rho\omega(|f_I|^2 - |f_T|^2 - |f_R|^2). \tag{184}$$

From (162), (180) and (182) we can rewrite this as

$$4|C_1|^2E = \tfrac{1}{4}\rho\omega\{4C_1C_1^*(F_{0a}C_0-Q_aC_2)(F_{0a}^*C_0^*-Q_a^*C_2^*)$$
$$-[(F_{0a}C_0-Q_aC_2)C_1^*+(F_{0a}C_0^*-Q_aC_2^*)C_1][(F_{0a}^*C_0^*-Q_a^*C_2^*)C_1+(F_{0a}^*C_0-Q_a^*C_2)C_1^*]$$
$$-[(F_{0a}^*C_0-Q_a^*C_2)C_1^*-(F_{0a}^*C_0^*-Q_a^*C_2^*)C_1][(F_{0a}C_0^*-Q_aC_2^*)C_1-(F_{0a}C_0-Q_aC_2)C_1^*]\} \tag{185}$$

where in each of the last two lines the first factor in square brackets is the right-hand side of (180) or (182) respectively, and the second factor is its complex conjugate. The terms in C_1C_1 and $C_1^*C_1^*$ in the last two lines cancel, leaving only terms with the factor $C_1C_1^* = |C_1|^2$, giving

$$E = \tfrac{1}{16}\rho\omega\{2(F_{0a}C_0-Q_aC_2)(F_{0a}^*C_0^*-Q_a^*C_2^*)-2(F_{0a}C_0^*-Q_aC_2^*)(F_{0a}^*C_0-Q_a^*C_2)\}$$
$$= \tfrac{1}{8}\rho\omega(F_{0a}Q_a^*-F_{0a}^*Q_a)(C_0^*C_2-C_0C_2^*). \tag{186}$$

We compare this with the rate of working by duct pressures, with complex amplitude

$$p_a = -\rho i\omega\phi_a, \tag{187}$$

driving a flux with complex amplitude Q_a. This form of the rate E of energy absorption by the duct is

$$E = \tfrac{1}{4}(p_aQ_a^*+p_a^*Q_a) = -\tfrac{1}{4}\rho i\omega(\phi_aQ_a^*-\phi_a^*Q_a), \tag{188}$$

which in turn gives

$$E = -\tfrac{1}{4}\rho i\omega(F_{0a}Q_a^*-F_{0a}^*Q_a) \tag{189}$$

since, by (163) and (128), ϕ_a differs from F_{0a} by a *real* multiple of Q_a; namely,

$$\phi_a-F_{0a} = [\phi_{Da}-(Q_a/n\lambda)(y+h)]-(\phi_{Da}+bQ_a) = -(Q_a/n\lambda)(y+h+bn\lambda). \tag{190}$$

To complete the check that the rate (189) of energy absorption by the duct is equal to the balance (186) of incident wave energy flux that is neither transmitted nor reflected, we must prove that

$$C_0^*C_2-C_0C_2^* = -2i. \tag{191}$$

Actually, we calculate from (154) that

$$C_0^*C_2-C_0C_2^* = -2i\frac{\pi}{\sin n\pi}se^{-s}[U_n(s)M_n'(s)-U_n'(s)M_n(s)], \tag{192}$$

which is not obviously a constant! However, we complete the proof by recalling that, for any two solutions $U_n(s)$ and $M_n(s)$ of the second-order differential equation (147), the Wronskian

$$U_n(s)M_n'(s)-U_n'(s)M_n(s) \tag{193}$$

is exactly proportional to $s^{-1}e^s$ (that is, to the exponential of minus the integrated coefficient of dw/ds). We may find the constant of proportionality from the asymptotic forms (148) and (149). They show that (193) is asymptotic (as $s\to\infty$) to

$$\frac{s^{-n}}{(-n)!}e^s\frac{s^{n-1}}{(n-1)!} = \frac{\sin n\pi}{\pi}s^{-1}e^s, \tag{194}$$

so that this must be its exact value for all s, verifying the energy balance requirement (191).

It is interesting to write the expression (182) for the reflected wave f_R in terms of f_I and Q_a, by substituting for F_{0a} from (162). This gives

$$f_R = \tfrac{1}{2} f_I^* \left(\frac{C_0}{C_0^*} - \frac{C_1}{C_1^*}\right) + \tfrac{1}{2} Q_a^* \frac{C_0 C_2^* - C_0^* C_2}{C_0^*}. \tag{195}$$

Using (176) in the first term and (191) in the second and (165) in both, we can write this as

$$f_R = f_I^* i \exp[i(\alpha + \alpha_1)] \sin(\alpha - \alpha_1) + Q_a^* i \exp(i\alpha) K e^{-2\pi h/\lambda}. \tag{196}$$

Similarly, from (180) we find

$$f_T = f_I \exp[-i(\alpha + \alpha_1)] \cos(\alpha - \alpha_1) - Q_a i \exp(-i\alpha) K e^{-2\pi h/\lambda}. \tag{197}$$

Equations (196) and (197) show that, when there is zero flux in the duct, the proportions of incident energy that are reflected and transmitted are $\sin^2(\alpha - \alpha_1)$, as stated in (19), and $\cos^2(\alpha - \alpha_1)$, respectively. These proportions add up to 1 because there is no energy absorption in that case.

There is also interest in the case $f_I = 0$ of zero incident wave, when any waves (196) and (197) must be generated by motions in the duct powered by some internal source of energy. Then we see that f_R and f_T are complex conjugates of each other, implying symmetrical wave generation. The energy flux in the waves is

$$\tfrac{1}{4}\rho\omega(|f_R|^2 + |f_T|^2) = \tfrac{1}{2}\rho\omega |Q_a|^2 D_r \tag{198}$$

where D_r is the radiation damping coefficient, given by (196) and (197) as

$$D_r = (K e^{-2\pi h/\lambda})^2 = |C_0|^{-2}. \tag{199}$$

Equation (191) is easily used to show that our definitions (170) and (199) of D_r agree. The general check on energy balance, equating the values of energy absorption E calculated as (184) and as (188), shows that E is negative in this case, and that the quantity $-E$ represents wave-energy output resulting from internal pressures driving the duct motions.

This may be independently verified: by (169) with $f_I = 0$, the internal pressure in the duct has complex amplitude

$$p_a = -\rho i\omega \phi_a = \rho\omega Q_a [i(y + h - l)/(n\lambda) - D_r]. \tag{200}$$

The part 90° out of phase with the flux Q_a does no work, but the part $-\rho\omega Q_a D_r$ in antiphase with Q_a does work at the rate (198).

The limiting case $n \to 0$ is of some interest. Then (137a) shows that

$$C_0 \to \int_{-i\infty}^{1} \tfrac{1}{2} s e^{\frac{1}{2}s\zeta} d\zeta = e^{\frac{1}{2}s}, \tag{201}$$

while (138) and (114) give

$$s = 4n(a^2 - 1) \to 4\pi h/\lambda. \tag{202}$$

Therefore, by (165), $\alpha \to 0$ and $K \to 1$; in words, a narrow duct records the pressure that would be found at the level of its mouth if the duct were absent. Equation (137b) also shows that $C_1 \to 0$, but we need the value of

$$\lim_{n \to 0} (n^{-1} C_1) = 2a \int_{-i\infty}^{1} (1 - \zeta^2)^{-\frac{1}{2}} e^{\frac{1}{2}s\zeta} d\zeta = 2a [\pi I_0(\tfrac{1}{2}s) + i K_0(\tfrac{1}{2}s)]. \tag{203}$$

This representation in terms of Bessel functions (Watson 1944, art. 6.22) shows, by (176), that

$$\alpha_1 \to \tan^{-1}[K_0(\tfrac{1}{2}s)/\pi I_0(\tfrac{1}{2}s)]. \tag{204}$$

Therefore, the reflexion coefficient $R = \sin^2(\alpha - \alpha_1)$ for zero duct flow tends to the value

$$\{1 + [\pi I_0(2\pi h/\lambda)/K_0(2\pi h/\lambda)]^2\}^{-1} \tag{205}$$

which was given by Ursell (1947), following Dean (1945), for the case of a single submerged vertical barrier.

At a rather lower, but not negligible, level of interest is the limiting case $n \to \frac{1}{2}$, when it is easy to show from (137) that $A_1 \to \infty$ while B_1 remains finite. By (176) this makes $K_1 \to 0$ (see figure 9) and $\alpha_1 \to 0$ (see figure 10). On the other hand, C_0 has by (137) a finite limit as $n \to \frac{1}{2}$, which can again (if desired) be expressed in terms of Bessel functions, although it can be calculated very readily from (154) as was done in obtaining the values in figures 7 and 10.

The fully interactive model for the mouth-upwards case, described above in some detail, gives results that are by no means unique even when the incident wave f_I is fixed, because they include the extra degree of freedom represented by Q. In fact, the solution becomes unique only when the internal duct dynamics are specified. Any such specification, if linear, can be represented by an internal impedance Z relating the complex amplitude of a duct reference pressure p_D to the complex amplitude of the flux Q. We may take that reference pressure p_D as the value in the depths of the duct extrapolated linearly back to the mouth, just as ϕ_D was defined in (94). Then the complex amplitude p_{Da} is $-\rho i\omega\phi_{Da}$, giving for the impedance

$$Z = p_{Da}/Q_a = -\rho i\omega\phi_{Da}/Q_a = -\rho i\omega(F_{0a} + bQ_a)/Q_a = -\rho i\omega(X + b), \tag{206}$$

where $X = F_{0a}/Q_a$ and, by (128), b is real. Therefore, the rate of energy absorption (189) can be written

$$E = \tfrac{1}{4}(ZQ_aQ_a^* + Z^*Q_a^*Q_a) = \tfrac{1}{2}(\operatorname{Re} Z)\,|Q_a|^2 = \tfrac{1}{2}\rho\omega(\operatorname{Im} X)\,|Q_a|^2, \tag{207}$$

involving, as must be expected, the real part of the impedance Z and therefore the imaginary part of X. Also the energy flux in the incident wave, (183), can be written (by (162), and again using $X = F_{0a}/Q_a$) as

$$\tfrac{1}{4}\rho\omega|C_0F_{0a} - C_2Q_a|^2 = \tfrac{1}{4}\rho\omega|C_0|^2\,|Q_a|^2\,|X - C_2C_0^{-1}|^2. \tag{208}$$

Comparing this with (207), we see that the proportion of the incident wave energy (208) which is absorbed is

$$\frac{2(\operatorname{Im} X)\,|C_0|^{-2}}{(\operatorname{Re} X - \operatorname{Re} C_2C_0^{-1})^2 + (\operatorname{Im} X + |C_0|^{-2})^2}, \tag{209}$$

where the fact that $\operatorname{Im}(C_2C_0^{-1}) = -|C_0|^{-2}$ [because of (191)] has again been used.

The proportion (209) so calculated takes the maximum value $\frac{1}{2}$ already derived for frictionless systems in §1.2 by a related method. This maximum is attained when

$$\operatorname{Re} X = \operatorname{Re} C_2C_0^{-1}, \quad \operatorname{Im} X = |C_0|^{-2} = -\operatorname{Im} C_2C_0^{-1}, \tag{210}$$

where the first equation is the condition for resonance and the second puts the energy

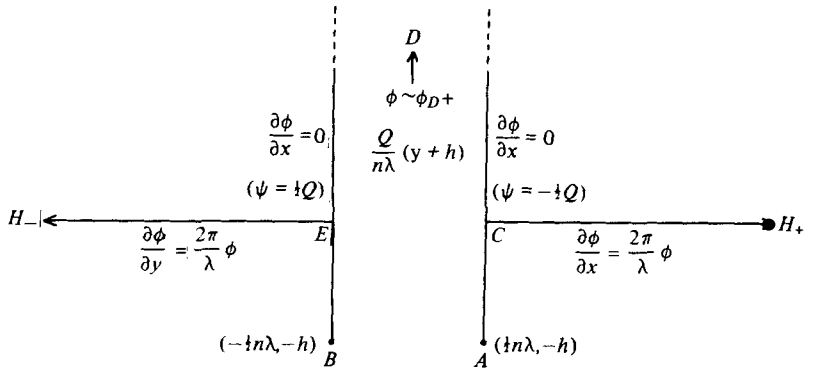

FIGURE 31. Boundary-value problem, in terms of the velocity potential ϕ and stream function ψ, to be solved in the fully interactive theory of the mouth-downwards case.

absorption rate equal to the external rate of loss of energy by generation of new waves. Under these conditions (optimal for linear duct dynamics)

$$F_{0a} = XQ_a = (C_2 C_0^{-1})^* Q_a, \tag{211}$$

so that (180) gives

$$f_T = i(C_1^*/C_1)(Q_a/C_0^*) = i\exp[i(\alpha - 2\alpha_1)](K e^{-2\pi h/\lambda}) Q_a. \tag{212}$$

Similarly, (182) shows that f_R is the complex conjugate f_T^*, implying a symmetrical re-radiation of that half of the incident wave energy which is not absorbed (a quarter of the incident energy being transmitted and a quarter reflected). These results for the optimal-absorption regime are characteristic of all symmetrical two-dimensional wave-energy-absorption systems (Evans 1976). It must be emphasized, however, that such results depend on the assumption that the internal dynamics of the duct is linear. When energy extraction is by means of a highly nonlinear device such as an 'overspill' system, a more favourable optimum may be possible.

After describing in detail the fully interactive theory for the mouth-upwards case, we can end this paper by quickly deriving all the analogous results for the mouth-downwards case. The theory is, indeed, completely identical once we have found the new set of equations corresponding to (154), and even the route to that set of equations is closely parallel to that already followed.

Figure 31 specifies the mouth-downwards problem to be solved in terms of the velocity potential ϕ. Here, we take Q as the upward flux in the duct, so that energy absorption will depend as before on duct pressures *in phase with* Q. Thus, (94) is replaced by

$$\phi - (Q/n\lambda)(y+h) \to \phi_D \tag{213}$$

in the 'depths' D which now, however, are where $y+h$ becomes large and *positive*. The duct walls are $x = \pm\frac{1}{2}n\lambda$, $y > -h$ and all other conditions, (95) to (99), are as before.

Figure 32 specifies the same problem in terms of the complex potential (102) and the auxiliary function (105). The changed sense in the flux Q means that now

$$\mathrm{Im} f = \mp\tfrac{1}{2}Q, \quad \mathrm{Im} F = \pm(\pi Q/\lambda) \quad \text{on} \quad x = \pm\tfrac{1}{2}n\lambda, \quad y \geqslant -h; \tag{214}$$

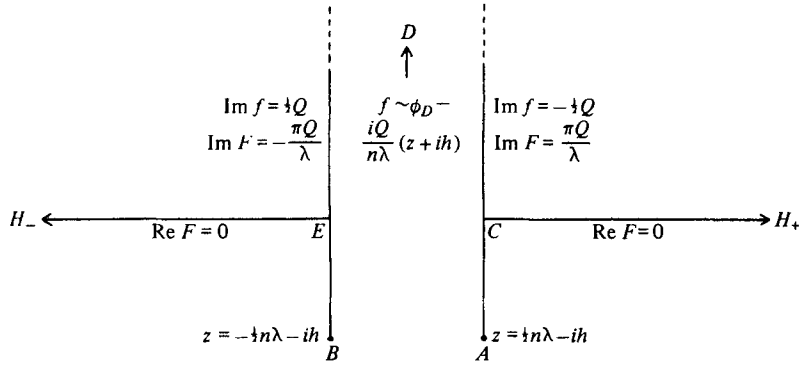

FIGURE 32. Boundary-value problem, in terms of the complex potential f and the auxiliary function F, to be solved in the complex z plane in the mouth-downwards case.

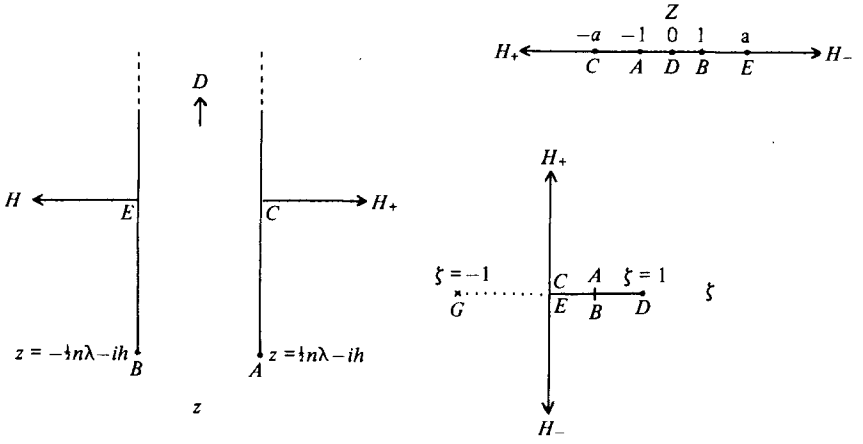

FIGURE 33. The three complex planes (z plane, Z plane and ζ plane) used in the mouth-downwards case. Dotted line: this illustrates the extended cut, running from $\zeta = -1$ to $\zeta = +1$, which is applicable when the complete complex ζ plane is used.

while in the 'depths'

$$f + (iQ/n\lambda)(z+ih) - \phi_D \to 0, \quad F - (Q/n\lambda) + (2\pi/\lambda)[\phi_D - (iQ/n\lambda)(z+ih)] \to 0. \tag{215}$$

Equation (110) remains correct, and the condition (111) becomes

$$f_\pm = \lim_{z \to +i\infty} \left\{ [\phi_D - (iQ/n\lambda)(z+ih)] \exp(2\pi i z/\lambda) + i \int_{\pm\infty}^{z} F(z_1) \exp(2\pi i z_1/\lambda)\, dz_1 \right\}. \tag{216}$$

Figure 33 shows the appropriate Schwarz–Christoffel mapping (62) of the required polygon in the z plane which now, in addition to the vertices A, B and D with internal angles 2π, 2π and 0, has vertices C and E with internal angles $+\frac{1}{2}\pi$. This gives

$$\frac{dz}{dZ} = -\frac{n\lambda}{i\pi} \frac{(Z-1)(Z+1)}{Z} \frac{a}{(a-Z)^{\frac{1}{2}}(a+Z)^{\frac{1}{2}}}, \tag{217}$$

if C, E correspond to $Z = \mp a$, respectively. The changed sign in front of (217) expresses the fact that the duct width $n\lambda$, being now the change in z as D is half-encircled in the *positive* sense in the upper half Z plane, is $+\pi i$ times the residue of (217) at $Z = 0$.

The resulting value of z is

$$z = \frac{n\lambda}{i\pi}\left[a(a^2-Z^2)^{\frac{1}{2}} - \tfrac{1}{2}\log\frac{(a^2-Z^2)^{\frac{1}{2}}+a}{(a^2-Z^2)^{\frac{1}{2}}-a}\right], \tag{218}$$

with the constant of integration chosen this time so that the points at infinity on the real axis correspond (figure 33). The value of a such that $\operatorname{Im} z = -h$ when $Z = \pm 1$ satisfies an equation

$$h = \frac{n\lambda}{\pi}\left[a(a^2-1)^{\frac{1}{2}} - \tfrac{1}{2}\log\frac{a+(a^2-1)^{\frac{1}{2}}}{a-(a^2-1)^{\frac{1}{2}}}\right], \tag{219}$$

where the changed sign from (114) makes the value of a *larger* (for given $h/n\lambda$) than in the mouth-upwards case. This is the main feature responsible for the asymptotic properties corresponding to the local model (§2.1) being reached *sooner*, as $h/n\lambda$ increases, than in the mouth-upwards case.

The appropriate auxiliary variable ζ is now

$$\zeta = (a^2-Z^2)^{\frac{1}{2}}/a, \tag{220}$$

which fills the right-hand half-plane cut from 0 to 1 (figure 33). Then (218) gives

$$z = \frac{n\lambda}{i\pi}\left(a^2\zeta - \tfrac{1}{2}\log\frac{\zeta+1}{\zeta-1}\right), \quad dz = \frac{n\lambda}{i\pi}\left(a^2+\frac{1}{\zeta^2-1}\right)d\zeta. \tag{221}$$

It is now the function

$$\log\frac{\zeta+1}{\zeta-1} \tag{222}$$

whose imaginary part has boundary values (119) and whose real part is zero on EH_- and H_+C. Next, the boundary values (214) on F give (120) as before, and we conclude this time that

$$F_m = \zeta^{-1}\left(F + \frac{Q}{\lambda}\log\frac{\zeta+1}{\zeta-1}\right) \tag{223}$$

is real on the whole boundary. The same argument as before then demonstrates that $(Z^2-1)F_m$ is a first-order polynomial in Z, and thus establishes the solution

$$F = \frac{2\pi}{\lambda}\zeta\frac{F_0+F_1Z}{Z^2-1} - \frac{Q}{\lambda}\log\frac{\zeta+1}{\zeta-1}, \tag{224}$$

where F_0, F_1 and Q are real.

In the 'depths' where $Z \to 0$, $\zeta \to 1$, the equations (215) and (224) now require that

$$\phi_D = F_0 + bQ, \quad \text{where} \quad b = \frac{a^2}{\pi} - \frac{h}{n\lambda} + \frac{1}{2n\pi}. \tag{225}$$

Furthermore, (216) now becomes

$$f_\pm = \lim_{\zeta\to 1}\left\{\left[F_0 + \frac{Q}{2\pi}\left(\log\frac{\zeta+1}{\zeta-1} + \frac{1}{n}\right)\right]\exp(2\pi iz/\lambda) + i\int_{\pm\infty}^{\zeta} F\exp(2\pi iz/\lambda)\,\frac{n\lambda}{i\pi}\,\frac{a^2(\zeta^2-1)+1}{\zeta^2-1}\,d\zeta\right\}, \tag{226}$$

where, by (224),

$$F = -\frac{2\pi}{\lambda}\zeta\frac{F_0+F_1 ia(\zeta^2-1)^{\frac{1}{2}}}{a^2(\zeta^2-1)+1} - \frac{Q}{\lambda}\log\frac{\zeta+1}{\zeta-1} \tag{227}$$

and, by (221),

$$\exp(2\pi iz/\lambda) = \exp(2na^2\zeta)\left(\frac{\zeta-1}{\zeta+1}\right)^n. \tag{228}$$

The fact that (228) becomes, not infinite, but zero in the 'depths', that is, as $\zeta \to 1$, eliminates any convergence problem when we take the limit in (226). Nevertheless, the same integration by parts as was performed in (134) proves useful in (226) for simplifying the form of the integral. Writing the first line of (226) as the integral

$$\int_{\pm i\infty}^{\zeta}$$

of its derivative and combining it with the second line, we obtain

$$f_\pm = F_0(A_0 \mp iB_0) - iF_1(A_1 \mp iB_1) - Q(A_2 \mp iB_2) \tag{229}$$

exactly as in (136), where now

$$A_0 \mp iB_0 = \int_{\pm i\infty}^{1} e^{\frac{1}{2}s\zeta}\left(\frac{\zeta-1}{\zeta+1}\right)^n\left[\tfrac{1}{2}s - \frac{2n}{\zeta+1}\right]d\zeta, \tag{230a}$$

$$A_1 \mp iB_1 = 2na\int_{\pm i\infty}^{1} e^{\frac{1}{2}s\zeta}\left(\frac{\zeta-1}{\zeta+1}\right)^n\frac{\zeta\,d\zeta}{(\zeta^2-1)^{\frac{1}{2}}}, \tag{230b}$$

$$A_2 \mp iB_2 = -\frac{s}{4\pi n}\int_{\pm i\infty}^{1} e^{\frac{1}{2}s\zeta}\left(\frac{\zeta-1}{\zeta+1}\right)^n d\zeta. \tag{230c}$$

This time, the variable s is

$$s = 4na^2. \tag{231}$$

The integrals (230) are very similar to those in (137) but with a few changes. The most important is the replacement of n by $-n$, just as we found for the corresponding local model (§2.1). It is also important that the complex ζ plane is now cut from -1 to $+1$ (rather than from $-\infty$ to -1 and from 1 to ∞), owing to the change in sign in the term in large round brackets. Finally, there is an additional ζ factor in the second integrand, resulting from the replacement of expression (132) for Z by

$$Z = +ia(\zeta^2-1)^{\frac{1}{2}}. \tag{232}$$

The first of these changes means that we must use integral expressions like (145) and (151) with n replaced by $-n$. On the other hand, the second change means that the corresponding integral expressions in (230), with the changed sign for the large round bracket, involve the extra factor $e^{in\pi}$ or $e^{-in\pi}$ on the new cut's upper or lower edges, which now coincide with the range $-1 < \zeta < 1$ of the integral (145), but involve no such modifying factor in the range $-\infty < \zeta < 1$ of the integral (151). Finally, the last change produces an extra modification in C_1. We obtain

$$C_0 = A_0 + iB_0 = \frac{\pi}{\sin n\pi}e^{-\frac{1}{2}s}\{-e^{-in\pi}[sM'_{-n}(s) - 2nM_{-n}(s)] + sU'_{-n}(s) - 2nU_{-n}(s)\}, \tag{233a}$$

$$C_1 = A_1 + iB_1 = \frac{2n\pi a}{\cos n\pi}e^{-\frac{1}{2}s}\{e^{-i(n-\frac{1}{2})\pi}[2M'_{\frac{1}{2}-n}(s) - M_{\frac{1}{2}-n}(s)] - 2U'_{\frac{1}{2}-n}(s) + U_{\frac{1}{2}-n}(s)\}, \tag{233b}$$

$$C_2 = A_2 + iB_2 = \frac{s}{2n\sin n\pi}e^{-\frac{1}{2}s}[e^{-in\pi}M'_{-n}(s) - U'_{-n}(s)]. \tag{233c}$$

The presence here of the factor $e^{-in\pi}$ in the leading terms involving the M function, instead of in the asymptotically much smaller terms involving the U function as in (154), confirms the important difference in phase between the responses of mouth-downwards and mouth-upwards ducts, foreshadowed in §2.1. The values of K and α calculated from (165), with C_0 given by (233), are plotted in figure 18 and show a phase lead $-\alpha$ close to (but slightly exceeding) $n\pi$ in each case. Asymptotically, the value of K tends to the broken-line expression (81), while the phase lead $-\alpha$ tends to $n\pi$. This is because when $h/n\lambda$ is large (219) makes a also large, with

$$\pi h/n\lambda = a^2 - \tfrac{1}{2} - \log(2a) + o(1), \tag{234}$$

while (148) and (233) for large $s = 4na^2$ give

$$C_0 \sim \frac{n\pi}{\sin n\pi}\, e^{\frac{1}{2}s}\, \frac{s^{-n}}{(-n)!}\, e^{-in\pi}. \tag{235}$$

Accordingly, by (165),

$$\begin{aligned} Ke^{-i\alpha} &= \exp(2\pi h/\lambda)\, C_0^{-1} \\ &\sim \exp[2n(a^2 - \tfrac{1}{2})]\,(2a)^{-2n}\, \frac{\sin n\pi}{n\pi}\, \exp(-\tfrac{1}{2}s)\,(-n)!\, s^n \exp(in\pi) = \frac{(n/e)^n}{n!}\, e^{in\pi}, \end{aligned} \tag{236}$$

giving the asymptotic limits

$$K \to (n/e)^n/n!, \quad (-\alpha) \to n\pi \tag{237}$$

stated above.

The necessary check on energy balance then proceeds as in (183) to (190), and requires us once more to prove (191); this time, as follows. By (233),

$$C_0^* C_2 - C_0 C_2^* = 2i\, \frac{\pi}{\sin n\pi}\, s e^{-s}[U_{-n}(s) M'_{-n}(s) - U'_{-n}(s) M_{-n}(s)]; \tag{238}$$

which, as required, is equal to $-2i$ because the Wronskian in square brackets is

$$-\pi^{-1} \sin(n\pi)\, s^{-1} e^s. \tag{239}$$

The added mass in the mouth-downwards case is derived from the equation (162) relating F_{0a} to Q_a, with the new values (233) of C_0 and C_2. This, with the new value (225) of b, makes ϕ_{Da} equal to (163) as before. Therefore, in the 'depths' of the duct (213) gives

$$\phi_a = \phi_{Da} + (Q_a/n\lambda)(y + h) = C_0^{-1} f_I + (Q_a/n\lambda)(y + h + l) - iD_r Q_a, \tag{240}$$

with the previous values (170) for the added length l and for the radiation damping coefficient

$$D_r = -\operatorname{Im}(C_2 C_0^{-1}) = |C_0|^{-2}. \tag{241}$$

Accordingly, using (225) for b, we have

$$\frac{l}{n\lambda} = \left\{\frac{a^2}{\pi} - \frac{h}{n\lambda}\right\} - \operatorname{Re}\left[-\frac{1}{2n\pi} - \frac{C_2}{C_0}\right]. \tag{242}$$

Here, the term in braces is once more separated out, as the value of $l/n\lambda$ with gravity neglected, corresponding to a solution

$$f = \frac{Q}{2\pi} \log \frac{\zeta + 1}{\zeta - 1} \sim \frac{Q[-iz + (h + l)]}{n\lambda} \quad \text{as} \quad \zeta \to 1 \quad \text{with} \quad \frac{l}{n\lambda} = \left\{\frac{a^2}{\pi} - \frac{h}{n\lambda}\right\}. \tag{243}$$

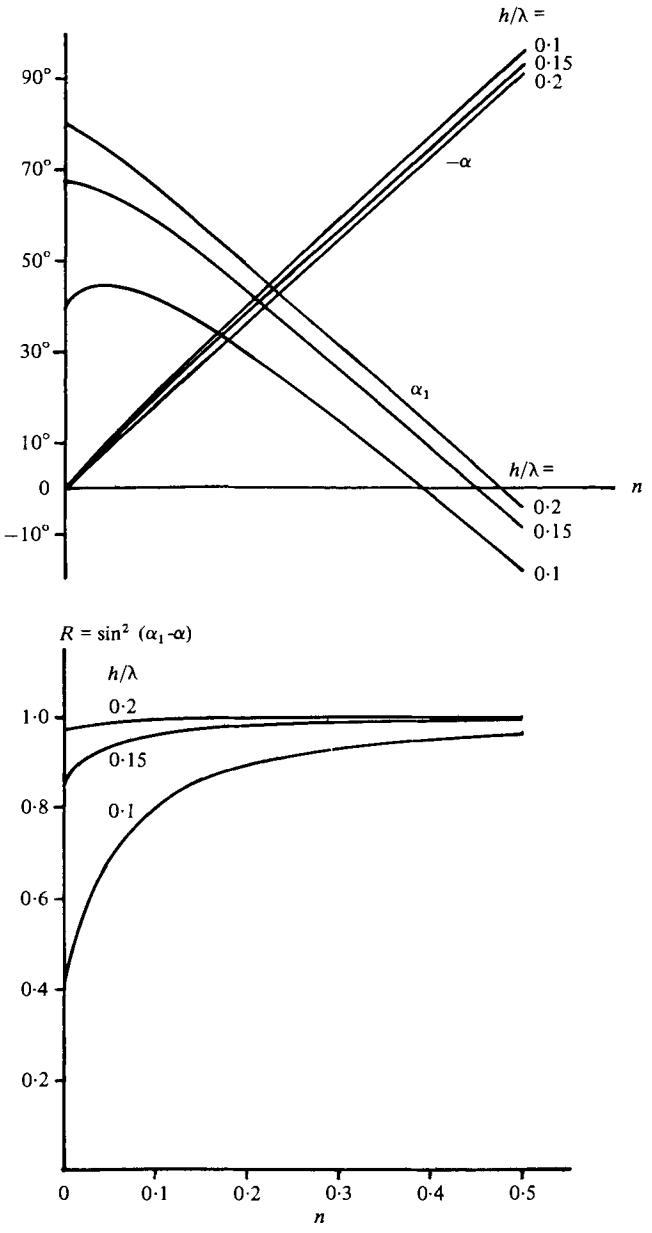

FIGURE 34. The phase lead $-\alpha$ and phase lag α_1 in the symmetrical and antisymmetrical components of duct response, respectively, plotted in the mouth-downwards case as functions of the width–wavelength ratio n. Lower graph: deduced values of the ratio R of reflected energy to incident energy in circumstances when there is no flow in the duct.

The term in square brackets in (242) can be written in a form

$$\frac{1}{\pi}\frac{M_{-n}(s)-e^{in\pi}U_{-n}(s)}{sM'_{-n}(s)-2nM_{-n}(s)-e^{in\pi}[sU'_{-n}(s)-2nU_n(-s)]} \tag{244}$$

which as with (175) can be expected to have positive real part, and does so for all cases which the author has calculated. This term represents a level of reduction

from the zero-gravity value similar to that found in the mouth-upwards case. A major difference between the two cases, however, is that the zero-gravity value (term in braces) is far bigger in the mouth-downwards condition. This is why added-mass values are considerably larger in the mouth-downwards than in the mouth-upwards condition (figures 20 and 14).

In the limiting case $n \to 0$, we obtain from (230) and (219) that once more (201) and (202) hold, giving $\alpha \to 0$ and $K \to 1$. However, the extra ζ factor in the integral for C_1 means that

$$\lim_{n\to 0}(n^{-1}C_1) = 2a\int_{-i\infty}^{1}\zeta(\zeta^2-1)^{-\frac{1}{2}}e^{\frac{1}{2}s\zeta}d\zeta = 2a[K_1(\tfrac{1}{2}s)+i\pi I_1(\tfrac{1}{2}s)], \tag{245}$$

showing by (176) that for the mouth-downwards case

$$\lim_{n\to 0}(\alpha_1) = \tan^{-1}[\pi I_1(\tfrac{1}{2}s)/K_1(\tfrac{1}{2}s)]. \tag{246}$$

Therefore, as $n \to 0$, the reflexion coefficient $R = \sin^2(\alpha-\alpha_1)$ for zero duct flow tends to the value

$$\{1+[K_1(2\pi h/\lambda)/\pi I_1(2\pi h/\lambda)]^2\}^{-1}, \tag{247}$$

which was given by Ursell (1947) for the case of a single vertical barrier extending downwards from the surface to depth h.

Figure 34 shows how for each value of h/λ the reflexion coefficient increases above the value (247) as n increases. These graphs imply that, under typical conditions in a two-dimensional mouth-downwards system with zero duct flow, almost all the energy is reflected.† On the other hand, when motions in the duct are responding to the waves, all the results of (206) to (212) apply. In particular, in the condition for optimum absorption, half of the incident wave energy is once more absorbed while the remainder is symmetrically re-radiated (one-quarter as a reflected, and one-quarter as a transmitted, wave).

For all other aspects of the use of results calculated from two-dimensional fully interactive theories, and for the extent to which different results so calculated may give reliable indications of the behaviour of three-dimensional systems, see §1.2. Also, see the end of §1.2 for a highly tentative set of conclusions from these studies.

I am most grateful to Dennis Carey, Brian Count, David Evans, Graeme Knott, and Michael Longuet-Higgins for their helpful comments on the materials in this paper.

REFERENCES

CAREY, D. J. & MERATLA, Z. 1976 *Brit. Patent Appl.* no. 38490/76, dated 16 September 1976; cognated with *Brit. Patent Appl.* no. 820/77, dated 10 January 1977.

DEAN, W. R. 1945 *Proc. Camb. Phil. Soc.* **41**, 231.

EVANS, D. V. 1976 *J. Fluid Mech.* **77**, 1.

EVANS, D. V. & MORRIS, C. A. N. 1972 *J. Inst. Math. Applics.* **10**, 1.

EVERY, M. J., PRIDDIN, K. G. & PROSSER, M. J. 1977 *Tests on a Device for Extracting Wave Power*. Cranfield, England: BHRA Fluid Engineering.

† This result for the system of figure 33 is in contrast with that found in the quite different mouth-downwards problem, with a free surface inside the duct at the same level as the external free surface, solved by Evans & Morris (1972). There, the reflexion coefficient can vanish for particular combinations of mouth depth and duct width.

FOCK, V. 1926 *Archiv für Elektroteknik* **16**, 331.

JARVIS, R. J. 1971 *J. Inst. Math. Applics.* **7**, 111.

JEFFREYS, H. & JEFFREYS, B. S. 1950 *Methods of Mathematical Physics*, 2nd edn. Cambridge University Press.

KNOTT, G. F. & FLOWER, J. O. 1979 *J. Fluid Mech.* **90**, 327–336.

LEVINE, H. & RODEMICH, E. 1958 *Stanford Univ. Tech. Rep.* no. 78.

MACDONALD, A. D. 1949 *J. Math. & Phys.* **28**, 183.

NEWMAN, J. N. 1975 *J. Fluid Mech.* **71**, 273.

URSELL, F. 1947 *Proc. Camb. Phil. Soc.* **43**, 374.

WATSON, G. N. 1944 *A Treatise on the Theory of Bessel Functions*, 2nd edn. Cambridge University Press.